Doctoral Dissertation

Preparation and Gas Separation Performance of Mixed Matrix Membranes Using SAPO-34 and ZIF-8

(SAPO-34 と ZIF-8 を用いた Mixed Matrix Membranes の 作製とガス分離特性)

LIU YONGSHENG

劉 永生

Graduate School of Sciences and Technology for Innovation

Yamaguchi University, Japan

山口大学大学院創成科学研究科環境共生系専攻

2021 年 3 月

Abstract

Compared with the conventional separation process, membrane technology is a promising alternative for hydrogen purification, natural gas purification and olefin/paraffin separation because of the low energy cost and small footprint. Polymer membranes have excellent processability and high reproducibility. Highly permeable polymer membranes have low selectivity. Therefore, the gas transport properties of polymer membranes are below an upper bound. Inorganic membranes exhibit excellent separation property and mechanical stability; however, their fabrication process is costly. The separation performance of polymer membranes could be improved to surpass the upper bound by blending inorganic particles. The obtained hybrid membranes are the so-called mixed matrix membranes (MMMs). In the MMMs, the inorganic particles are the dispersion phase (filler) and polymer as the continuous phase (matrix). The preparation cost of MMMs with inorganic particle powder and polymer matrix is expected to be lower than that of inorganic membranes. Hence, much attention has been paid on the development and application of MMMs. Various inorganic materials, such as zeolite, silica carbon molecule sieve, and metal organic frameworks (MOFs), have been employed in the preparation of MMMs.

The silicoaluminophosphate-34 (SAPO-34) zeolite with 0.38 nm pore size and zeolitic imidazolate framework-8 (ZIF-8) particles with 0.34 nm aperture size are the promising filler candidate in the preparation of the MMMs, due to their pore size approaches the range of the sizes of the gas molecules. In this thesis, we had blended the SAPO-34 zeolite

and ZIF-8 particles into the polyethersulfone (PES) and polyimides (PI) to prepared the MMMs. The separation performance and mechanism of the MMMs had been investigated.

In Chapter 2, the mechanochemically synthesized ZIF-8 nanoparticles were blended in the 4,4'- (hexafluoroisopropylidene)diphthalic anhydride-2,4,6-trimethyl-1,3-phenylenediamine (6FDA-TrMPD) polyimide to prepare the MMMs. The reported ZIF-8 MMMs all used particles synthesized by solvothermal-synthesized method which requires organic solvents. Mechanochemically synthesis can avoid the use of organic solvent. The C_3H_6/C_3H_8 separation performance of the mechano-synthesized ZIF-8 MMM was similar to that of the conventional solvothermal-synthesized ZIF-8 MMM. This separation performance was in good agreement with the theoretical values predicted by using Maxwell model. Compared with the solvothermal synthesized ZIF-8, the mechanochemically synthesis method has some advantages including solvent-free, simple synthesis process, high yield, and large-scale production availability. These merits can be expected to promote the application of mechano-synthesized ZIF-8 in the membrane separation.

In Chapter 3, the commercialized SAPO-34 zeolite had been added to the PES membrane for the CO_2/CH_4 separation. It is not only confirmed that the diffusivity selectivity was essential to the ideal selectivity but also identified that the commercial SAPO-34 was better than the lab-made SAPO-34 sample. The performance of the MMMs in this study was also superior to that of the reported SAPO-34/PES MMMs in literature. The comparison with the reported MMMs and our MMMs reveals that it is possible to further improve the separation performance of the SAPO-34/PES MMMs.

In Chapter 4, the 6FDA-2,6-diaminotoluene (6FDA-mDAT) polyimide was selected as the polymer matrix to be blended with the SAPO-34 zeolite. Sieve-in-a-cages (defects)

appeared in the MMMs due to the poor compatibility of the zeolite particles and polymer matrix. The silane coupling reagent, *N*-phenylaminopropyltrimethoxysilane (PhAPTMS), was the first time applied to modify the surface of the SAPO-34 particles in order to improve the compatibility of the zeolite particles and 6FDA-mDAT matrix. When the filler content was 5 wt%, the PhAPTMS-modified SAPO-34 both increased the gas permeability and selectivity compared with the neat polymer membrane and the original SAPO-34 MMM. This was attributed to that the aminosilane enhanced the affinity of the filler particles with polymer matrix. When the filler content over 10 wt%, the separation performance of the PhAPTMS-modified SAPO-34 MMMs was lower than the original SAPO-34. This was due to the agglomeration of the PhAPTMS-modified filler in the MMMs. Therefore, the PhAPTMS was effective to enhance the separation performance of the SAPO-34/6FDA-mDAT MMMs when the filler content less than 10 wt% in this study.

Finally, Chapter 5 summarized the main contents and prospects of this thesis.

要　旨

膜分離は、水素精製、天然ガス精製、オレフィン/パラフィン分離など、ガス分離の有望な有効手段である。従来の分離プロセスと比較して、膜分離はエネルギーコストが低く、装置の設置面積が小さい。高分子膜は優れた加工性と高い再現性を備えている。一般に透過性の高い高分子膜は選択性が低い。したがって、高分子膜のガス分離特性は上限を示す。一方、無機膜は優れた分離特性と機械的安定性を示す。ただし、膜の製造コストは高い。無機粒子のブレンドにより、高分子膜の分離性能を改善して上限を超える高分子膜を作製する方法が注目されている。得られるハイブリッド膜は mixed matrix membranes（MMM）と呼ばれる。 MMM では、無機粒子は分散相（フィラー）であり、連続相（マトリックス）がポリマーである。無機粒子粉末とポリマーマトリックスを用いた MMM の製造コストは、無機膜よりも低いと予想される。したがって、MMM の開発と適用に多くの注目が集まっている。ゼオライト、シリカ、分子ふるい炭素、および有機金属フレームワーク（MOF）などのさまざまな無機材料が MMM の調製に検討されている。

0.38 nm の孔サイズのシリコアルミノホスフェート（SAPO-34）ゼオライトと 0.34 nm のアパーチャサイズのゼオライトイミダゾレートフレームワーク（ZIF-8）粒子は、ガス分子のサイズに近いため、MMM の調製における有望なフィラー候補である。この論文では、無機微粒子として SAPO-34 ゼオライトと ZIF-8 粒子を、マトリックスとしてポリエーテルスルホン（PES）とポリイミド（PI）に注目し、欠陥の無い MMM の作製法、分離性能、およびメカニズムを研究した。

第 2 章では、高分子膜に ZIF-8 をブレンドして C_3H_6 /C_3H_8 分離性能を向上させた MMM を研究した。環境負荷が小さく高収率で大量生産が可能なメカノケミカル法により合成された ZIF-8 ナノ粒子を MMM に初めて用いた。マトリックスには C_3H_6 /C_3H_8 分離に使える可能性のある数少ない高分子の一つである 4,4 '-（ヘキサフルオロイソプロピリデン）ジフタル酸無水物-2,4,6-トリメチル-1,3-フェニレンジアミン（6FDA-TrMPD）ポリイミドを用いた。微粒子の合成過程で生じる凝集をボールミルで粉砕する方法の採用が、マクスウェルモデルを使用して予測される理論値と一致する分離性能を持つ MMM の作製を可能にすることを明らかにした。この MMM の性能は従来のソルボサーマル合成された ZIF-8 を用いた MMM と同等であった。この成果は、多くのメリットを持つメカノケミカル法で合成できる MOF を用いる MMM の作製法に有益な情報を与えることが期待できる。

第 3 章では、SAPO-34 ゼオライトによる高分子膜の CO_2/CH_4 分離性能の向上を研究した。微粒子には市販品およびラボで合成したナノサイズのものを用いた。マトリックスとして PES 膜を用いた。２種類の微粒子を用いて作製した MMM の分離性能を拡散選択性と溶解度選択性に分けて検討した。どちらの MMM も拡散選択性が MMM の分離性の主要因子であることを確認した。市販の SAPO-34 を用いた MMM の方が優れた分離性能を示すことも確認した。微粒子に対する物理化学的考察から、市販の SAPO-34 はラボで合成した微粒子よりも CO_2/CH_4 分離性能の向上に適した結晶構造を持つことを明らかにした。ただ、どちらの MMM にも、微粒子表面とマトリックスとの間に Sieve-in-a-Cage と呼ばれる欠陥が部分的に残っていることも電子顕微鏡（SEM）による観察で分かった。本研究の成果は SAPO-34 を用いた MMM の微粒子の選択に有益な指針を与えると期待される。

第 4 章では、Sieve-in-a-cage と呼ばれる欠陥を完全に解消する方法として微粒子のシリル化を検討した。微粒子として SAPO-34 ゼオライトを用いた。マトリックスとして、高分子膜素材の中で最もガス分離性能が高いポリイミドの一つである 6FDA-2,6-ジアミノトルエン（6FDA-mDAT）ポリイミドを選択した。シランカップリング試薬である N-フェニルアミノプロピルトリメトキシシラン（PhAPTMS）は SAPO-34 粒子の表面修飾に初めて適用した。シリル化 SAPO-34 を 5wt%充填した MMM は、未修飾 SAPO-34 微粒子を用いた MMM よりも優れたガス透過性と選択性を示した。この膜の SEM 観察により Sieve-in-a-cage の欠陥は存在しないことが分かった。シリル化がフィラー粒子とポリマーマトリックスとの親和性を高めたためと考えられる。フィラー含有量が 10wt%を超える MMM でも界面状態は良好であった。この研究はシリル化が微粒子とマトリックスとの界面における欠陥を無くすことが可能であること、フェニル基を含むシリル化剤が効果的であることを明らかにした。しかし、10wt%を越える充填率の MMM の分離性能は未修飾 SAPO-34 を用いた MMM よりも低くなった。これは、MMM 内のシリル化フィラー同士の凝集によるものと考えられる。この凝集はシリル化フィラーと高分子溶液との混合およびその後の溶媒蒸発による製膜の過程で生じたと考えられる。高いフィラー含有率の MMM の作製には凝集を防ぐ方法の開発が不可欠であることが分かった。

最後に、第 5 章でこの論文の主な内容と展望を要約した。

Contents

Chapter 1 General Introduction

1.1 Gas Separation

Gas separation is an important process and be widely applied in the industrial production. Table 1-1 lists the major practical application of gas separation.

1.1.1 Purification of Natural Gas

The increasingly serious energy crisis and environmental pollution urgently require the development and utilization of clean energy source. It is necessary to search for potential energy alternatives [1]. Natural gas consists primarily of methane (CH_4) and some contaminating substances such as CO_2, hydrogen sulfide (H_2S), vapor and other higher alkane [2]. It produces less carbon dioxide (CO_2) when burned than other fossil fuels, result in a lower greenhouse effect, and thus can fundamentally improve environmental quality. Hence, natural gas is a clean, environmentally friendly, and high-quality energy source. However, the presence of contaminates especially acid gas would corrode the transport pipeline and reduce the heating value of natural gas. Hence, it is necessary to remove the acid gas and other impurities from natural gas.

Table 1-1 Major practical application of gas separation

Practical application	**Gas pairs**
Purification of natural gas	CO_2/CH_4, H_2S/CH_4, vapor/CH_4
Purification of hydrogen	H_2/CH_4, H_2/N_2, H_2/CO, H_2/H_2S
Separation of olefin/paraffin	C_2H_4/C_2H_6, C_3H_6/C_3H_8, C_4H_8/C_4H_{10}

1.1.2 Purification of Hydrogen

Hydrogen is one kind of the most promising energy sources because of its high energetic efficiency and zero carbon emission (the byprodcut is only water). Therefore, promoting the application of hydrogen energy not only reduces the energy crisis, but also helps to eliminate the greenhouse effect and environmental pollution. The current major method of hydrogen production is the steam reforming of light hydrocarbons methane and other fossil fuels [3]. The CH_4, CO, and H_2S are the major impurities in the production. In the downstream process of the hydrogen energy industrial production, the separation of H_2/CH_4 and other gas pairs contribute to breaking the chemical balance to obtain high quality of H_2 and enhance production efficiency.

1.1.3 Separation of Olefin/Paraffin

In the chemical and petroleum industries, light olefins including ethylene and propene play a vital role due to their wide use as raw materials for many products. Ethylene (C_2H_4) is the basic chemical raw material for synthetic ethanol (alcohol), synthetic fibers, synthetic rubber, synthetic plastics, and other petrochemical production [4]. In 2016, the worldwide production of ethylene was over 150 million tons [5]. This value exceeded that of any other organic compound. Propylene (C_3H_6) can be used to prepare important industrial products such as polypropylene, propylene oxide, isopropanol, phenol, and acetone. It is one of the important raw materials for the three major chemical materials. The world production of propene is currently about half that of ethylene [6].

The dominant technology for producing olefins is gasoline cracking or catalytic dehydrogenation of paraffins [7]. In this case, the actual production of olefins usually

contains the paraffin as the impurity. However, the similar physical and chemical properties of olefin and paraffin such as molecular size and boiling point, make their separation very difficult, especially the separation of C_2H_4/C_2H_6 and C_3H_8/C_3H_{10} [8].

1.2 Membrane Separation Technology

The major technologies for gas separation are absorption [9], adsorption [10], and distillation [11] and the membrane separation [12]. Compared to other technologies, the membrane separation has environmentally friendly (no extra chemicals/solvent addition), simple operation, low energy consumption, small footprint, sustainable production, and other advantages. Therefore, the membrane materials have been widely investigated in gas separation [13].

1.2.1 Milestones

A membrane is defined as a selective barrier that allows some substances (molecules, ions, or other small particles) to pass through but stops others. The background/milestone of the development of the membrane gas separation are shown in Figure 1-1 [14–16].

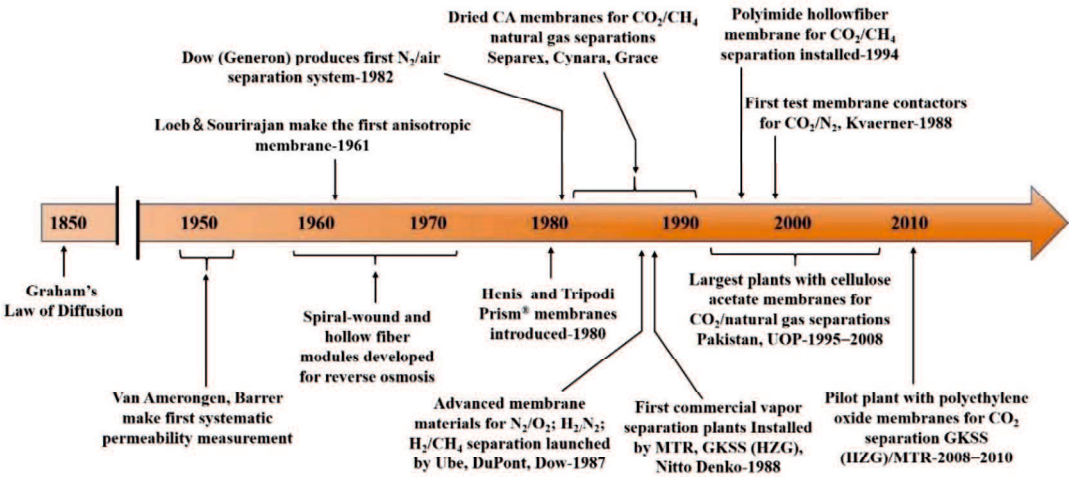

Figure 1-1. Milestone on the development of membrane gas separation [14–16].

The research of membrane science can be traced back two centuries. In 1831, John Kearsley Mitchell had investigated the gas diffusion through the wall of balloons which made of natural rubber [17]. This observation has been verified as the first scientific research on the membrane gas separation. In 1850, Thomas Graham, the father of membrane science, had studied the diffusion of gases and liquids through various media [18]. He discovered that the glue, gelatin, starch, and other certain substances passed through a barrier more slowly than inorganic salts and other substances, leading to establishing a distinction between the two types of particles made by the separating media or barrier. In 1855, Adolf Eugen Fick had studied the gas transport mechanism through the nitrocellulose membrane and then postulated the concept of diffusion, the "Fick's First Law" [19]. This law is a quantitative description of material transport through barriers. In 1866, Thomas Graham proposed the solution-diffusion model [20]. In 1980, Permea (Monsanto) company launched the first large industrial application of membrane-based separation that separating hydrogen from the purge gas stream of ammonia plants by using the Prism membrane [21]. Since then, the membrane gas separation technology has been developed rapidly [22].

Membranes are generally classified into three main categories based on the nature of the materials: polymeric membrane, inorganic membrane, and mixed matrix membranes.

1.2.2 Polymeric Membrane

The polymeric membrane is the first and also the most industrial applied membrane materials for gas separation. The polymeric membrane can be divided into the glassy and rubbery polymer membrane according to the glass transition temperatures (T_g) [23]. The values of *Tg* can be measured by differential scanning calorimetry (DSC) [24], as shown

in Figure 1-2. Table 1-2 lists the classification of the polymeric membranes [25–30].

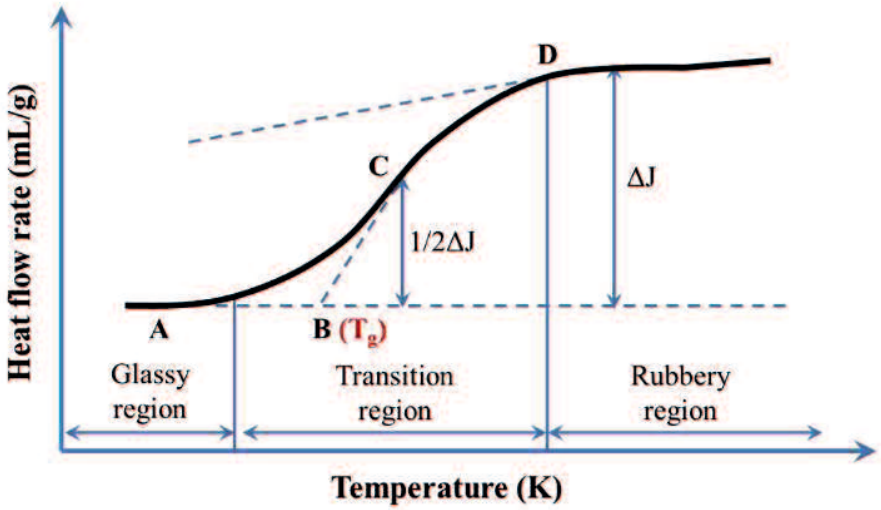

Figure 1-2. Glass transition temperature (T_g) of polymeric membrane measured by DSC analysis.

Table 1-2 List of polymeric membranes [25–30]

Type	Materials	Abbreviation	T_g (°C)
Glassy	Cellulose Acetate	CA	100–130
	Polycarbonate	PC	150
	Polyetherimide	PEI	217
	Polyethersulfone	PES	210–230
	Polyethylene terephthalate	PET	73–78
	Polyimide	PI	250–340
	Poly(p-phenylene oxide)	PPO	215
	Polyphenylene sulfide	PPS	88–93
Rubbery	Polyethylenes	PE	−125 to −130
	Poly(ethylene oxide)	PEO	−67
	Polycaprolactone	PCL	−60
	Polypropylenes (atactic)	PP	−20 to −5
	Polydimethyl siloxane	PDMS	−125
	Poly(vinyl acetate)	PVAc	25 −30
	Polyvinylidene Fluoride	PVDF	−42 to −25

Rubbery polymers have T_g below room temperature and usually contain flexible chains [31]. Glassy polymers have T_g above room temperature and possess rigid chains with restricted segmental motion [32]. In general, the glassy membranes possess relatively high gas selectivity and low gas permeability, whereas rubbery membranes show high gas permeability but low gas selectivity. In a word, high permeable polymer membranes have low selectivity and vice versa. Figure 1-3 shows that these gas separation properties of polymeric membranes are below an upper bound as illustrated by Robeson [33,34]. The commonly application of polymeric membrane is due to their excellent processability, high reproducibility, and other merits. However, the properties including the trade-off between gas permeability and selectivity, and easy aging and plasticization limit the promotion of application for the polymeric membranes.

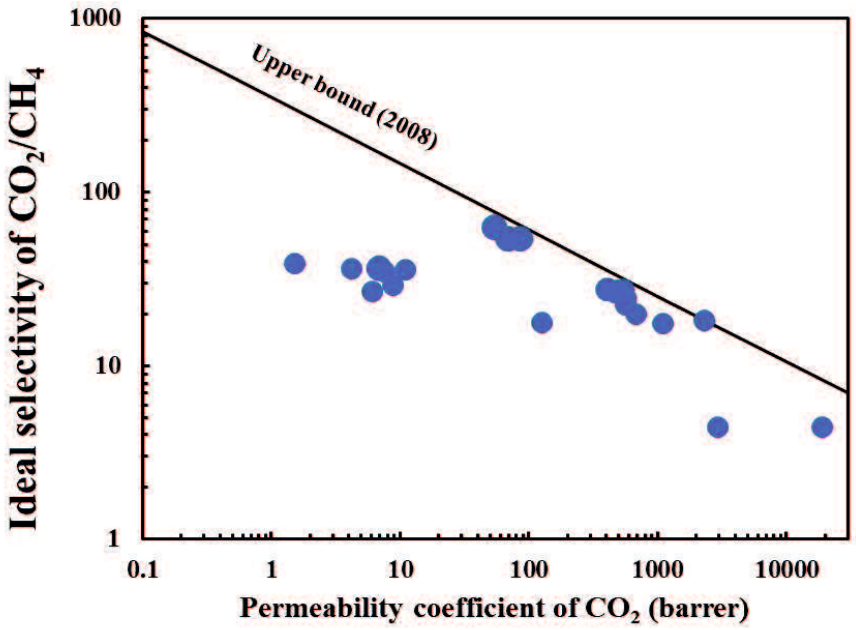

Figure 1-3. Robeson upper bound of polymeric membrane for CO_2/CH_4 separation [34].

1.2.3 Inorganic Membrane

Inorganic membranes can be classified into porous membrane and nonporous (dense) membrane based on the structure of the materials. The membrane made of zeolite [35], metal organic frameworks (MOFs) [36], porous silica [37], carbon and its derivatives [38] belong to porous membrane. The membrane made of nonporous silica [39], metal [40], metal oxide [41], and their derivatives membranes are assigned to the dense membrane [42]. Compared with the dense membranes, the porous membranes have been studied more because of the lower gas permeability and higher cost. The inorganic membranes have excellent separation property and mechanical stability and other advantages due to their orderly framework. Hence, the porous inorganic membranes have attracted a lot of interest in membrane gas separation. Herein, the zeolite membrane and MOFs membrane are introduced as follows.

1.2.3.1 Zeolite Membrane

The zeolite crystal has porous framework made of TO_4 units. The T presents the tetrahedral framework atoms including Si, Al, B, P, Fe, Ti and so on. Zeolite can be divided into two categories, pure silica zeolite and heteroatom zeolite. Heteroatom zeolites are considered to be formed by replacing silicon atoms in pure silicon zeolite with other atoms such as metals. The difference in number, size, charge and arrangement of heteroatoms produces different types of zeolite. Table 1-3 lists the framework types and pore size of the zeolite materials [43–46]. International Union of Pure and Applied Chemistry (IUPA) recommend that: (1) the microporous materials have pore diameters of less than 2 nm; (2) mesoporous materials have pore diameters between 2 nm and 50 nm

(3) macroporous materials have pore diameters of greater than 50 nm [47]. In this case, the zeolites belong to the microporous materials.

Table 1-3 Major structures of zeolite/zeolite membrane [43–46]

Structure	Example	Pore size (nm)
AEI	AlPO-18, SAPO-18	0.38×0.38
CHA	SAPO-34, SSZ-13	0.38×0.38
DDR	ZSM-58, DD3R	0.36×0.44
ERI	T, AlPO-17	0.36×0.51
FAU	NaX, NaY	0.74×0.74
LTA	NaA, ITQ-19	0.41×0.41
MFI	Silicalite-1, TS-1, ZSM-5	0.51×0.53
RHO	Rho, LZ-214	0.36×0.36

The zeolite membranes are formed by loading the zeolite crystals on the support by *in-situ* growth, secondary hydrothermal synthesis and other method. The first zeolite membrane was reported by Suzuki in 1987 [48]. Since then, the development and application of the zeolite membrane has been widely investigated. The types and quality of the zeolite membrane has been improved. Due to the pore size of zeolite crystal close to the diameter of gas molecules, the zeolite membrane is a promising candidate for the gas separation. Currently, the gas-separation available zeolite membrane includes MFI [49], LTA [50], CHA [51], FAU [52], AEI [53], RHO [54], ERI [55], and DDR[56] and so on [35].

1.2.3.2 MOFs Membrane

Metal-organic frameworks (MOFs) are a class of compounds consisting of metal ions

or clusters coordinated to organic ligands to form one dimensional (1D), 2D or 3D structures [57,58]. Since the MOFs was first reported by O.M. Yaghi and his research group in 1999 [59], there are more than 20000 MOFs including zeolitic imidazole frameworks (ZIFs) [60], MIL-101 [61], UiO-66 [62] and NU-110 [63] have been synthesized and studied [57]. They have fixed pore sizes that show potential for excellent size-sieving ability depending on the pore aperture and the molecular diameter of the gases to be separated. Due to this property, MOFs are of interest for the storage of gases such as hydrogen and carbon dioxide.

1.2.4 Mixed Matrix Membranes

The application of polymeric membrane is limited by the trade-off between gas permeability and selectivity. Inorganic membranes have high cost (expensive support) and poor processability and other disadvantages. Recently years, the researchers have blended the porous inorganic particles to the polymer to prepare a novel membrane material, so-called mixed matrix membranes (MMMs, as shown in Figure 1-4) [64–66].

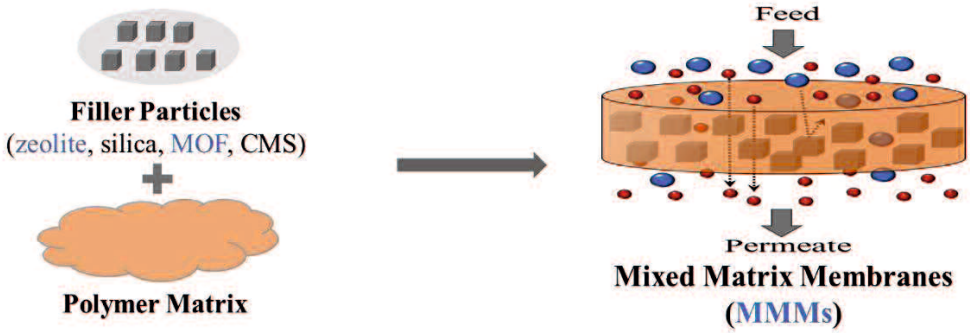

Figure 1-4. Mixed matrix membranes (MMMs) composited of inorganic filler and polymer matrix.

The preparation cost of MMMs with inorganic particle powder and polymer matrix is expected to be lower than that of inorganic membranes. The porosity framework of the

filler promotes the separation performance of the polymeric membrane. Hence, the MMMs can combine the both merits of the polymeric membrane and inorganic membrane. Therefore, much attention has been paid on the development and application of MMMs.

Normally, the inorganic particles act as the dispersion phase (filler) and the polymer as the continuous phase (matrix). Most of researchers focus on the choice of the filler for the preparation of MMMs. Owing to their uniform porosity and excellent thermal, mechanical, and chemical stability, the zeolites are widely investigated in the MMMs. The first investigation of the gas separation using the MMMs was LTA/PDMS for CO_2/CH_4 separation as reported by Paul and Kemp in 1973 [67]. They discovered the addition of the zeolite had greatly affected the diffusion time-lag of the polymeric membrane and minor influenced the steady steady-state permeation. MOFs have adaptable chemical properties and porosities. Especially, interaction of the linker with polymer chains enhance the affinity of MOFs and polymer. Carbon, silica and others substances, have also been blended the polymer matrix to prepare the MMMs for the gas separation [68].

1.3 Separation Mechanism

Membrane gas separation is based on the difference in the permeation of the gas molecules driven by the pressure gradient imposed between upstream and downstream streams. Except the pressure, the permeation of membrane also varies from the temperature, flow rate, and membrane area. This leads to the difference in the selective performance of the membrane. The permeability of different gases components was calculated as the permeate flux through the effective area of the membrane under its partial pressure. And the selectivity was calculated by the ratio of the permeance with different components. According to the pore

sizes in membrane materials, the gas transport process is described by four kinds of mechanism: Convective/Poiseuille Flow [69], Knudsen Diffusion [70], Molecular Sieving [71], and Solution-Diffusion [72]. These four mechanisms were expressed by in Figure 1-5. The detailed explanation as follows.

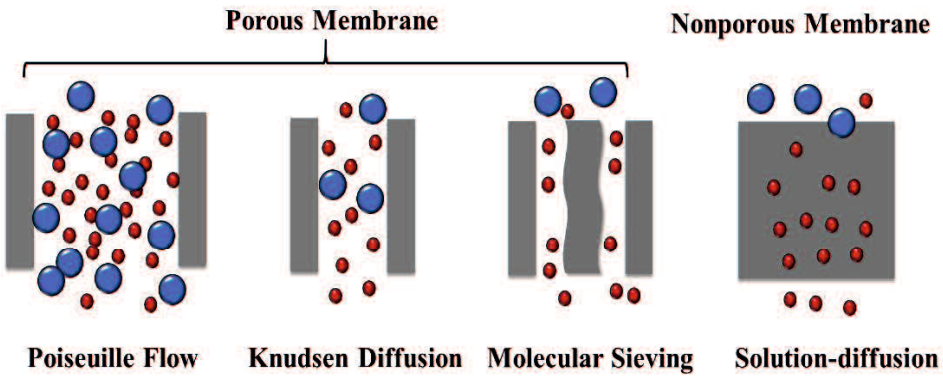

Figure 1-5. Gas separation mechanism using membrane.

1.3.1 Convective Flow

The Convective Flow occurs if the porous membranes have the relatively large pore (> 100 nm) [69]. This value is much bigger than the diameter of the gas molecules. There are no separations when the gas molecules in the presence of this mechanism.

1.3.2 Knudsen Diffusion

When the pore sizes of the porous membrane materials are in a range of 5–100 nm and less than the mean free path of the gas molecules, the gas separation behavior is described by Knudsen Diffusion [70]. This separation is based on the difference between these two gases molecular weights which is proportional to the inverse square root ratio of the molecular weights. Gas molecules interact with the pore walls much more frequently than with one another and allow lighter molecules to preferentially diffuse through pores to

achieve separation. Due to the gas permeate through the membrane almost independent of one another, the Knudsen diffusion coefficient is independent of pressure. Table 1-4 lists the Knudsen diffusion selectivity varies from different gas pairs [73–76].

Table 1-4 Gas properties and Knudsen diffusion selectivity [73–76].

Gas	Molecular weight	Kinetic diameter(Å)	Gas pairs	Knudsen selectivity
He	4	2.60	H_2/O_2	4.00
H_2	2	2.89	H_2/N_2	3.74
O_2	32	3.46	H_2/CO_2	4.69
N_2	28	3.64	H_2/CH_4	2.83
CO_2	44	3.30	CO_2/N_2	0.80
CH_4	16	3.80	CO_2/CH_4	0.60
n-C_4H_{10}	58	4.69	N_2/CH_4	0.76
i-C_4H_{10}	58	5.28	O_2/N_2	0.94
SF_6	146	5.50		

1.3.3 Molecular Sieving

The gas separation mechanism will be expressed by Molecular Sieving when the pore size of the membrane materials less than 0.7 nm [71]. Due to the high productivity and selectivity, molecular sieving membranes become increasingly important in gas separation especially for inorganic membranes. The gas separation through the zeolite and MOFs belongs to this type.

1.3.4 Solution and Diffusion

The difference from the other three is that Solution and Diffusion occurs in non-porous membranes includes polymeric membrane [72]. It is considered that the gas molecules from the upstream gas phase first adsorb into the nonporous membrane, then diffuse across it and finally desorb into the downstream gas phase side. The gas separation mechanism in polymer membrane can be expressed by the Solution-Diffusion model.

Figure 1-6 detail shows the comparison of the Molecular Sieving and Solution-Diffusion which are the commonly used model of porous inorganic membrane and polymer membrane.

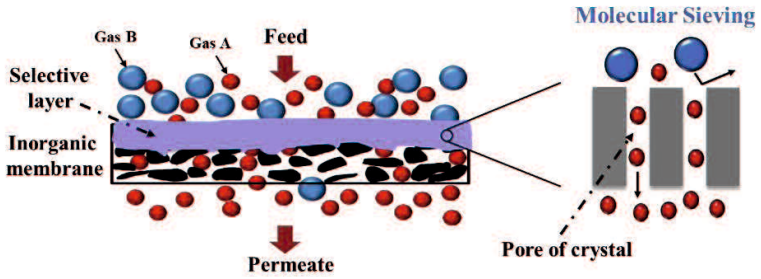

Porous inorganic membrane separation

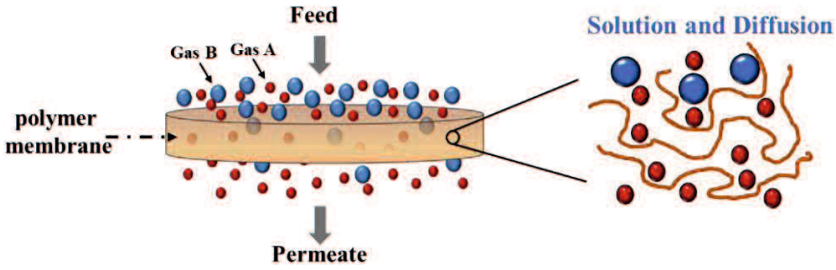

Polymeric membrane separation

Figure 1-6. Representative molecular sieving and solution-diffusion process.

The gas transportation is complicated for the practical application which may combine of the above mechanisms. Nevertheless, the permeability (P) used to express the capability of a membrane to permeate gas is common method [76,77].

$$P = D \times S \tag{1-1}$$

$$\alpha P = \frac{P_i}{P_j} \tag{1-2}$$

$$\alpha D = \frac{D_i}{D_j} \tag{1-3}$$

$$\alpha S = \frac{S_i}{S_j} \tag{1-4}$$

Permeability is controlled by the gas the diffusivity (D) and solubility (S), as expressed by the equation (1-1). The gas selectivity (αP), diffusion selectivity (αD), and solution selectivity (αS) of gas i to gas j is the ratio of their P, D and S, respectively [77–79].

1.4 Challenge in Mixed Matrix Membranes

The MMMs prepared by incorporating inorganic fillers into the polymer matrix combines the merits of each material and provides superior gas separation performance. However, the ideal structure of the MMMs always not be successful fabricated due to the difference in the nature of the inorganic filler and polymeric matrix. Some defects or unexpected phenomenon such as sieve-in-a-cages, agglomeration, rigidification, may occurred in preparation of the MMMs, as shown in Figure 1-7.

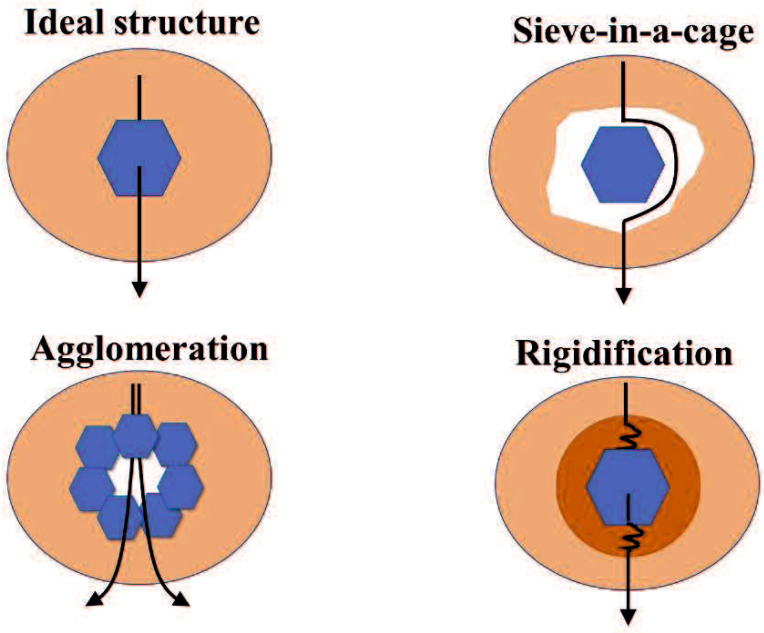

Figure 1-7. Schematic diagram of ideal structure, sieve-in-a-cage, agglomeration and rigidification. Yellow circle, blue hexagon and black arrow presents the polymer matrix, inorganic particles and the gas transmission, respectively.

1.4.1 Sieve-in-a-cage

Figure 1-7 shows the schematic diagram of the sieve-in-a-cage (voids). This structure appeared in the 4A/Matrimid membrane was first reported by W.J. Koros in 2002 [80]. The presence of the sieve-in-a-cage is due to the poor compatibility of the zeolite particles and polymer matrix. The void space between the two phases allows the gas molecules to pass through, and then result in a low ideal selectivity. In general, the backbone of polymer chain is more rigid, the sieve-in-a-cage is more possible appears. Matrimid is one kind of polyimide and has T_g over 200 °C, as shown in Table 1-2. The PVAc is a rubbery polymer that has lower T_g and flexible structure than the glassy polymer. This is why the sieve-in-cage didn't appear in the 4A/PVAc MMMs.

1.4.2 Agglomeration

The porous particles with large surface area are welcome to the gas separation of MMMs. However, the agglomeration is always unavoidable for particles in the preparation of MMMs. S.T. Oyama et al. found that the SAPO-34 zeolite microparticles were agglomerated in the PEI based membrane when the filler content over 10 wt% [81]. In this case, the molecular sieving effect of the SAPO-34 zeolite cannot be completely utilized. Another negative influence is that the intergranular spaces between particles in the agglomerates allow the gas molecules to pass through, and then result in a low ideal selectivity.

1.4.3 Rigidification

The rigidification of the polymer is caused by effective polymer-filler interactions [82].

After incorporation, the polymer chains may penetrate into the pores of fillers. Hence, this phenomenon usually occurred near the surface of the filler particles. Rigidification reduce the mobility of polymer chain. The additional negative effect of this is to block the pores of the filler. In this case, the gas permeability is decreased and the selectivity increased. This contrast to the effect of sieve-in-a-cage. Normally, the blockage of the zeolite pore simultaneously occurs with rigidification of the polymer chains which will harm the gas permeability.

1.4.4 Improving Methods

In order to fabricate a high quality of membrane without defect, the priming [83], ion-liquids (ILs) modification [84], amine functionalization [85], silane coupling reaction [86], cross-linking [87], mechanical treatment of filler [88], and other methods [89,90] have been used to promote the compatibility of the filler particles and polymeric matrix. Herein, the priming, amine functionalization, silane coupling reaction and mechanical treatment are described in details as follows.

In 2000, W.J. Koros introduced the priming that mixing a small amount of polymer with filler particles in the solvent to form a thin polymer layer on the surface of filler following by addition of the residual polymer [91]. The residual polymer was then added into the slurry of the coated filler and solvent before the preparation of the MMMs. The priming leads to a better dispersion of the filler particles and no contact between bare zeolite surfaces. Hence, the priming can be used to improve the sieve-in-a-cage as well as the agglomeration. In this process, not only the interaction of polymer-filler but also to interactions of the polymer and filler with the solvent was required for attention.

Since 2010, Halil Kalipcilar et al. have applied the amine reagents, including 2-

hydroxy-5-methyl aniline (HMA), ethylenediamine (EDA) and hexylamine (HA), to modify the SAPO-34 zeolite [92,93]. The functionalized zeolite particles provided a better wettability with PES matrix compared with the original filler. Thus, the CO_2/CH_4 separation performance had been enhanced.

Silane coupling agents consists of both the inorganic and organic functional groups such as methoxy, or ethoxy, and amino [90]. The general formula of $R_n–Si–X_{4n}$ (R: the functional organic group, X: an easily hydrolysable group such as methoxy, ethoxy or acetoxy. The amino-organosilane is commonly used to functionalize inorganic fillers, including 3-aminopropyltrimethoxysilane (APTMS) [86], 3-aminopropyltriethoxysilane (APTES) [96] and 3-aminopropyldimethylethoxysilane (APDMES) [97] and 3-aminopropyldiethoxymethylsilane (APDEMS) [98]. The hydrolyzed to silanols, $R_n–Si–(OH)_{4-n}$, they react with hydroxyl groups on the zeolite surface and amino groups or other functional groups in the polymer matrix to enhance the compatibility between the phase boundaries [90]. The mechanism of silane coupling with zeolite is shown in Figure 1-8. The methoxy group of the aminosilane can react with the silanol which locates on the surface of zeolite particles.

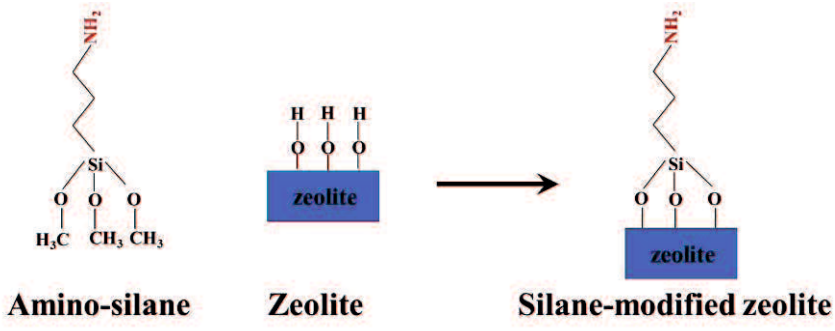

Figure 1-8. Surface modification of zeolite using silane reagent [94–98].

The first study of silane modification on the zeolite is that S.W. Kim et al. had used the

APTES to increase the hydrophobic property of the natural zeolite [94]. Asghari et al. had used APTMS to modify the FAU zeolite for enhancing the CO_2/CH_4 separation performance of the poly (ether-block-amide) (PEBA) membrane [99]. Masoud Aghajani et al. had blended the APTES modified ZIF-8 in PEBA for CO_2/CH_4 separation [100]. Chung et al. had applied the APDEMS o increase the content of 4A zeolite in the PVAc membrane up to 40 wt% [95].

Unlike the above two methods involving chemical reactions, mechanical treatment such as ball milling (Figure 1-9) and ultrasonic belongs to physical process. These methods are majorly applied to improve the dispersion of filler particles.

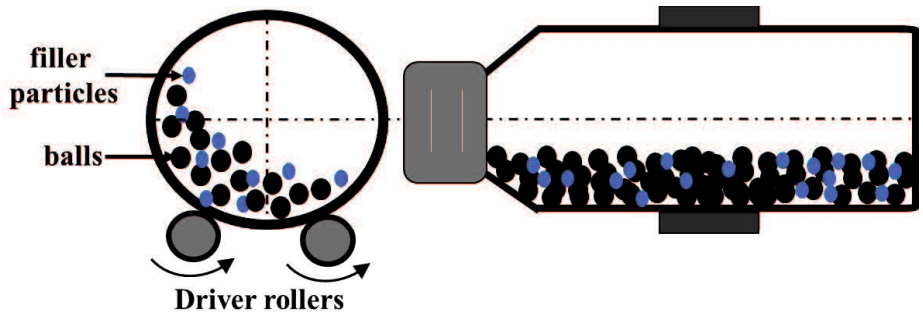

Figure 1-9. Ball mill process: colored balls and black balls present the sample and grand medium.

Z.H. Zhu et al. had used ball milling to disperse the Cd-6F, one kind of MOFs, in the 6FDA-ODA polyimide for CO_2/N_2 separation [101]. J.A. Thompson et al. had reported that sonication-induced Ostwald ripening of ZIF-8 nanoparticles and formation of ZIF-8/Matrimid composite membranes [102]. The sonication made significant difference on the shape, size distribution and structure of ZIF-8 particles suspended in an organic solvent during the preparation of the membrane. The membrane prepared by high-intensity sonication provided an obvious enhancement in the CO_2 permeability and CO_2/CH_4 selectivity.

1.5 Research Objectives

As described in the above introduction, the zeolite and MOFs have a promising potential for separation performance using the MMMs. The ZIF-8 has flexible structure with effective pore size in a range of 0.4–0.42 nm which between the molecular diameter of C_3H_6 (0.40 nm) and C_3H_8 (0.42 nm) [103,104]. The SAPO-34 zeolite has pore size of 0.38 nm which is suit for the separation of CO_2 and CH_4, due to their molecular diameter are 0.33 nm and 0.38 nm, respectively [105,106] . Therefore, there are some research on the ZIF-8 MMMs for the C_3H_6/C_3H_8 separation and SAPO-34 MMMs for the CO_2/CH_4 separation. These were the research objects in this thesis. The overview of this thesis is as follows.

The general introduction as described in Chapter 1. This chapter provided the information of the significance of the membrane-based gas separation, the separation mechanism, and the merits of the mixed matrix membranes as well as the challenges/problem in the preparation of the MMMs.

I first focused on the enhancement of C_3H_6/C_3H_8 selectivity by blending mechanochemically synthesized ZIF-8 into a polymer membrane in Chapter 2. The ZIF-8 in the reported MMMs were all using the solvothermal synthesis method, which requires organic solvent such as methanol and *N*,*N*-dimethylformamide [107]. These solvents are toxic and can result in environmental contamination and human health problems [108]. In a previous research, the ZIF-8 can be synthesized by a solvent-free mechanochemically method [109]. Besides, this method provided other advantages, including simple synthesis process, high yield, and large-scale production availability. In this case, the preparation and separation performance of the MMMs using

mechanochemically synthesized ZIF-8 was worth to be investigated. In order to analysis the effect of mechano-synthesized ZIF-8, temperature and pressure dependence of the gas permeability and ideal selectivity also had been investigated.

The influence of the commercial SAPO-34 on the gas permeability and selectivity of the PES MMMs had been investigated in Chapter 3. Some researchers had studied the SAPO-34/PES MMMs for CO_2/CH_4 separation [84,85,92,93]. They reported the gas permeability and selectivity of the membrane using lab-made and commercial SAPO-34 zeolite, except for a detailed discussion on the gas diffusivity and solubility. We had reported the effect of the lab-made SAPO-34 zeolite on the CO_2 and CH_4 diffusivity and solubility had been investigated as well as their permeability and ideal selectivity [110]. In terms of the general applicability and synthesis cost, the commercial zeolite is more promising than the lab-made zeolite. In this study, we tried to make a comparison of the influence of the commercial and the lab-made SAPO-34 zeolite on the CO_2 and CH_4 diffusivity and solubility of the PES membrane as well as the gas permeability and ideal selectivity.

The sieve-in-a-cage (defect) in the zeolite filled MMMs can be improved by using silane coupling reagent. However, one of the most common-used silanes, 3-aminopropyltrimethoxysilane (APTMS), would block the pore of zeolite to reduce the gas permeability [99,111,112]. Herein, I have first tried to apply a novel aminosilane, *N*-phenylaminopropyltrimethoxysilane (PhAPTMS) instead of the APTMS to modify the zeolite MMMs. The presence of the benzene-ring can prevent the PhAPTMS block the zeolite pore. The *N*-phenyl trimethoxysilane (PhTMS) which contains benzene-ring and no amino group was used as a reference. The influence of these different silane on the

morphology and separation performance of the MMMs composited of SAPO-34 zeolite and 6FDA-mDAT polyimide had been investigated in Chapter 4.

The results of Chapter 2, Chapter 3 and Chapter 4 are summarized in Chapter 5. The prospects of this study are also described in this chapter.

1.6 References

[1] H. Bahrampour, A.K. Beheshti Marnani, M.B. Askari, M.R. Bahrampour, Evaluation of renewable energies production potential in the Middle East: Confronting the world's energy crisis, Front. Energy. 14 (2020) 42–56.

[2] B. Shimekit, H. Mukhtar, Natural gas purification technologies–Major Advances for CO_2 separation and future directions, Adv. Nat. Gas Technol. ISBN 978-953-51-0507-7, Chapter 9 (2012) 235–270.

[3] N.W. Ockwig, T.M. Nenoff, Membranes for hydrogen separation, Chem. Rev. 107 (2007) 4078–4110.

[4] J. Hou, P. Liu, M. Jiang, L. Yu, L. Li, Z. Tang, Olefin/paraffin separation through membranes: From mechanisms to critical materials, J. Mater. Chem. A. 7 (2019) 23489–23511.

[5] I. Amghizar, L.A. Vandewalle, K.M. Van Geem, G.B. Marin, New Trends in Olefin Production, Engineering. 3 (2017) 171–178.

[6] A. Farshi, F. Shaiyegh, S.H. Burogerdi, A. Dehgan, FCC process role in propylene demands, Pet. Sci. Technol. 29 (2011) 875–885.

[7] J.J.H.B. Sattler, J. Ruiz-Martinez, E. Santillan-Jimenez, B.M. Weckhuysen, Catalytic dehydrogenation of light alkanes on metals and metal oxides, Chem. Rev. 114 (2014) 10613–10653.

[8] Z. Zhang, K.R. Yang, X. Xu, Understanding the separation mechanism of C_2H_6/C_2H_4 on zeolitic imidazolate framework ZIF-7 by periodic DFT investigations, J. Phys. Chem. C. 124 (2020) 256–266.

[9] C.A. Scholes, C.J. Anderson, G.W. Stevens, S.E. Kentish, Membrane gas

separation physical solvent absorption combined plant simulations for pre-combustion capture, Energy Procedia. 37 (2013) 1039–1049.

[10] P. Pullumbi, F. Brandani, S. Brandani, Gas separation by adsorption: technological drivers and opportunities for improvement, Curr. Opin. Chem. Eng. 24 (2019) 131–142.

[11] X. Li, J. Li, B. Yang, Design and control of the cryogenic distillation process for purification of synthetic natural gas from methanation of coke oven gas, Ind. Eng. Chem. Res. 53 (2014) 19583–19593.

[12] G.Q. Lu, J.C. Diniz da Costa, M. Duke, S. Giessler, R. Socolow, R.H. Williams, T. Kreutz, Inorganic membranes for hydrogen production and purification: A critical review and perspective, J. Colloid Interface Sci. 314 (2007) 589–603.

[13] C. Castel, E. Favre, Membrane separations and energy efficiency, J. Memb. Sci. 548 (2018) 345–357.

[14] R.W. Baker, Future directions of membrane gas separation technology, Ind. Eng. Chem. Res. 41 (2002) 1393–1411.

[15] P. Bernardo, G. Clarizia, 30 Years of membrane technology for gas separation, Chem. Eng. Trans. 32 (2013) 1999–2004.

[16] X.H. Ma, S.Y. Yang, Polyimide gas separation membranes, Adv. Polyimide Mater., Chapter 6 (2018) 257–322.

[17] J.K. Mitchell, On the penetrativeness of fluids, J. Memb. Sci. 100 (1995) 11–16.

[18] T. Graham, On the Law of the diffusion of gases, J. Memb. Sci. 100 (1995) 17–21.

[19] A. Fick, Ueber Diffusion, Annalen der Physik, 94 (1851) 58–86.

[20] T. Graham, On the absorption and dialytic separation of gases by colloid septa, J. Memb. Sci. 100 (1995) 21–31.

[21] D. Pont, Nas Report Doubles Estimates of Ozone Loss, Chem. Eng. News. 57 (1979) 6.

[22] R.W. Baker, B.T. Low, Gas separation membrane materials: A perspective, Macromolecules. 47 (2014) 6999–7013.

[23] J.L. Keddie, R.A.L. Jones, R.A. Cory, Size-dependent depression of the glass transition temperature in polymer films, Europhys Lett. 27 (1994) 59–64.

[24] A. Mushtaq, H. Bin Mukhtar, A.M. Shariff, Effect of Glass Transition Temperature in Enhanced Polymeric Blend Membranes, Procedia Eng. 148 (2016) 11–17.

[25] O.H. Fred-Ahmadu, G. Bhagwat, I. Oluyoye, N.U. Benson, O.O. Ayejuyo, T. Palanisami, Interaction of chemical contaminants with microplastics: Principles and perspectives, Sci. Total Environ. 706 (2020) 135978.

[26] C.L. Beyler, M.M. Hirschler, Thermal Decomposition of Polymers, Chem. Mater. 23 (2011) 3495–3508.

[27] A. Afantitis, G. Melagraki, K. Makridima, A. Alexandridis, H. Sarimveis, O. Iglessi-Markopoulou, Prediction of high weight polymers glass transition temperature using RBF neural networks, J. Mol. Struct. ThemoChem. 716 (2005) 193–198.

[28] R.O. Corrêa, A.S. Telles, J.E. Ourique, A graph-structural method for prediction of polymer properties, Brazilian J. Chem. Eng. 21 (2004) 621–628.

[29] H.T.H. Nguyen, P. Qi, M. Rostagno, A. Feteha, S.A. Miller, The quest for high glass transition temperature bioplastics, J. Mater. Chem. A. 6 (2018) 9298–9331.

[30] J. Liu, H. Ni, Z. Wang, S. Yang, W. Zhou, Colorless and transparent high – temperature-resistant polymer optical films–Current status and potential applications in optoelectronic fabrications, Optoelectron. –Mater. Devices.

Chapter 3 (2015) 57-81.

[31] P.J. Ludovice, Structure-property relationships–rubbery polymers, Mechanical Properties and Testing of Polymers, ISBN 978-94-01509231-4 (1999) 238–241.

[32] E.F. Oleinik, Glassy polymers as matrices for advanced composites, Polym. J. 19 (1987) 105–117.

[33] L.M. Robeson, Correlation of separation factor versus permeability for polymeric membranes, J. Memb. Sci. 62 (1991) 165–185.

[34] L.M. Robeson, The upper bound revisited, J. Memb. Sci. 320 (2008) 390–400.

[35] N. Kosinov, J. Gascon, F. Kapteijn, E.J.M. Hensen, Recent developments in zeolite membranes for gas separation, J. Memb. Sci. 499 (2016) 65–79.

[36] Q. Qian, P.A. Asinger, M.J. Lee, G. Han, K. Mizrahi Rodriguez, S. Lin, F.M. Benedetti, A.X. Wu, W.S. Chi, Z.P. Smith, MOF-based membranes for gas separations, Chem. Rev. 120 (2020) 8161–8266.

[37] M.A. Pizzoccaro-Zilamy, C. Huiskes, E.G. Keim, S.N. Sluijter, H. Van Veen, A. Nijmeijer, L. Winnubst, M.W.J. Luiten-Olieman, New generation of mesoporous silica membranes prepared by a Stöber-Solution pore-growth approach, ACS Appl. Mater. Interfaces. 11 (2019) 18528–18539.

[38] T. Koga, H. Kita, K. Uemura, K. Tanaka, I. Kawafune, M. Funaoka, Structure and separation performance of carbon membranes from lignin-based materials, Trans. Mater. Res. Soc. Japan. 34 (2009) 371–374.

[39] S.T. Oyama, D. Lee, P. Hacarlioglu, R.F. Saraf, Theory of hydrogen permeability in nonporous silica membranes, J. Memb. Sci. 244 (2004) 45–53.

[40] S. Uemiya, State-of-the-art of supported metal membranes for gas separation, Sep. Purif. Methods. 28 (1999) 51–85.

[41] A. Darmawan, J. Motuzas, S. Smart, A. Julbe, J.C. Diniz da Costa, Binary iron cobalt oxide silica membrane for gas separation, J. Memb. Sci. 474 (2015) 32–38.

[42] S.P. Cardoso, I.S. Azenha, Z. Lin, I. Portugal, A.E. Rodrigues, C.M. Silva, Inorganic membranes for hydrogen separation, Sep. Purif. Rev. 47 (2018) 229–266.

[43] J.D.F. Ramsay, S. Kallus, Zeolite membranes, Elsevier Masson SAS, 2000.

[44] A. Tavolaro, E. Drioli, Zeolite membranes, Adv. Mater. 11 (1999) 975–996.

[45] C. Feng, K.C. Khulbe, T. Matsuura, R. Farnood, A.F. Ismail, Recent progress in zeolite/zeotype membranes, J. Membr. Sci. Res. 1 (2015) 49–72.

[46] M. Pera-Titus, Porous inorganic membranes for CO_2 capture: Present and prospects, Chem. Rev. 114 (2014) 1413–1492.

[47] K.K.U. J. Rouquerol, D. Avnir, C.W. Faibridge, D.H. Everetit, J.H. HAaynes, N. PEernicone, J.D.F. Ramsay, K.S.W. Sing, Recommendations for the characterization of porous solids, Pure Appl. Chem, 66 (1994) 1739–1758.

[48] H. Suzuki, Composite membrane having a surface layer of an ultrathin film of cage-sharped zeolite and process for production thereof, United States Patent, UP4699892 (1987).

[49] J. Lindmark, J. Hedlund, Carbon dioxide removal from synthesis gas using MFI membranes, J. Memb. Sci. 360 (2010) 284–291.

[50] H. Li, C. Qiu, S. Ren, Q. Dong, S. Zhang, F. Zhou, X. Liang, J. Wang, S. Li, M. Yu, Na+-gated water-conducting nanochannels for boosting CO_2 conversion to liquid fuels, Science, 367 (2020) 667–671.

[51] B. Liu, R. Zhou, K. Yogo, H. Kita, Preparation of CHA zeolite (chabazite) crystals and membranes without organic structural directing agents for CO_2 separation, J.

Memb. Sci. 573 (2019) 333–343.

[52] X. Gu, J. Dong, T.M. Nenoff, Synthesis of defect-free FAU-type zeolite membranes and separation for dry and moist CO_2/N_2 mixtures, Ind. Eng. Chem. Res. 44 (2005) 937–944.

[53] T. Zhan, T. Wu, Y. Shi, X. Chen, Y. Li, M. Zhu, F. Zhang, I. Kumakiri, X. Chen, H. Kita, Influence of synthesis parameters on preparation of AlPO-18 membranes by single DIPEA for CO_2/CH_4 separation, J. Memb. Sci. 601 (2020) 117853.

[54] B. Liu, I. Kumakiri, K. Tanaka, X. Chen, H. Kita, Preparation of Rho zeolite membranes on tubular supports, membrane, MEMBRANE. 41 (2016) 81–86.

[55] Y. Cui, H. Kita, K.I. Okamoto, Preparation and gas separation performance of zeolite T membrane, J. Mater. Chem. (2004) 924–932.

[56] J. Okazaki, H. Hasegawa, N. Chikamatsu, K. Yajima, K. Shimizu, M. Niino, DDR-type zeolite membrane: A novel CO_2 separation technology for enhanced oil recovery, Sep. Purif. Technol. 218 (2019) 200–205.

[57] H. Furukawa, K.E. Cordova, M. O'Keeffe, O.M. Yaghi, The chemistry and applications of metal-organic frameworks, Science. 341 (2013) 1230444.

[58] N. Stock, S. Biswas, Synthesis of metal-organic frameworks (MOFs): Routes to various MOF topologies, morphologies, and composites, Chem. Rev. 112 (2012) 933–969.

[59] Design and synthesis of an exceptionally stable and highly, Nature. 402 (1999) 276–279.

[60] J.C. Tan, T.D. Bennett, A.K. Cheetham, Chemical structure, network topology, and porosity effects on the mechanical properties of zeolitic imidazolate frameworks, Proc. Natl. Acad. Sci. U. S. A. 107 (2010) 9938–9943.

[61] S. Bhattacharjee, C. Chen, W.S. Ahn, Chromium terephthalate metal-organic framework MIL-101: Synthesis, functionalization, and applications for adsorption and catalysis, RSC Adv. 4 (2014) 52500–52525.

[62] M. Nasrabadi, M.A. Ghasemzadeh, M.R.Z. Monfared, The preparation and characterization of UiO-66 metal-organic frameworks for the delivery of the drug ciprofloxacin and an evaluation of their antibacterial activities, New J. Chem. 43 (2019) 16033–16040.

[63] O.K. Farha, I. Eryazici, N.C. Jeong, B.G. Hauser, C.E. Wilmer, A.A. Sarjeant, R.Q. Snurr, S.T. Nguyen, A.Ö. Yazaydin, J.T. Hupp, Metal-organic framework materials with ultrahigh surface areas: Is the sky the limit?, J. Am. Chem. Soc. 134 (2012) 15016–15021.

[64] T.S. Chung, L.Y. Jiang, Y. Li, S. Kulprathipanja, Mixed matrix membranes (MMMs) comprising organic polymers with dispersed inorganic fillers for gas separation, Prog. Polym. Sci. 32 (2007) 483–507.

[65] B. Shimekit, H. Mukhtar, T. Murugesan, Prediction of the relative permeability of gases in mixed matrix membranes, J. Memb. Sci. 373 (2011) 152–159.

[66] H. Vinh-Thang, S. Kaliaguine, Predictive models for mixed-matrix membrane performance: A review, Chem. Rev. 113 (2013) 4980–5028.

[67] D.R. Paul, D.R. Kemp, The diffusion time lag in polymer membranes containing adsorptivellers, J. Polym. Sci. Polym. Symp. 41 (1973) 79–93.

[68] M. Galizia, W.S. Chi, Z.P. Smith, T.C. Merkel, R.W. Baker, B.D. Freeman, 50th Anniversary perspective: Polymers and mixed matrix membranes for gas and vapor separation: A review and prospective opportunities, macromolecules. 50 (2017) 7809–7843.

[69] V. V. Ugrozov, A. V. Volkov, The Effects of the viscous flow of a gas and the porous structure of a support on the permeability of a composite membrane, Colloid J. 82 (2020) 597–603.

[70] J. Gilron, A. Soffer, Knudsen diffusion in microporous carbon membranes with molecular sieving character, J. Memb. Sci. 209 (2002) 339–352.

[71] M. Jia, K.V. Peinemann, R.D. Behling, Molecular sieving effect of the zeolite-filled silicone rubber membranes in gas permeation, J. Memb. Sci. 57 (1991) 289–292.

[72] H.T.C. R.M. Barrer, Solution and diffusion of gases and vapors in silicone rubber membrades, J. Polym. Sci. Part C. 10 (1965) 111–138.

[73] P. Pandey, R.S. Chauhan, Membranes for gas separation, Prog. Polym. Sci. 26 (2001) 853–893.

[74] S. Sridhar, S. Bee, S. Bhargava, Membrane-based gas separation: principle, applications and future potential, Chem. Eng. Dig. 1 (2014) 1–25.

[75] Kawakami, J. Hajims, N. Muruganadam, L. George, Semipermeable membranes based on specified tetrabromobisphenol type polyesters, EP Patents, EP0376234B2 (1999).

[76] D.F. Sanders, Z.P. Smith, R. Guo, L.M. Robeson, J.E. McGrath, D.R. Paul, B.D. Freeman, Energy-efficient polymeric gas separation membranes for a sustainable future: A review, Polymer (Guildf). 54 (2013) 4729–4761.

[77] S.A. Stern, The “Barrer” permrbility unit, J. Polym. Sci. Part A. 6 (1968) 1933–1934.

[78] S. Bisoi, A.K. Mandal, A. Singh, V. Padmanabhan, S. Banerjee, Soluble, optically transparent polyamides with a phosphaphenanthrene skeleton: Synthesis,

characterization, gas permeation and molecular dynamics simulations, Polym. Chem. 8 (2017) 4220–4232. 7j.

[79] D. Bastani, N. Esmaeili, M. Asadollahi, Polymeric mixed matrix membranes containing zeolites as a filler for gas separation applications: A review, J. Ind. Eng. Chem. 19 (2013) 375–393.

[80] R. Mahajan, R. Burns, M. Schaeffer, W.J. Koros, Challenges in forming successful mixed matrix membranes with rigid polymeric materials, J. Appl. Polym. Sci. 86 (2002) 881–890.

[81] S. Belhaj Messaoud, A. Takagaki, T. Sugawara, R. Kikuchi, S.T. Oyama, Mixed matrix membranes using SAPO-34/polyetherimide for carbon dioxide/methane separation, Sep. Purif. Technol. 148 (2015) 38–48.

[82] R. Lin, B. Villacorta Hernandez, L. Ge, Z. Zhu, Metal organic framework based mixed matrix membranes: An overview on filler/polymer interfaces, J. Mater. Chem. A. 6 (2018) 293–312.

[83] R.T. Adams, J.S. Lee, T.H. Bae, J.K. Ward, J.R. Johnson, C.W. Jones, S. Nair, W.J. Koros, CO_2-CH_4 permeation in high zeolite 4A loading mixed matrix membranes, J. Memb. Sci. 367 (2011) 197–203.

[84] R. Nasir, N.N.R. Ahmad, H. Mukhtar, D.F. Mohshim, Effect of ionic liquid inclusion and amino-functionalized SAPO-34 on the performance of mixed matrix membranes for CO_2/CH_4 separation, J. Environ. Chem. Eng. 6 (2018) 2363–2368.

[85] U. Cakal, L. Yilmaz, H. Kalipcilar, Effect of feed gas composition on the separation of CO_2/CH_4 mixtures by PES-SAPO 34-HMA mixed matrix membranes, J. Memb. Sci. 417–418 (2012) 45–51.

[86] R. Mahajan, W.J. Koros, Mixed matrix membrane materials with glassy polymers.

Part 1, Polym. Eng. Sci. 42 (2002) 1420–1431.

[87] A.M.W. Hillock, S.J. Miller, W.J. Koros, Crosslinked mixed matrix membranes for the purification of natural gas: Effects of sieve surface modification, J. Memb. Sci. 314 (2008) 193–199.

[88] L. Ge, W. Zhou, V. Rudolph, Z. Zhu, Mixed matrix membranes incorporated with size-reduced Cu-BTC for improved gas separation, J. Mater. Chem. A. 1 (2013) 6350–6358.

[89] G. Dong, H. Li, V. Chen, Challenges and opportunities for mixed-matrix membranes for gas separation, J. Mater. Chem. A. 1 (2013) 4610–4630.

[90] N.N. Rosyadah Ahmad, H. Mukhtar, D.F. Mohshim, R. Nasir, Z. Man, Surface modification in inorganic filler of mixed matrix membrane for enhancing the gas separation performance, Rev. Chem. Eng. 32 (2016) 181–200.

[91] R. Mahajan, W.J. Koros, Factors controlling successful formation of mixed-matrix gas separation materials, Ind. Eng. Chem. Res. 39 (2000) 2692–2696.

[92] E. Karatay, H. Kalipçilar, L. Yilmaz, Preparation and performance assessment of binary and ternary PES-SAPO-34-HMA based gas separation membranes, J. Memb. Sci. 364 (2010) 75–81.

[93] N.N.R. Ahmad, H. Mukhtar, D.F. Mohshim, R. Nasir, Z. Man, Effect of different organic amino cations on SAPO-34 for PES/SAPO-34 mixed matrix membranes toward CO_2/CH_4 separation, J. Appl. Polym. Sci. 133 (2016) 1–6.

[94] J.Y. Lee, S.H. Lee, S.W. Kim, Surface tension of silane treated natural zeolite, Mater. Chem. Phys. 63 (2000) 251–255.

[95] Y. Li, H.M. Guan, T.S. Chung, S. Kulprathipanja, Effects of novel silane modification of zeolite surface on polymer chain rigidification and partial pore

blockage in polyethersulfone (PES)-zeolite A mixed matrix membranes, J. Memb. Sci. 275 (2006) 17–28.

[96] C. Takai, M. Fuji, M. Takahashi, A novel surface designed technique to disperse silica nano particle into polymer, Colloids Surfaces A Physicochem. Eng. Asp. 292 (2007) 79–82.

[97] H. Salmio, D. Brühwiler, Distribution of amino groups on a mesoporous silica surface after submonolayer deposition of aminopropylsilanes from an anhydrous liquid phase, J. Phys. Chem. C. 111 (2007) 923–929.

[98] H. Sanaeepur, A. Kargari, B. Nasernejad, Aminosilane-functionalization of a nanoporous Y-type zeolite for application in a cellulose acetate based mixed matrix membrane for CO_2 separation, RSC Adv. 4 (2014) 63966–63976.

[99] M. Mosadegh, F. Amirkhani, H. Riasat Harami, M. Asghari, M.J. Parnian, Effect of Nafion and APTEOS functionalization on mixed gas separation of PEBA-FAU membranes: Experimental study and MD and GCMC simulations, Sep. Purif. Technol. 247 (2020).

[100] H.R. Amedi, M. Aghajani, Aminosilane-functionalized ZIF-8/PEBA mixed matrix membrane for gas separation application, Microporous Mesoporous Mater. 247 (2017) 124–135.

[101] R. Lin, L. Ge, L. Hou, E. Strounina, V. Rudolph, Z. Zhu, Mixed matrix membranes with strengthened MOFs/polymer interfacial interaction and improved membrane performance, ACS Appl. Mater. Interfaces. 6 (2014) 5609–5618.

[102] J.A. Thompson, K.W. Chapman, W.J. Koros, C.W. Jones, S. Nair, Sonication-induced Ostwald ripening of ZIF-8 nanoparticles and formation of ZIF-8/polymer composite membranes, Microporous Mesoporous Mater. 158 (2012) 292–299.

[103] C. Zhang, R.P. Lively, K. Zhang, J.R. Johnson, O. Karvan, W.J. Koros, Unexpected molecular sieving properties of zeolitic imidazolate framework-8, J. Phys. Chem. Lett. 3 (2012) 2130–2134.

[104] D. Fairen-Jimenez, S.A. Moggach, M.T. Wharmby, P.A. Wright, S. Parsons, T. Düren, Opening the gate: Framework flexibility in ZIF-8 explored by experiments and simulations, J. Am. Chem. Soc. 133 (2011) 8900–8902.

[105] Y. Luo, H.H. Funke, J.L. Falconer, R.D. Noble, Adsorption of CO_2, CH_4, C_3H_8, and H_2O in SSZ-13, SAPO-34, and T-Type Zeolites, Ind. Eng. Chem. Res. 55 (2016) 9749–9757.

[106] B. Engineering, Alumina-Supported SAPO-34 Membranes for CO_2/CH_4 Separation Moises A. Carreon, J Am Chem Soc. 130 (2008) 5412–5413.

[107] D.R. Joshi, N. Adhikari, An overview on common organic solvents and their toxicity, J. Pharm. Res. Int. 28 (2019) 1–18.

[108] D.R. Joshi, N. Adhikari, An overview on common organic solvents and their toxicity, J. Pharm. Res. Int. 28 (2019) 1–18.

[109] S. Tanaka, K. Kida, T. Nagaoka, T. Ota, Y. Miyake, Mechanochemical dry conversion of zinc oxide to zeolitic imidazolate framework, Chem. Commun. 49 (2013) 7884–7886.

[110] T. Wu, Y. Liu, I. Kumakiri, K. Tanaka, X. Chen, H. Kita, Preparation and permeation properties of PESU-based mixed matrix membranes with nano-sized CHA zeolites, J. Chem. Eng. Japan. 52 (2019) 514–520.

[111] Y. Li, H.M. Guan, T.S. Chung, S. Kulprathipanja, Effects of novel silane modification of zeolite surface on polymer chain rigidification and partial pore blockage in polyethersulfone (PES)-zeolite A mixed matrix membranes, J. Memb.

Sci. 275 (2006) 17–28.

[112] Y. Cheng, Z. Wang, D. Zhao, Mixed Matrix Membranes for Natural Gas Upgrading: Current Status and Opportunities, Ind. Eng. Chem. Res. 57 (2018) 4139–4169.

Chapter 2 Mechanochemically synthesized ZIF-8 nanoparticles blended into 6FDA-TrMPD membranes for gas separation

2.1 Introduction

Membrane separation is a promising alternative for gas separation, including CO_2 capture and storage, and olefin/paraffin separation [1–4]. Compared with the conventional separation process, membrane separation has low energy cost and small footprint. Polymer membranes have excellent processability and high reproducibility. Highly permeable polymer membranes have low selectivity. Therefore, the gas transport properties of polymer membranes are below an upper bound, as illustrated by Robeson [5]. Inorganic membranes exhibit excellent separation property and mechanical stability; however, their fabrication process is costly.

The separation performance of polymer membranes could be improved to surpass the upper bound by blending inorganic particles. The obtained hybrid membranes are the so-called mixed matrix membranes (MMMs) [6,7]. The preparation cost of MMMs with inorganic particle powder and polymer matrix is expected to be lower than that of inorganic membranes. Hence, much attention has been paid on the development and application of MMMs. Various inorganic materials, such as zeolite [8], silica [9,10],

carbon molecule sieve (CMS) [11], and metal organic frameworks (MOFs) [12–15] have been employed in the preparation of MMMs.

Zeolitic imidazolate framework-8 (ZIF-8) is a typical MOF and is a promising filler for MMMs owing to its flexible structure and an effective pore size in the range of 0.40–0.42 nm [16,17]. Compared with other MOFs, ZIF-8 can remain stable during the preparation of MMMs owing to its good thermal stability [18]. The critical diameters of C_3H_6 and C_3H_8 molecules are 0.40 and 0.42 nm, respectively. Some studies reported that ZIF-8 crystals can be applied into the separation of C_3H_6 and C_3H_8 [19,20].

ZIF-8 crystals can be synthesized using solvothermal, microwave-assisted, sonochemical, mechanochemical, dry-gel conversion, or microfluidic methods [21]. Solvothermal synthesis requires *N*,*N*-dimethylformamide (DMF), methanol or other organic solvents. This can result in environmental contamination and human health problems [22]. These harmful solvents are also used in microwave-assisted, sonochemical, and microfluidic methods. In contrast, mechanochemical synthesis and dry-gel conversion are solvent-free synthesis methods. Dry-gel conversion is carried out at 393 K, and the mechanochemical method at room temperature. Therefore, the advantages of solvent-free and low energy-cost make the mechanochemical synthesis most attractive for ZIF-8. In our previous research, we optimized the mechanochemical method by the salt-free process to reduce the impurity content [23]. The pore structure of the mechano-synthesized ZIF-8 were proved to be comparable with the solvothermal synthesized ZIF-8 in our previous study.

A highly permeable polyimide (PI) made from 4,4'-(hexafluoroisopropylidene)diphthalic anhydride (6FDA) and 2,4,6-trimethyl-1,3-

phenylenediamine (TrMPD) can be used as a polymeric matrix in the preparation of MMMs for the separation of C_3H_6 and C_3H_8 [24,25]. Koros et al. [26,27] had blended original solvothermal-synthesized ZIF-8 particles into 6FDA-TrMPD by physical mixing. The C_3H_6 permeability and C_3H_6/C_3H_8 ideal selectivity of a 48 wt% ZIF-8/6FDA-TrMPD membrane were 258% and 150% higher than those of the neat 6FDA-TrMPD membrane. A new paradigm of ZIF-8/6FDA-TrMPD MMMs fabrication based on solvothermal synthesis was presented by Jeong et al., named as polymer modification-enabled *in-situ* MOF formation (PMMOF) [28]. The method enhanced the C_3H_6/C_3H_8 ideal selectivity of the neat membrane by 230% with loading 26 wt% ZIF-8. The separation performance of the MMMs were further improved by *in-situ* linker doping [29].

The above results remind us that the solvothermal synthesized ZIF-8 can be used to improve the separation performance of 6FDA-TrMPD polymer. The mechanochemically synthesized ZIF-8 is expected to further promote the application of ZIF-8 in the MMMs due to the solvent-free synthesis and other merits. In this study, the mechanochemical-synthesized ZIF-8 sample (hereinafter referred to as “mechano-synthesized ZIF-8”) was added to 6FDA-TrMPD polymer to prepare flat ZIF-8/6FDA-TrMPD MMMs. Commercial ZIF-8 particles synthesized using the solvothermal method were also dispersed in the 6FDA-TrMPD matrix. The single gas permeation of C_3H_6 and C_3H_8 was used to evaluate the separation performance of the MMMs.

2.2 Experimental

2.2.1 Materials and Instrumental

Table 2-1 lists the information of the materials and instrumental for the preparation of ZIF-8/6FDA-TrMPD MMMs. If some materials and instruments in this table are used in other chapters, they will not be listed again to avoid duplication.

Table 2-1 Materials and Instrumental of ZIF-8/6FDA-TrMPD MMMs

Materials	**Abbreviation/Code**	**Manufacturer, Model**	**Purity** (wt%)
ZnO	—	Wako	—
2-methylimidazole	2-MeIm	Sigma-Aldrich	99
Ceramic ball (ϕ10mm)	—	®YTZ,	–
Ceramic ball (ϕ1.5mm)	—	100®YTZ	
Commercial ZIF-8	Z2	BASF, Basolite®Z1200	—
4,4'-(Hexafluoroisopropylidene)diphthalic Anhydride	6FDA	Tokyo Chemical Industry (TCI)	99
2,4,6-Trimethyl-1,3-phenylenediamine	TrMPD	TCI	98
N-methylpyrrolidone	NMP	Wako	99
Acetic anhydride	—	Wako	97
Triethylamine	—	Wako	99
Ethanol	EtOH	Wako	95
Pot mill turntable	—	Nitto Kagaku, ANZ-50S	—
Stainless-steel test sieve	—	Tokyo Screen, SANPO	—
Vacuum oven	—	EYE04,	—
Oil pump/vacuum pump	—	ULVAC, GLD-051	—
X-ray diffraction	XRD	Rigaku, SmartLab9/SWXD	—
Scanning electron microscope	SEM	JEOL, JSM-6335F	—
Fourier transform infrared spectrometer	FTIR	JASCO, FTIR-610	—
Energy dispersive X-Ray	EDX	JEOL, JSM-7600F	

2.2.2 Purification of Monomer

The raw monomers were purified by using sublimation in this study. Figure 2-1 shows that the schematic diagram of monomer sublimation with vacuum method. The raw monomer powder was added into a glass tube with two-necks, and then start the heating after the vacuum gauge pointing the pressure in the tube was lower than 0.05 Torr. The oil pump provided the vacuum condition. The sublimation condition and results were summarized in Table 2-2. The sublimation temperature of diamine monomers was lower than that of the 6FDA monomers to avoid the decomposition.

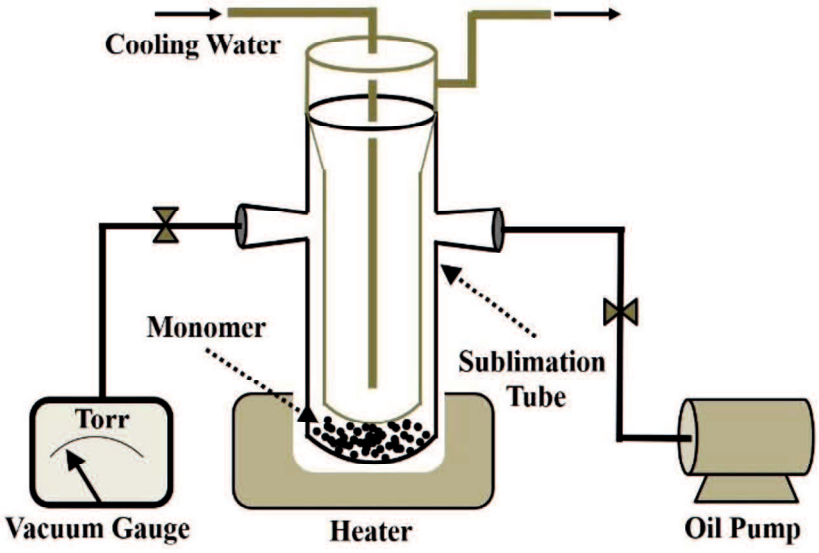

Figure 2-1 Schematic diagram of monomer sublimation with vacuum method.

Table 2-2 Sublimation condition and results of monomer with vacuum method

Monomer	Temperature (°C)	Time (hour)	Input (g)	Output (g)	Yield (%)
6FDA	240	2	6.4	6.2	97
TrMPD	65	3	5.0	3.3	66

Note: The data of input and output was the average experimental value.

2.2.3 Synthesis of 6FDA-TrMPD Polymer

The 6FDA-TrMPD polyimides were synthesized by the imidization of the polyamic acid which was generated from the 6FDA monomer reacted with the TrMPD diamine monomer as shown in the Scheme 2-1. The reaction of 6FDA with TrMPD monomers was carried out in a four-neck round flask (Figure 2-2) under nitrogen atmosphere. Acetic anhydride and triethylamine were used as the catalysts. The molar ratio of TrMPD monomer: 6FDA: acetic anhydride: triethylamine was 1: 1: 4: 4. The detail experimental process is as follows:

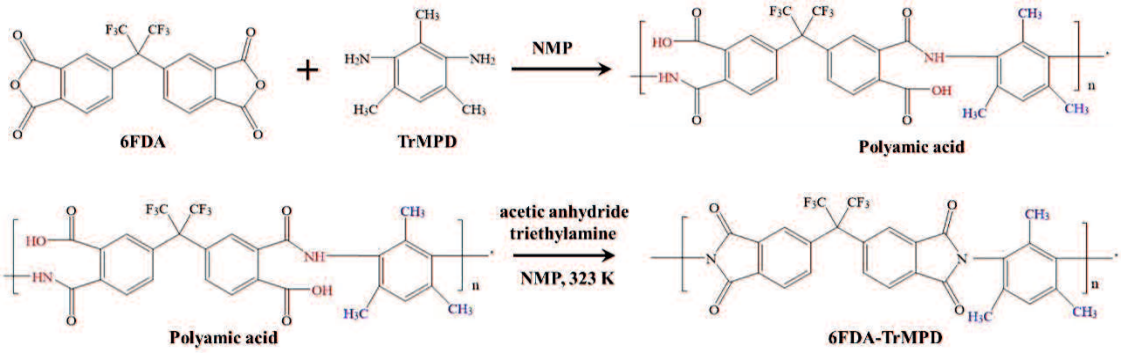

Scheme 2-1. Synthesis mechanism of 6FDA-TrMPD polyimide.

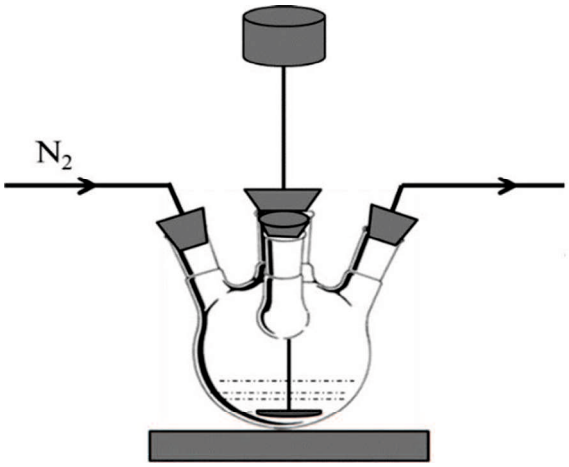

Figure 2-2. Synthesis apparatus of 6FDA-TrMPD polyimide.

(1) TrMPD monomer was mixed with the NMP solvent for 30 minutes to form a clear solution, and then the 6FDA was separately added to the solution.

(2) After mixing 6FDA and TrMPD monomers in the NMP, the solution was kept overnight to form a medium product, polyamic acid.

(3) The polyamic acid was converted to the polyimide at 50 °C in the presence of acetic anhydride and triethylamine.

(4) The obtained solution was slowly poured into 800 mL of ethanol and washed thrice.

(5) The washed polymer was dried at 80 °C overnight.

2.2.4 Synthesis of ZIF-8

Mechano-synthesized ZIF-8 powder was produced by using the method reported previously [23]. A mixture with 0.1 mmol nano-sized ZnO powders and 0.2 mmol 2-MeIm was milled by ceramic balls at a rotation speed of 100 rpm and room temperature. The products were rinsed with deionized water for the removal of unreacted 2-MeIm and then dried under reduced pressure at 313 K. The commercial ZIF-8 powder purchased from Aldrich-Sigma was used for reference. It is well known to be synthesized by solvothermal method [30]. The mechano-synthesized ZIF-8 and commercial ZIF-8 powders are referred to as Z1 and Z2, respectively. A preliminary experiment showed that a milling treatment can promote a better dispersion of ZIF-8 particles in MMMs, as described in the supporting information.

2.2.5 Ball Milling of ZIF-8

The mechano-synthesized ZIF-8 and solvothermal synthesized ZIF-8 powders were treated by ball milling. This was due to that the as-synthesized ZIF-8 nanoparticles would

agglomerate after drying. Agglomerates is not good for preparation of an MMM with ideal structure. The mixture containing 1 g of ZIF-8 powder, 13 g of *N*-methylpyrrolidone (NMP) and 30 g of ceramic ball (1.5 mm diameter) were added in a polypropylene (PP) bottle, and then put on a pot mill turntable. Rotation rate and time were 120 rpm and 3 days, respectively. After milling, the balls were separated from the ZIF-8 and NMP through a stainless-steel test sieve with aperture size of 0.85 mm. The obtained ZIF-8/NMP slurry was used for the preparation of the mixed matrix membranes (MMMs).

2.2.6 Preparation of Neat 6FDA-TrMPD Membrane

The 6FDA-TrMPD powder was divided into four equal parts to be dissolved in the NMP solvent to prepare a 15 wt% PI/NMP solution. After stirring for 20 hours, the solution was treated by ultrasonic for 4 hours and then bubble removal for 30 min. The solution was cast on the glass plate with a glass rod. After vacuum drying at 200 °C for 20 hours, the membrane was peeled from the glass plate.

2.2.7 Preparation of ZIF-8/6FDA-TrMPD MMMs

A slurry of ZIF-8 and NMP was obtained from the ball milling. The 6FDA-TrMPD polymer was divided into three equal parts to be added in the ZIF-8/NMP slurry sequentially and then formed a solution that had a weight ratio of filler-to-polymer in the range of approximately 0–30 wt%. After ultrasonic treatment for 4 h, the solution was cast onto a glass plate. The membrane was formed after drying the solution at 473 K for 20 h. It was then peeled off from the glass plate. The neat polymer membrane was prepared using the same method but without adding any filler particle. Table 2-3 summarizes the preparation conditions of the as-synthesized membranes. The volume

fraction of the filler particles (ν_f) in the MMMs was calculated by the following equation:

$$\nu_f = \frac{W_f}{W_f + \frac{d_f}{d_p}(1-W_f)} \quad (2\text{-}1)$$

where the W_f is the weight ratio of filler in the MMMs; d_f and d_p is the density of the ZIF-8 filler (0.95 g/cm^3) and 6FDA-TrMPD polymer (1.35 g/cm^3), respectively [3,24,30].

Table 2-3 Preparation condition of ZIF-8/6FDA-TrMPD MMMs

No.	Filler source	W_f (wt%)	ν_f (vol%)
N	—	0	0
M1	Mechanochemical	20	26
M2	Mechanochemical	30	38
C1	Commercial	20	26
C2	Commercial	30	38

Notes:
(1) "N" represents the neat 6FDA-TrMPD membrane. It is the T0 membrane presented in Chapter 4.

(2) "W_f" and "ν_f" denote the filler weight content and volume fraction in the polymer matrix, respectively.

2.2.8 Characterization Methods

The X-ray diffraction (XRD) was used to analyze the structure of the filler and membranes. The scanning electron microscopy (SEM) was applied to observe the morphology. The chemical structure of the membranes was measured by the FTIR spectrometer in the wavenumber range of 400–4000 cm^{-1}. The distribution situation of ZIF-8 particles in the cross-section of MMMs was measured by energy dispersive X-Ray (EDX) mapping of Zn elements

2.2.9 Single Gas Permeation

The single gas permeation through the membranes was tested by a home-made

apparatus (Figure 2-3) with the vacuum method at 0.1–0.6 MPa and 35–100 °C (308–437 K). Before the gas permeation, the membrane in the apparatus was degassed at 100 °C for more than 2 hours and then cooling to 35 °C.

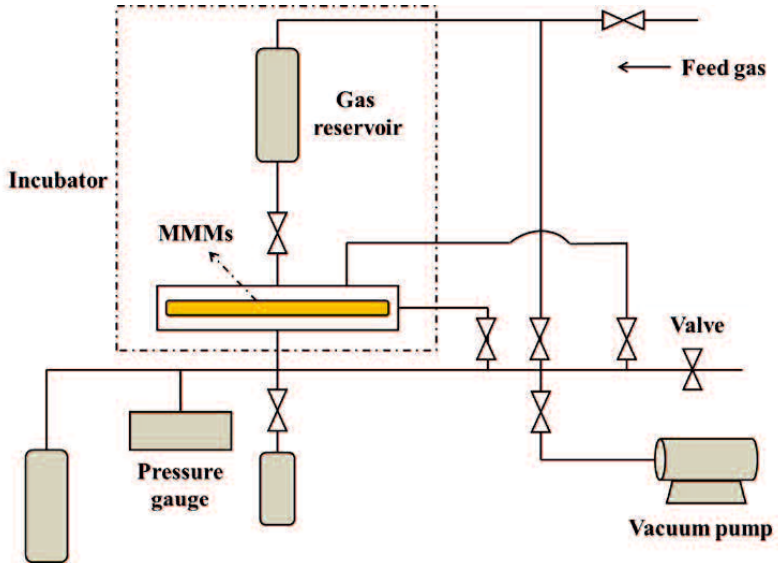

Figure 2-3. Schematic diagram of gas permeation apparatus with vacuum method

The gas permeability (P), diffusivity (D) and solubility (S) were calculated using the following three equations.

$$P = Nl/\Delta p \quad (2\text{-}2)$$

$$D = l^2/6\theta \quad (2\text{-}3)$$

$$S = P/D \quad (2\text{-}4)$$

where the N, Δp, and l was the number of gas molecule passing per unit time through per unit membrane area, the transmembrane partial pressure difference, and the thickness of membrane, respectively. The θ is the time lag [31,32]. The unit of P, D and S was in barrer, cm^2/s, $cm^3(STP)/(cm^3\ cmHg)$, respectively (1 barrer = 10^{-10} $cm^3(STP)\ cm/(cm^2\ s\ cmHg)$).

The ideal selectivity (αP), diffusivity selectivity (αD), and solubility selectivity (αS) were the permeability ratio, diffusivity ratio, and solubility ratio, respectively. The

relationship of these three parameters was expressed by equation (2-5):

$$\alpha P = \alpha D \times \alpha S \tag{2-5}$$

2.3 Results and Discussion

2.3.1 XRD Analysis

Figure 2-4 shows the XRD patterns of the original ZIF-8 powder and MMMs. The Z1 and Z2 are the mechano-synthesized and solvothermal-synthesized ZIF-8 powders. The N presents the neat 6FDA-TrMPD membrane; M0 membrane contains 20 wt% of original Z1, M1 and M2 membranes contain 20 wt% and 30 wt% ball-milled Z1; C1 and C2 membranes contain 20 wt% and 30 wt% Z2; respectively.

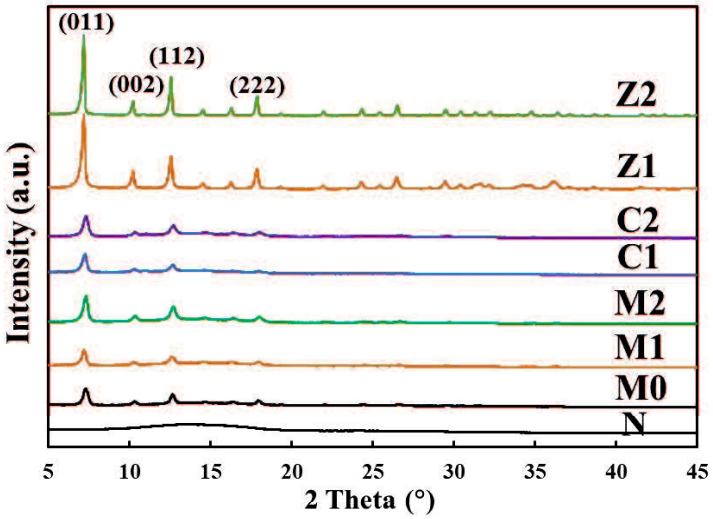

Figure 2-4. XRD patterns of original ZIF-8 powder and ZIF-8/6FDA-TrMPD MMMs: N presents the neat 6FDA-TrMPD membrane; M0 membrane contains 20 wt% original Z1, M1 and M2 membranes contain 20 wt% and 30 wt% ball-milled Z1; C1 and C2 MMMs contain 20 wt% and 30 wt% Z2; Z1 and Z2 are the mechano-synthesized and solvothermal-synthesized ZIF-8 powders, respectively.

The mechano-synthesized filler powder (Z1) had four main XRD peaks at 2theta = 7.3°, 10.3°, 12.6° and 18.0° corresponding to the crystal plane of (011), (002), (112) and (222), respectively. The relative intensity and position of these peaks in a good agreement with the XRD peaks of ZIF-8 reported by the literature [3,18]. Therefore, the mechano-synthesized filler powder exhibits typical XRD peaks of ZIF-8. The XRD pattern of the commercial ZIF-8 prepared using the solvothermal method (Z2) is similar to that of Z1. This suggests that there is no significant difference in the crystalline structure of the two ZIF-8 powders.

The neat 6FDA-TrMPD membrane (N) exhibits an amorphous structure. With the ZIF-8 filler added to the matrix, the XRD patterns of the MMMs exhibit ZIF-8 crystal peaks. Due to the presence of the amorphous matrix, the intensity of the ZIF-8 peak exhibited by the MMMs is weaker than that exhibited by the original powder. The sharp peaks in MMMs attributed to the ZIF-8 particles are similar to peaks for the Z1 and Z2 powders. In addition, the intensity of XRD peaks belong to ZIF-8 in the M1 membrane prepared using 20 wt% of ball-milled Z1 was same to that in the membrane (M0) prepared using original Z1. This indicates that the ZIF-8 particles remained stable during ball milling.

2.3.2 SEM Results

Figure 2-5 shows the SEM images of the original ZIF-8 powders. The mechano-synthesized ZIF-8 powder (Z1) was shown in Figure 2-5(a) and Figure 2-5(b) which with 50000 and 20000 of magnification. The solvothermal-synthesized ZIF-8 powder (Z2) was shown in Figure 2-5(c) and Figure 2-5(d) which with 50000 and 20000 of magnification. With 50000 of magnification, the shape of particles could be observed clearly; with the 20000 of magnification, the agglomeration of the particles could be observed clearly. The

mechano-synthesized ZIF-8 powder exhibits uniform spherical crystals with a particle size of approximately 100 nm, whereas the solvothermal-synthesized ZIF-8 powder exhibits cubic crystals with a particle size of approximately 200 nm. The agglomeration both appeared in these two kinds of ZIF-8 powder. This was due that nanoparticles have high surface area and tend to agglomerate.

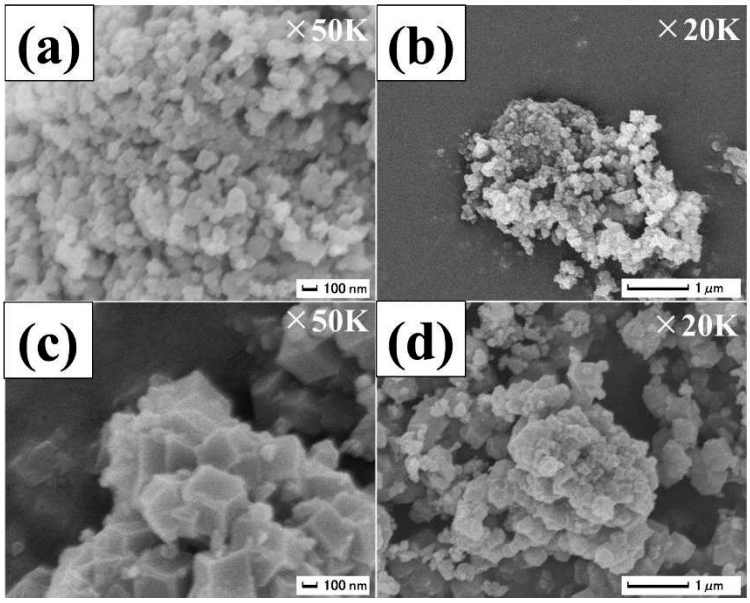

Figure 2-5. Scanning electron microscope (SEM) images of original ZIF-8 powder: (a,b) mechano-synthesized ZIF-8 (Z1), (c,d) commercial ZIF-8 (Z2).

Figure 2-6 shows the cross-sectional SEM images of the MMMs prepared using 20 wt% of ZIF-8. The M0, M1 and C1 membranes were using original Z1, ball-milled Z1, and ball-milled Z2 particles. The agglomerates of the original Z1 particles can be observed in the M0 membrane. After ball milling treatment, the Z1 particles were homogenously dispersed in M1 membrane. The particle size of ball-milled Z1 filler was approximately 50 nm. This was much smaller than that of the original powder (100 nm). The XRD patterns confirmed that the XRD peak intensity of the filler in the M1

membrane was similar to that in the M0 membrane. Therefore, the ball milling treatment helps to break the ZIF-8 particles into small pieces without destroying the crystal structure, thereby improving the dispersibility of the ZIF-8 particles in the MMM. The solvothermal-synthesized ZIF-8 particles were also pre-treated by ball milling for three days and dispersed well in the polymer matrix of the C1 membranes, as shown in Figure 2-6d. The particle size of the ball-milled filler in C1 was about 100 nm, and smaller than that of the original ZIF-8 powder (200 nm). Hence, the influence of ball milling on mechano-synthesized ZIF-8 particles is the same as on the solvothermal-synthesized ZIF-8 particles.

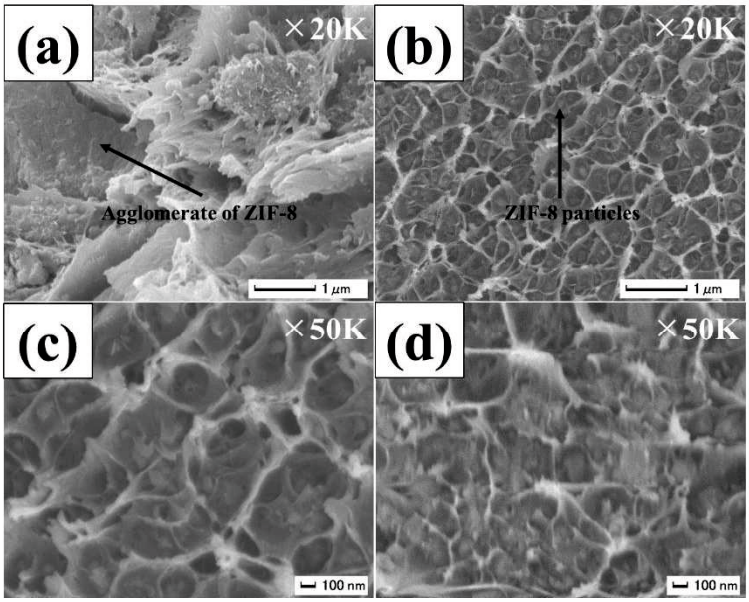

Figure 2-6. Cross-sectional SEM images of the MMMs contains 20 wt% of ZIF-8: (a) M0 membrane using 20 wt% of original Z1, (b,c) M1 membrane using 20 wt% of ball-milled Z1, (d) C1 membrane using 20 wt% of ball-milled Z2.

2.3.3 FTIR Measurement

Figure 2-7 shows the FTIR spectra of the neat 6FDA-TrMPD polyimide and the

MMMs with the wavenumber in range of 400–4000 cm^{-1}. The N presents the neat 6FDA-TrMPD membrane; M0 membrane contains 20 wt% of original Z1, M1 and M2 membranes contain 20 wt% and 30 wt% ball-milled Z1; C1 and C2 membranes contain 20 wt% and 30 wt% Z2; respectively.

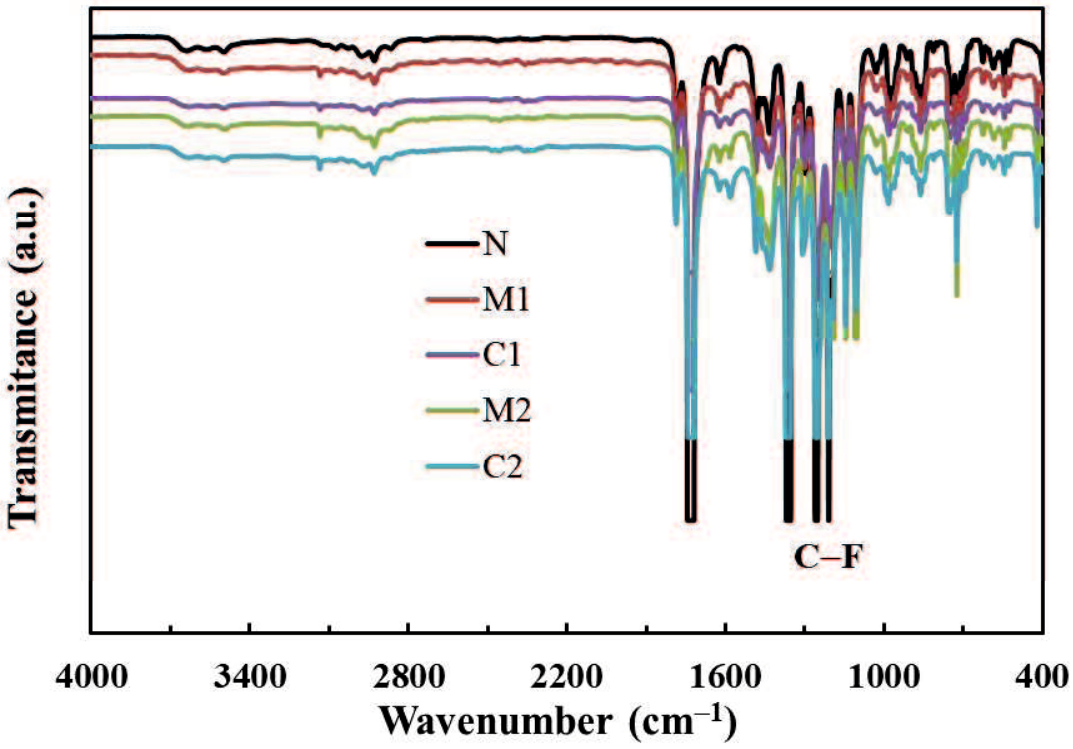

Figure 2-7. FTIR spectra of the membranes: N presents the neat 6FDA-TrMPD membrane in range of **400–4000** cm^{-1}; M1 and M2 MMMs contain 20 wt% and 30 wt% of ball-milled Z1 particles; C1 and C2 MMMs contain 20 wt% and 30 wt% of ball-milled Z2.

The polyimide was synthesized by the imidization of the polyamic acid which was generated from the 6FDA reacted with TrMPD, as shown in the Scheme 2-1. The medium product, polyamic acid, has O–H and N–H bond. Their stretching peaks are around 3200 and 3350 cm^{-1}, respectively [33]. There is no peak that appeared in Figure 2-7 assigned to these two stretches. It indicates the polyimides was obtained.

Figure 2-8 displayed the wavenumber range of 400–440 cm^{-1} of the FTIR spectra of the membranes from Figure 2-7. A FTIR peak assigned to the Zn–N stretching from ZIF-8 will around 421 cm^{-1} [34]. Figure 2-8 shows that this peak appeared in the MMMs and not in the neat membrane. It further identified that the MMMs contained the ZIF-8 particles. The intensity of the Zn–N stretching was increased with increasing the filler content. This result was in accordance with the XRD results that the peak intensity of the ZIF-8 was increased with increasing the filler content.

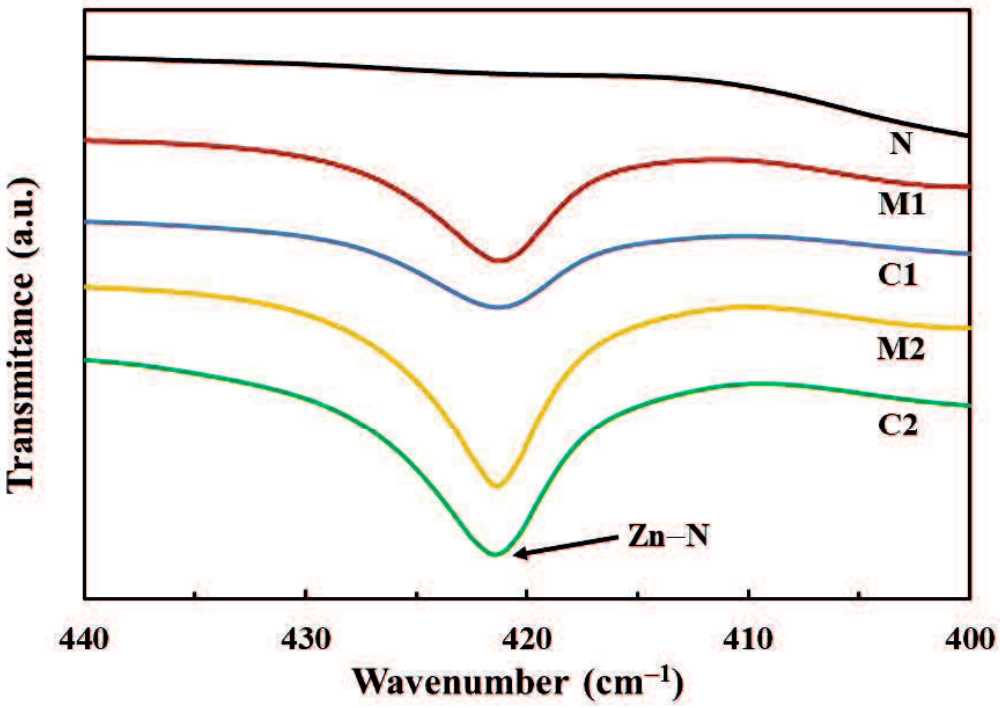

Figure 2-8. FTIR spectra of the membranes in range of **400–440** cm^{-1}: N presents the neat 6FDA-TrMPD membrane; M1 and M2 MMMs contain 20 wt% and 30 wt% of ball-milled Z1 particles; C1 and C2 MMMs contain 20 wt% and 30 wt% of ball-milled Z2.

2.3.4 Elemental Mapping

Figure 2-9 displays the EDX mapping of the cross-section of the M1 membrane and the M2 membrane. The right figures were from EDX mapping corresponding the SEM observation (left figures). The green color presented the Zn atoms from ZIF-8 particles.

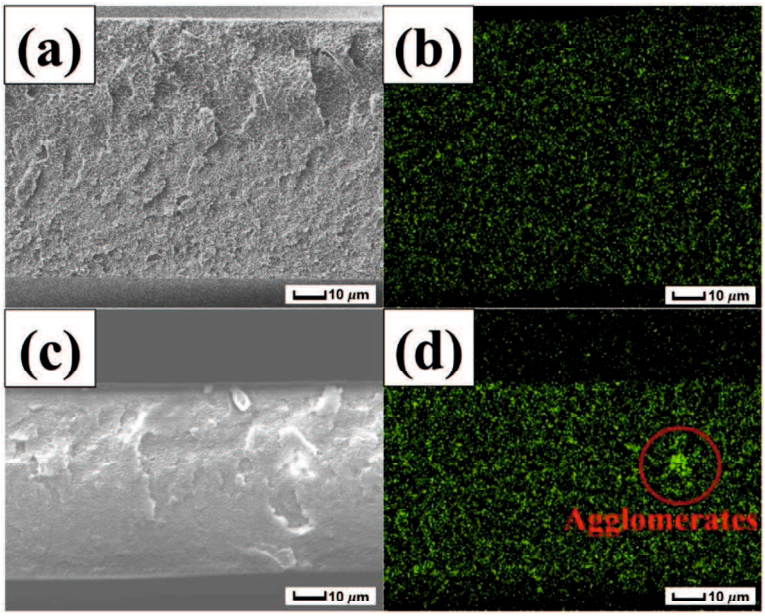

Figure 2-9. EDX mapping of Zn (green) in the MMMs and their cross-sectional SEM images: (a, b) M1 with 20 wt% of ball-milled Z1; (c, d) M2 with 30 wt% of ball-milled Z1. Each figure was taken at a magnification of 1000.

The M1 and M2 was prepared using 20 wt% and 30 wt% of mechano-synthesized ZIF-8, respectively. Figure 2-9(b) shows the Zn atoms were dispersed evenly, indicating a good ZIF-8 particle distribution across the M1 membrane. On the other hand, the accumulation of Zn atoms in the cross-section of the M2 membrane indicates agglomeration occurred, as shown in Figure 2-9(d). A high content of MOF particles in the polymer matrix can easily form agglomerates [35].

2.3.5 Gas Separation Performance

Figure 2-10 shows the C_3H_6/C_3H_8 separation performance of the membranes at 0.1 MPa and 35 °C. The X axis and Y axis presents the CO_2 permeability and CO_2/CH_4 ideal selectivity, respectively. Circle and triangle symbol are the MMMs using mechano-synthesized ZIF-8 (Z1) and solvothermal synthesized ZIF-8 (Z2) particles, respectively. The dotted line indicates the prediction value made using the Maxwell model. The solid circles on the dotted line are located at intervals of 10 vol%. The upper bound line indicates the results obtained by Koros et al. [25]

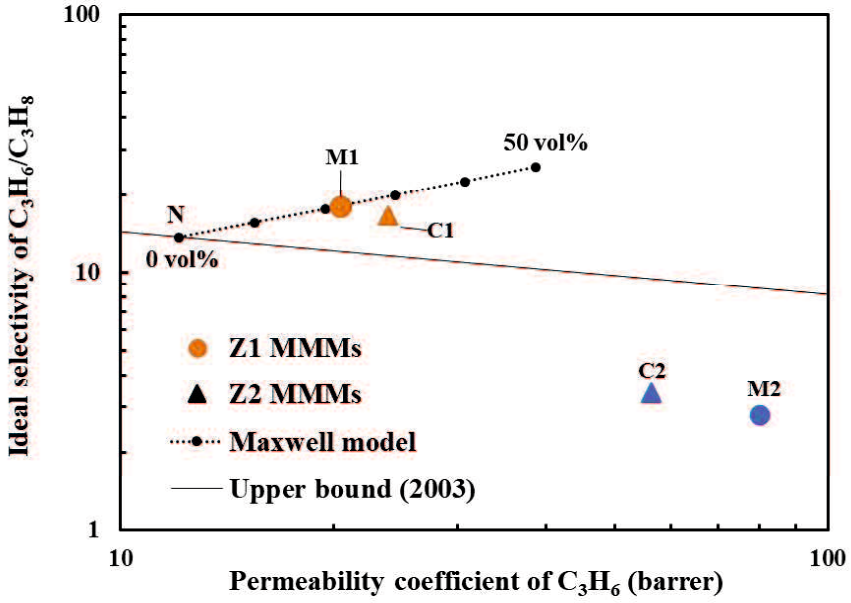

Figure 2-10. C_3H_6/C_3H_8 separation performance of the ZIF-8/6FDA-TrMPD MMMs at 0.1MPa and 35 °C. The Z1 and Z2 MMMs present the mechano-synthesized ZIF-8 and solvothermal-synthesized ZIF-8 particles. The dotted line indicates the prediction value made using the Maxwell model. The solid circles on the dotted line are located at intervals of 10 vol%. The upper bound line indicates the results obtained by Koros et al. [25].

The M1 membrane with 20 wt% mechano-synthesized ZIF-8 provides a C_3H_6 permeability of 20 barrer and C_3H_6/C_3H_8 ideal selectivity of 18, respectively. These values are 70% and 32% higher than those of the neat membrane (N), respectively. Table 2-4 summarized the detail value of the permeability as well as the diffusion coefficient and solubility coefficient at 308 K. These values of neat polymer membrane were affected by the addition of ZIF-8 particles.

Table 2-4 Permeability coefficient (*P*), diffusivity coefficient (*D*) and solubility coefficient (*S*) of C_3H_6 and C_3H_8 at 0.1MPa and 308 K.

Membrane	***l***	***P*** (barrer)		***D*** (10^{-10} cm^2/s)		***S*** [cm^3(STP)/ (cm^3 cm Hg)]		**α(*P*)**	**α(*D*)**	**α(*S*)**
	(μm)	**C_3H_6**	**C_3H_8**	**C_3H_6**	**C_3H_8**	**C_3H_6**	**C_3H_8**			
N	20	12	0.9	22	2	0.6	0.5	14	12	1
M1	96	20	1.1	41	(12)	0.5	(0.1)	18	(3)	(6)
C1	37	24	1.4	42	3	0.6	0.5	17	13	1
Pure ZIF-8	—	210	2.5	160	2	1.3	1.5	84	94	1

Notes:

(1) *l* is the thickness of membrane; α(*P*), α(*D*) and α(*S*) are the ideal selectivity, diffusivity selectivity and solubility selectivity of C_3H_6/C_3H_8, respectively.

(2) 1 barrer = 10^{-10} cm^3 (STP) cm/ (cm^2 s cm Hg).

(3) The data for pure ZIF-8 was obtained from a report of Koros et. al. [17].

(4) The *D* of C_3H_8 for the M1 membrane was not accurate due to the fact that the calculation of time-lag was greatly influenced by a long measurement time. It can be improved by reducing the membrane thickness or increasing the temperature.

After the addition of ZIF-8, the diffusivity coefficient of C_3H_6 was increased more than that of C_3H_8, and the solubility coefficient almost remained. Therefore, the increase in the permeability due to the increase in the diffusivity coefficient. The increase in the ideal selectivity was also attributed to the increase in diffusivity selectivity rather than the solubility selectivity. This result is consistent with the fact that the molecular diameters of C_3H_6 (0.40 nm) and C_3H_8 (0.42 nm) corresponding to the effective pore size of ZIF-8 crystal in the range of 0.40–0.42 nm [17]. This indicates that the C_3H_6 molecules can pass

through the pores of ZIF-8 in the MMMs easier than the C_3H_8 molecules.

In addition, Table 2-5 summarized the values of permeability, diffusivity coefficient, and solubility coefficient at 373 K, which can further verify the effect of the ZIF-8 particles in the M1 membrane.

Table 2-5 Permeability coefficient (*P*), diffusivity coefficient (*D*) and solubility coefficient (*S*) of C_3H_6 and C_3H_8 at 0.1MPa and 373 K.

Membrane	***l*** (μm)	***P*** (barrer)		***D*** ($\times 10^{-10}$ cm^2/s)		***S*** [cm^3(STP)/ (cm^3 cmHg)]		**α(*P*)**	**α(*D*)**	**α(*S*)**
		C_3H_6	**C_3H_8**	**C_3H_6**	**C_3H_8**	**C_3H_6**	**C_3H_8**			
N	20	19	3	112	15	0.2	0.2	7	7	1
M1	96	26	2	146	12	0.2	0.2	11	12	1
C1	37	28	3	171	15	0.2	0.2	11	11	1
Pure ZIF-8	—	256	4.2	800	10	0.3	0.4	61	80	1

Notes: The data for pure ZIF-8 membrane was calculated by combing the adsorption isotherm in the ZIF-8 crystals at 308 K reported by Koros et. al. and the activation energies for the pure ZIF-8 membrane reported by Hara et. al. [17,19].

The 20 wt% solvothermal-synthesized ZIF-8-filled MMM (C1) exhibited a performance similar to that of the M1 membrane. Separation performances of the MMMs can be evaluated by comparing with the Maxwell model, which is considered a simple and effective tool for predicting the separation performance of MMMs [26]. In this study, the detailed calculation method was as follows.

$$P = P_1 \times \frac{P_1 + 2P_2 - 2v_f(P_1 - P_2)}{P_2 + 2P_1 + v_f(P_1 - P_2)} \tag{2-6}$$

where P, P_1, and P_2 are the gas permeabilities of the MMM, pure polymer matrix (continuous phase), and pure filler (dispersed phase), respectively; v_f is the volume fraction of the filler particles. The permeability value of the pure ZIF-8 particles was obtained from the study by Koros et. al. [17].

The theoretical values from the Maxwell model for the C_3H_6/C_3H_8 separation at 308 K

were indicated by dotted lines in Figure 2-10. The separation performance of the M1 membrane is consistent with that predicted using the Maxwell model. The performance of the C1 membrane was also comparable with the theoretical value. This confirms there is no defect in the M1 and C1 membranes. In addition, the C_3H_6/C_3H_8 separation performance of M1 and C1 surpass the upper bound of the polymer membrane illustrated by Koros et al. [25]. We can conclude that the mechano-synthesized ZIF-8 particles were applied for the preparation of the ZIF-8/6FDA-TrMPD MMMs.

The M2 membrane containing 30 wt% of the mechano-synthesized ZIF-8 exhibited a higher permeability but poor ideal selectivity than that of the M1. It was due to the agglomeration of filler particles in the M2, as shown in Figure 2-9d. With increasing content, the fine filler particles tend to form agglomerates and result in some filler-polymer interfacial defects. The intergranular spaces between particles in the agglomerates allow the gas molecules to pass through, and then result in a low ideal selectivity. The C2 membrane containing 30 wt% solvothermal-synthesized ZIF-8 also displayed a higher permeability and lower ideal selectivity than the C1 with 20 wt% filler. This may also be due to the agglomerates. The defect in the M2 and C2 membranes can be improved by further optimizing the milling condition.

2.3.6 Investigation on the role of ZIF-8 particles

The results of the separation performance indicate that the ZIF-8 could affect the gas permeability and ideal selectivity of the MMMs. This is due to the micropore of ZIF-8 made a difference on the permeation of the C_3H_6 and C_3H_8. In order to analyze the role of ZIF-8 in the MMMs, the temperature dependence and pressure dependence were investigated in this study.

2.3.6.1 Temperature Dependence

The temperature dependence of C_3H_6 and C_3H_8 permeability of the neat membrane (N), 20 wt% mechano-synthesized ZIF-8 filled MMM (M1), and 20 wt% solvothermal-synthesized ZIF-8 MMM (C1) at 0.1 MPa had been investigated in this study. Figure 2-11 shows the plots of the gas permeabilities as a function of the temperature ranging from 308 to 373 K (35–100 °C). The X axis in each graph presents the reciprocal temperature value. The Y axis in Figure 2-11(a), Figure 2-11(b) and Figure 2-11(c) was the C_3H_6 permeability, C_3H_8 permeability and C_3H_6/C_3H_8 ideal selectivity, respectively.

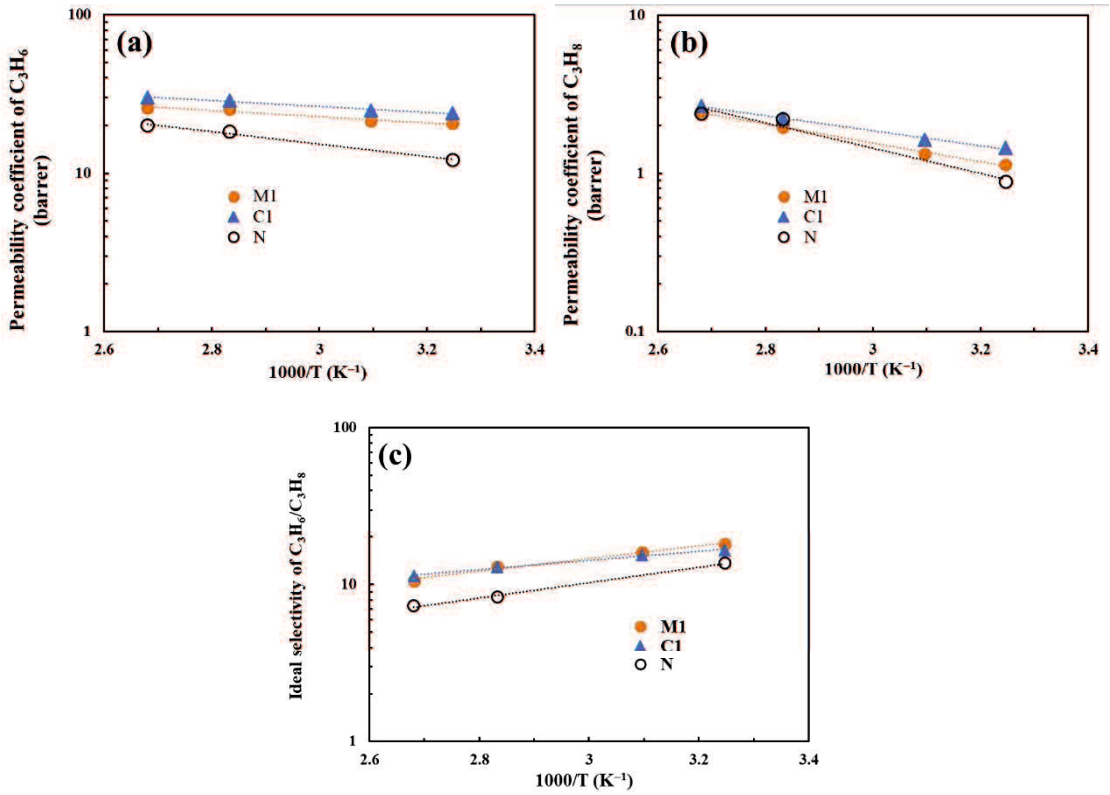

Figure 2-11. Temperature dependence of the permeability and ideal selectivity of C_3H_6/C_3H_8 of the neat 6FDA-TrMPD membrane (N), M1 membrane using 20 wt% of ball-milled Z1 particles, and C1 membrane using 20 wt% of ball-milled Z2 particles at 0.1MPa.

The gas permeabilities linearly decreases with the reciprocal of the temperature for all

the membranes. With an increase in the temperature from 308 to 373 K, the C_3H_6 permeabilities of the neat membrane, M1, and C1 were increased by 54%, 29%, and 26% respectively. For each membrane, the temperature influenced the C_3H_8 permeability more than the C_3H_6 permeability. The C_3H_6/C_3H_8 ideal selectivity was decreased with increasing the temperature, as shown in Figure 2-11(c). The increase in the gas permeability was due to the increase in the diffusivity coefficient, based on the comparison between the values at 308 K in Table 2-4 and at 373 K in Table 2-5. The decrease in the ideal selectivity was also attributed to the decrease in the diffusivity selectivity because the solubility selectivity didn't change.

The temperature dependence on the gas permeability of the N, M1, and C1 membranes can be expressed by the Arrhenius equation [19].

$$P = P_0 \times exp(-\frac{E_P}{RT}) \quad (2\text{-}7)$$

where E_P, P_0, T, and R are the activation energy, pre-exponential factor, absolute temperature, and universal gas constant, respectively. Table 2-6 lists the E_P values of C_3H_6 and C_3H_8 in the neat membrane, M1, and C1 membranes. The activation energy data in the pure ZIF-8 membrane was obtained from the study by Hara et al. [19].

Table 2-6 Activation energies for C_3H_6 and C_3H_8 permeation.

Membrane	**C_3H_6** (kJ/mol)	**C_3H_8** (kJ/mol)
Neat polymer (N)	8	15
MMM (M1)	4	12
MMM (C1)	4	10
Pure ZIF-8	−3	8

Table 2-6 shows that he E_P values of C_3H_6 and C_3H_8 in the pure ZIF-8 membrane were lower than in the neat membrane. The diffusivity coefficient of C_3H_6 and C_3H_8 of the pure

ZIF-8 membrane at 308 K and 373 K were higher than in the neat membrane, as shown in Table 2-4 and Table 2-5. This indicates the diffusion of these gas molecules in the pores of ZIF-8 was easier than in the neat membrane at the temperature in a range of 308−373 K. This is the reason that why the permeation of the gas molecules in the pure ZIF-8 membrane requires a lower E_P than in the neat membrane.

Due to the presence of 20 wt% ZIF-8 particles, the E_P values of C_3H_6 and C_3H_8 in the M1 and C1 membranes were between the neat membrane and pure ZIF-8 membrane, and closer to that in the neat membrane than that in the pure ZIF-8 membrane. The C_3H_6 diffusivity coefficient of the MMMs at 308 K and 373 K were both higher than for the neat membrane. It confirmed that molecules diffuse more easily in MMMs than in pure membranes. Temperature increases tend to exhibit a greater effect on the diffusion of gas molecules with large resistance than that with less resistance [36]. This is why the change of the gas permeability of the neat membrane with increasing the temperature from 308 to 373 K was greater than that of the MMMs. In addition, the permeation of C_3H_8 in the membranes required more E_P than C_3H_6 resulted in the temperature influenced the permeability of C_3H_8 more than that of C_3H_6. These results suggested that the pores of ZIF-8 in the MMMs were available for the permeation of C_3H_6 and C_3H_8.

2.3.6.2 Pressure Dependence

To further analyze the effect of mechano-synthesized ZIF-8 particles in the 6FDA-TrMPD polymer matrix, the pressure dependence of C_3H_6 and C_3H_8 permeability of the neat membrane (N) and 20 wt% mechano-synthesized ZIF-8 MMM (M1) membrane was discussed in this study. Figure 2-12 shows the plots of C_3H_6 and C_3H_8 permeability of the neat membrane and M1 membrane as a function of the pressure. The gas permeation

measurement was carried out at 373 K to reduce the permeation time. The X axis in each graph presents the pressure. The Y axis in Figure 2-12(a), Figure 2-12(b) and Figure 2-12(c) was the C_3H_6 permeability, C_3H_8 permeability and C_3H_6/C_3H_8 ideal selectivity, respectively.

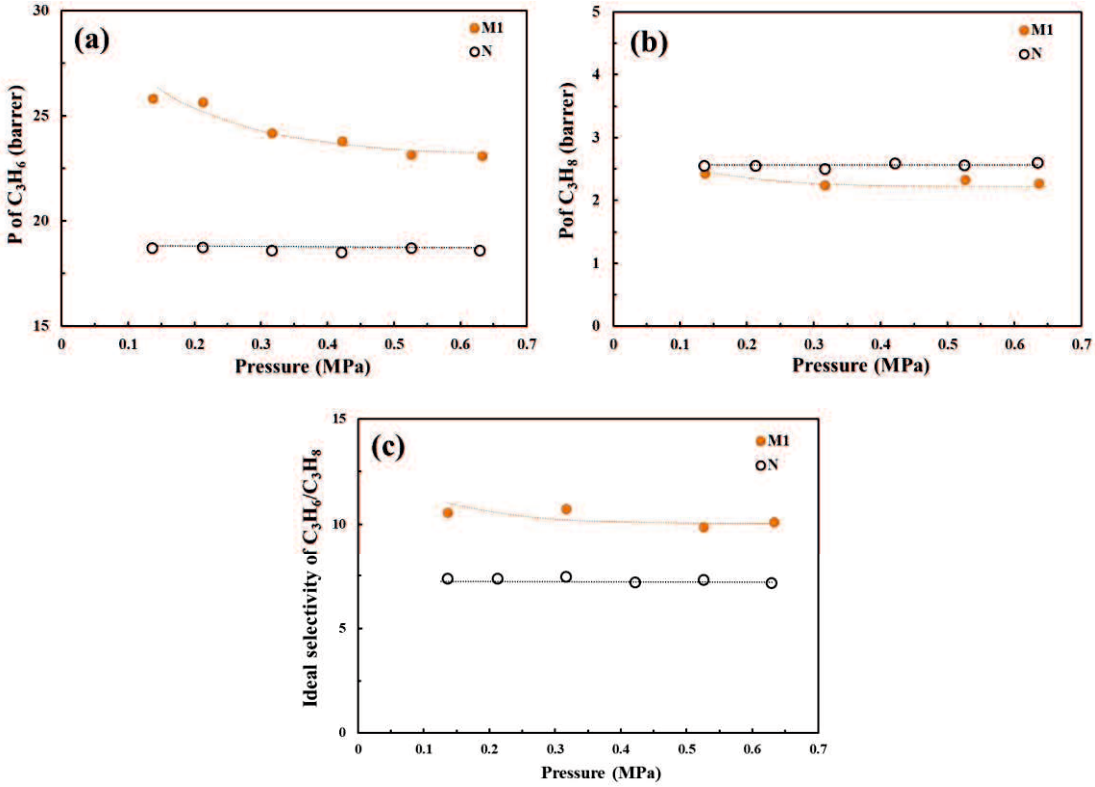

Figure 2-12. Pressure dependence of (a) C_3H_6 permeability, (b) C_3H_8 permeability, and (c) C_3H_6/C_3H_8 ideal selectivity for the N and M1 membranes at 373 K.

The C_3H_6 and C_3H_8 permeability of the neat membrane was almost independent of the pressure. Consequently, the C_3H_6/C_3H_8 ideal selectivity of the neat membrane was also independent of the pressure. On the other hand, the gas permeability of the M1 membrane was decreased with increasing the pressure. The variation in the C_3H_6 permeability was slightly larger than that of C_3H_8 permeability, resulting in a slight decrease in the ideal selectivity.

Pressure dependence on the gas permeability of the glassy polymeric membranes can be explained by using the dual-mode sorption and transport model, which is expressed in equation (2-8) [37].

$$P = k_D D_D + \frac{C'_H b D_H}{1+bp} \quad (2\text{-}8)$$

where k_D is the Henry's law solubility constant, C'_H is the Langmuir capacity constant, b is the Langmuir mode sorption affinity parameter, D_D and D_H are the diffusion coefficients of Henry's law population and Langmuir population, respectively. The first term is independent of the pressure. The additional second term corresponds to the permeability of the gas adsorbed in the micro-voids, which act as Langmuir-type sorption sites.

The equation (2-8) means the gas permeability is decreased with increasing the pressure. The values of C'_H and b are generally decreased with increasing the temperature [38]. In this case, the pressure-independent of C_3H_6 and C_3H_8 permeability of the neat membrane, as shown in Figure 2-12, was attributed to the high measurement temperature at 373 K. On the other hand, the gas permeability of the M1 membrane followed the above dual-mode model. Li et al. reported the sorption isotherms of C_3H_6 and C_3H_8 in ZIF-8 up to 73 kPa at temperatures ranging from 303 to 393 K [39]. The adsorption isotherms of the gases in the ZIF-8 micropores followed the Langmuir-type isotherms at 308 K. Although their isotherms gradually approach linearity, the isotherms at 378 K were still concave with respect to pressure axis. This indicates that the ZIF-8 micropores in the M1 membrane can act as Langmuir-type sorption sites even at 373 K. Hence, the gas permeation mechanism of the MMMs follows the dual mode sorption and transport model. This is why the gas permeability of the M1 membrane were decreased with increasing the

pressure. In summary, the pressure-dependent of the C_3H_6 and C_3H_8 permeability of the M1 membrane at 373 K indicates that the micropores of mechano-synthesized ZIF-8 particles were available for the permeation of these two kinds of gas molecules.

2.3.7 Comparison of the Study Results

Table 2-7 summarized the detail values of the C_3H_6/C_3H_8 separation performance of 20 wt% ZIF-8 filled MMMs as well as the synthesis condition of ZIF-8 in literatures [3,26,28,29,40–43].

Table 2-7 Summary of C_3H_6/C_3H_8 separation performance of ca. 20 wt% ZIF-8 filled MMMs.

Synthesis of ZIF-8		**Polymer**	**ZIF-8 content**	**C_3H_6 permeability**	**C_3H_6/C_3H_8 ideal**	**Reference**
Method/source	**Solvent**		**in MMMs (wt%)**	**(barrer)**	**selectivity**	
Basolite®Z1200	DMF	6FDA-TrMPD	16	28	19	[26]
In-situ ion-exchange (PMMOF)	MeOH	6FDA-TrMPD	20	5	31	[28]
In-situ linker doping (PMMOF)	MeOH	6FDA-TrMPD	19	17	18	[29]
In-situ linker doping (Blending)	MeOH	6FDA-TrMPD	19	43	15	[29]
Solvothermal	MeOH	6FDA-TrMPD	19	22	17	[29]
Solvothermal	MeOH	PEABA	20	32	5	[3]
Basolite®Z1200	DMF	PIM-6FDA-OH	20	10	34	[40]
Solvothermal	MeOH	PVAc	20	6	4	[41]
Solvothermal	MeOH	PVC-g-POEM	20	59	4	[42]
Solvothermal	MeOH	6FDA-Durene/DABA	20	19	26	[43]
Mechanochemical	Not used	6FDA-TrMPD	20	20	18	This study

Notes:

(1) "DMF" and "MeOH" are the *N*,*N*-dimethylformamide and methanol, respectively;

(2) The Basolite®Z1200 is the commercial ZIF-8 powder synthesized by solvothermal method [18].

The separation performance was also shown in Figure 2-13 which can provide a clear

comparison of the different ZIF-8 MMMs. The X axis and Y axis presents the C_3H_6 permeability and C_3H_6/C_3H_8 ideal selectivity, respectively. The circle and diamond symbols displayed the separation performance values of the MMMs using mechano-synthesized ZIF-8 in this study and using solvothermal synthesized ZIF-8 in literature.

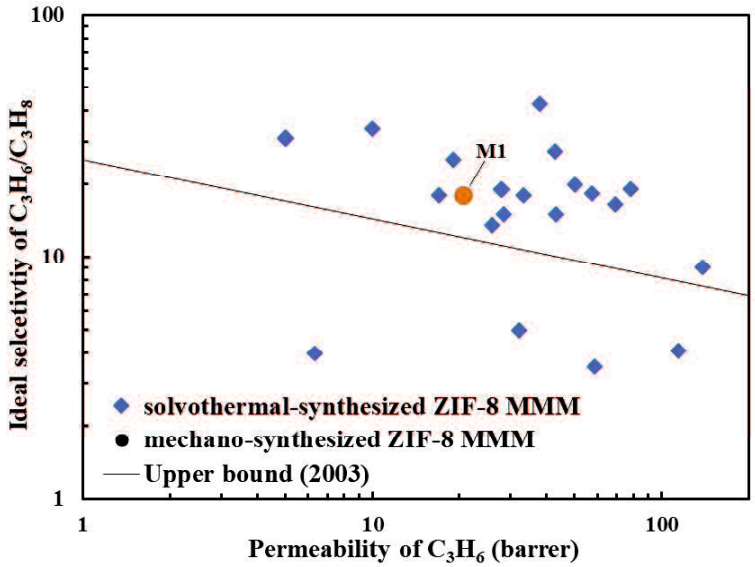

Figure 2-13. Separation performance comparison of 20 wt% mechano-synthesized ZIF-8 MMM (M1) and 20 wt% solvothermal-synthesized ZIF-8 MMMs in literatures [3,26,28,29,40–43]. The upper bound line indicates the results obtained by Koros et al. [25].

The M1 membrane using mechano-synthesized ZIF-8 provides a medium separation performance among these MMMs. There some MMMs showed higher performance than the M1 membrane. This may be due to the different polymer matrix and preparation method. Under the condition of ensuring proper performance, the eco-friendly synthesis and cost-effectiveness of the materials should be considered for the large-scale practical application. To the best of our knowledge, all the ZIF-8 used in the currently reported MMMs were obtained from the solvothermal synthesis method. It required 1500 mL of *N*,*N*-dimethylformamide (DMF) to synthesis 1 g of ZIF-8 at 413 K in a typical procedure

[18]. Other studies also used DMF or methanol to synthesis and wash the ZIF-8 powder. Mechanochemically synthesis method was carried out at room temperature and without organic solvent, so it can reduce synthesis cost as well as environmental pollution [22]. In addition, the mechanochemically synthesis method has other merits including simple synthesis process, high yield, and large-scale production availability [23]. These merits can be expected to promote the application of mechano-synthesized ZIF-8 in the membrane separation and other related industries.

2.4 Conclusions

Mechanochemical-synthesized ZIF-8 particles were blended into the 6FDA-TrMPD polymer to prepare the mixed matrix membranes for the C_3H_6/C_3H_8 separation. The mechano-synthesized ZIF-8 nanoparticles promoted the C_3H_6/C_3H_8 separation performance of the MMMs in accordance with the Maxwell model. Temperature and pressure dependence analysis confirmed the molecular sieving effect of the mechano-synthesized ZIF-8 in the polymer matrix for the permeation of C_3H_6 and C_3H_8. Compared to the conventional solvothermal-synthesis method, the advantages of solvent-less and low energy-cost are expected to extend the practical application of the mechano-synthesized ZIF-8 in the membrane industries.

2.5 References

[1] B. Liu, R. Zhou, K. Yogo, H. Kita, Preparation of CHA zeolite (chabazite) crystals and membranes without organic structural directing agents for CO_2 separation, J. Memb. Sci. 573 (2019) 333–343.

[2] B. Zhou, Q. Li, Q. Zhang, J. Duan, W. Jin, Sharply promoted CO_2 diffusion in a mixed matrix membrane with hierarchical supra-nanostructured porous coordination polymer filler, J. Memb. Sci. 597 (2020) 117772.

[3] H.R. Amedi, M. Aghajani, Modified zeolitic–midazolate framework 8/poly(ether-block-amide) mixed-matrix membrane for propylene and propane separation, J. Appl. Polym. Sci. 135 (2018) 1–13.

[4] Y. Alcheikhhamdon, I. Pinnau, M. Hoorfar, B. Chen, Propylene - propane separation using Zeolitic-Imidazolate Framework (ZIF-8) membranes: Process techno-commercial evaluation, J. Memb. Sci. 591 (2019) 117252.

[5] L.M. Robeson, The upper bound revisited, J. Memb. Sci. 320 (2008) 390–400.

[6] D. Bastani, N. Esmaeili, M. Asadollahi, Polymeric mixed matrix membranes containing zeolites as a filler for gas separation applications: A review, J. Ind. Eng. Chem. 19 (2013) 375–393.

[7] Y. Cheng, Z. Wang, D. Zhao, Mixed matrix membranes for natural gas upgrading: current status and opportunities, Ind. Eng. Chem. Res. 57 (2018) 4139–4169.

[8] M. Sen, N. Das, In situ carbon deposition in polyetherimide/SAPO-34 mixed matrix membrane for efficient CO_2/CH_4 separation, J. Appl. Polym. Sci. 134 (2017) 1–10.

[9] T. Suzuki, A. Saito, Preparation of polybenzoxazole–silica hybrid membranes for

CO_2/CH_4 separation, Polym. J. 51 (2019) 1037–1044.

[10] N. Sakaguchi, M. Tanaka, M. Yamato, H. Kawakami, Superhigh CO_2-Permeable Mixed Matrix Membranes Composed of a Polymer of Intrinsic Microporosity (PIM-1) and Surface-Modified Silica Nanoparticles , ACS Appl. Polym. Mater. 1 (2019) 2516–2524.

[11] R. Nasir, H. Mukhtar, Z. Man, M.S. Shaharun, M.Z. Abu Bakar, Effect of fixed carbon molecular sieve (CMS) loading and various di-ethanolamine (DEA) concentrations on the performance of a mixed matrix membrane for CO_2/CH_4 separation, RSC Adv. 5 (2015) 60814–60822.

[12] R. Lin, B. Villacorta Hernandez, L. Ge, Z. Zhu, Metal organic framework based mixed matrix membranes: An overview on filler/polymer interfaces, J. Mater. Chem. A. 6 (2018) 293–312.

[13] X. Zhang, T. Zhang, Y. Wang, J. Li, C. Liu, N. Li, J. Liao, Mixed-matrix membranes based on Zn/Ni-ZIF-8-PEBA for high performance CO_2 separation, J. Memb. Sci. 560 (2018) 38–46.

[14] M. Safak Boroglu, A.B. Yumru, Gas separation performance of 6FDA-DAM-ZIF-11 mixed-matrix membranes for H_2/CH_4 and CO_2/CH_4 separation, Sep. Purif. Technol. 173 (2017) 269–279.

[15] W. Guan, Y. Dai, C. Dong, X. Yang, Y. Xi, Zeolite imidazolate framework (ZIF)-based mixed matrix membranes for CO_2 separation: A review, J. Appl. Polym. Sci. 137 (2020) 1–13.

[16] D. Fairen-Jimenez, S.A. Moggach, M.T. Wharmby, P.A. Wright, S. Parsons, T. Düren, Opening the gate: Framework flexibility in ZIF-8 explored by experiments and simulations, J. Am. Chem. Soc. 133 (2011) 8900–8902.

[17] C. Zhang, R.P. Lively, K. Zhang, J.R. Johnson, O. Karvan, W.J. Koros, Unexpected molecular sieving properties of zeolitic imidazolate framework-8, J. Phys. Chem. Lett. 3 (2012) 2130–2134.

[18] K.S. Park, Z. Ni, A.P. Cote, J.Y. Choi, R. Huang, F.J. Uribe-Romo, H.K. Chae, M. O'Keeffe, O.M. Yaghi, Exceptional chemical and thermal stability of zeolitic imidazolate frameworks, Proc. Natl. Acad. Sci. 103 (2006) 10186–10191.

[19] N. Hara, M. Yoshimune, H. Negishi, K. Haraya, S. Hara, T. Yamaguchi, Diffusive separation of propylene/propane with ZIF-8 membranes, J. Memb. Sci. 450 (2014) 215–223.

[20] S. Zhou, Y. Wei, L. Li, Y. Duan, Q. Hou, L. Zhang, L.X. Ding, J. Xue, H. Wang, J. Caro, Paralyzed membrane: Current-driven synthesis of a metal-organic framework with sharpened propene/propane separation, Sci. Adv. 4 (2018).

[21] Y.R. Lee, M.S. Jang, H.Y. Cho, H.J. Kwon, S. Kim, W.S. Ahn, ZIF-8: A comparison of synthesis methods, Chem. Eng. J. 271 (2015) 276–280.

[22] D.R. Joshi, N. Adhikari, An overview on common organic solvents and their toxicity, J. Pharm. Res. Int. 28 (2019) 1–18.

[23] S. Tanaka, K. Kida, T. Nagaoka, T. Ota, Y. Miyake, Mechanochemical dry conversion of zinc oxide to zeolitic imidazolate framework, Chem. Commun. 49 (2013) 7884–7886.

[24] K. Tanaka, J. Taguchi, J.Q. Hao, H. Kita, K. Okamoto, Permeation and separation properties of polyimide membranes to olifins and paraffins, J. Memb. Sci. 121 (1996) 197–207.

[25] R.L. Burns, W.J. Koros, Defining the challenges for C_3H_6/C_3H_8 separation using polymeric membranes, J. Memb. Sci. 211 (2003) 299–309.

[26] C. Zhang, Y. Dai, J.R. Johnson, O. Karvan, W.J. Koros, High performance ZIF-8/6FDA-DAM mixed matrix membrane for propylene/propane separations, J. Memb. Sci. 389 (2012) 34–42.

[27] C. Zhang, K. Zhang, L. Xu, Y. Labreche, B. Kraftschik, W.J. Koros, Highly scalable ZIF-based mixed-matrix hollow fiber membranes for advanced hydrocarbon separations, AIChE J. 60 (2012) 2625–2635.

[28] S. Park, M.R. Abdul Hamid, H.K. Jeong, Highly propylene-selective mixed-matrix membranes by *in situ* metal-organic framework formation using a polymer-modification srategy, ACS Appl. Mater. Interfaces. 11 (2019) 25949–25957.

[29] S. Park, H.K. Jeong, In-situ linker doping as an effective means to tune zeolitic-imidazolate framework-8 (ZIF-8) fillers in mixed-matrix membranes for propylene/propane separation, J. Memb. Sci. 596 (2020) 117689.

[30] J.C. Tan, T.D. Bennett, A.K. Cheetham, Chemical structure, network topology, and porosity effects on the mechanical properties of zeolitic imidazolate frameworks, Proc. Natl. Acad. Sci. U. S. A. 107 (2010) 9938–9943.

[31] D.R. Paul, D.R. Kemp, The diffusion time lag in polymer membranes containing adsorptivellers, J. Polym. Sci. Polym. Symp. 41 (1973) 79–93.

[32] K. Tanaka, M.N. Islam, M. Kido, H. Kita, K. ichi Okamoto, Gas permeation and separation properties of sulfonated polyimide membranes, Polym. 47 (2006) 4370–4377.

[33] K.I. Okamoto, K. Tanaka, H. Kita, M. Ishida, M. Kakimoto, Y. Imai, Gas permeability and permselectivity of polyimides prepared from 4,4 艂-diaminotriphenylamine, Polym. J. 24 (1992) 451–457.

[34] H.T. Kwon, H.K. Jeong, A.S. Lee, H.S. An, J.S. Lee, Heteroepitaxially grown

zeolitic imidazolate framework membranes with unprecedented propylene/propane separation performances, J. Am. Chem. Soc. 137 (2015) 12304–12311.

[35] J. Dai, S. Li, J. Liu, J. He, J. Li, L. Wang, J. Lei, Fabrication and characterization of a defect-free mixed matrix membrane by facile mixing PPSU with ZIF-8 core–shell microspheres for solvent-resistant nanofiltration, J. Memb. Sci. 589 (2019) 117261.

[36] C.M. Zimmerman, W.J. Koros, Comparison of gas transport and sorption in the ladder polymer BBL and some semi-ladder polymers, Polym. 40 (1999) 5655–5664.

[37] W.J. Koros, D.R. Paul, Transient and steady-state permeation in poly(ethylene terephthalate) above and below the glass transition., J. Polym. Sci. Polym. Phys. Ed. 16 (1978) 2171–2187.

[38] W.J. Koros, D.R. Paul, CO_2 sorption in poly(ethylene terephthalate) above and below the glass transition, J. Polym. Sci. Polym. Phys. Ed. 16 (1978) 1947–1963.

[39] K. Li, D.H. Olson, J. Seidel, T.J. Emge, H. Gong, H. Zeng, J. Li, Zeolitic imidazolate frameworks for kinetic separation of propane and propene, J. Am. Chem. Soc. 131 (2009) 10368–10369.

[40] X. Ma, R.J. Swaidan, Y. Wang, C. en Hsiung, Y. Han, I. Pinnau, Highly compatible hydroxyl-functionalized microporous polyimide-ZIF-8 mixed matrix membranes for energy efficient propylene/propane separation, ACS Appl. Nano Mater. 1 (2018) 3541–3547.

[41] J. Yu, C. Wang, L. Xiang, Y. Xu, Y. Pan, Enhanced C_3H_6/C_3H_8 separation performance in poly(vinyl acetate) membrane blended with ZIF-8 nanocrystals,

Chem. Eng. Sci. 179 (2018) 1–12.

[42] W.S. Chi, S.J. Kim, S.J. Lee, Y.S. Bae, J.H. Kim, Enhanced performance of mixed-matrix membranes through a graft copolymer-directed interface and interaction tuning approach, ChemSusChem. 8 (2015) 650–658.

[43] M. Askari, T.S. Chung, Natural gas purification and olefin/paraffin separation using thermal cross-linkable co-polyimide/ZIF-8 mixed matrix membranes, J. Memb. Sci. 444 (2013) 173–183.

Chapter 3 Investigation of gas diffusivity and solubility of SAPO-34/PES mixed matrix membranes

3.1 Introduction

The membrane materials are widely studied to separate the CO_2 from natural gas, due to the contaminant is significant to increase the heat value and reduce the corrosion of the transport pipeline [1–4]. Polymeric membrane is one of the most applied membrane materials because of the good processability, low cost, and high flexibility. However, the polymeric membrane always meets a trade-off between gas permeability and selectivity [5]. Inorganic membrane materials have high permeability and selectivity than the conventional polymeric membranes, but the poor processability and high cost from expensive support result in the implementation difficulty [6]. Blending microporous inorganic particles to the polymer matrix to prepare a mixed matrix membranes (MMMs) is an effective strategy to break the limitation, because it could combine both advantages of the polymeric membrane and inorganic membrane [7]. Hence, various porous materials, such as zeolite, silica, carbon molecule sieve and metal organic frameworks, have been applied in MMMs preparation recently [8].

Among the polymers, the polyerthersulfone (PES) is known for its outstanding toughness, and tensile strength as well as the thermal stability, antioxidative ability and excellent flexibility [9,10]. Besides, PES is also typically not attacked by mineral- and silicone-based oils, dilute acids and bases [10]. Therefore, the PES is the material of choice for numerous membrane applications [11]. However, the CO_2/CH_4 separation performance of PES based membrane is also limited by the trade-off between

permeability and selectivity. One of effective modification method is addition of the filler to the membrane casting solution. The silicoaluminophosphate-34 (SAPO-34) zeolite has a CHA-type structure with a pore size of 0.38 nm. This is between the molecular diameter of CO_2 (0.33 nm) and CH_4 (0.38 nm). Hence, there are some studies on the SAPO-34/PES MMMs for the CO_2/CH_4 separation. Kalipcipar et al. had used a laboratory-made (lab-made) SAPO-34 to increase the CO_2 permeability but at loss of the CO_2/CH_4 ideal selectivity [12]. It was due to the interfacial voids around the zeolite. They applied the 2-hydroxy-5-methyl aniline (HMA) to improve the compatibility of the zeolite filler and polymer matrix [13]. The HMA modified SAPO-34 MMMs provided a CO_2/CH_4 ideal selectivity of 45. This was 35% higher than the neat membrane. However, the CO_2 permeability was lower than the neat membrane. This was due to the HMA resulted in the rigidification of the polymer chains. Mukhtar et al. had used a commercial SAPO-34 (ACS Materials) to blend in the PES matrix for the CO_2/CH_4 separation, but the interfacial void also appeared [14]. They modified the commercial SAPO-34 using ethylenediamine (EDA) and hexylamine (HA) to improve the compatibility of the zeolite particles and PES matrix. They further combined the ion liquids (ILs) with EDA or HA to improve the structure of their membranes [15]. The CO_2/CH_4 ideal selectivity of their membranes was up to 37 and still lower than the HMA-modified SAPO-34 MMMs reported by Kalipcipar et al. [13].

In the above studies, the researchers had described the modification of the membrane structure and the improvement of the gas permeability and selectivity. There was no detail discussion on the contribution of the SAPO-34 to the permeability and selectivity of the SAPO-34/PES MMMs in terms of the gas diffusivity and solubility. In our previous study, the effect of the lab-made SAPO-34 zeolite on the CO_2 and CH_4 diffusivity and solubility

had been investigated as well as the permeability and ideal selectivity [16]. After adding SAPO-34 zeolite, the permeability and ideal selectivity were increased with the solubility increased and the diffusivity decreased. We demonstrated that the diffusion selectivity was essential to the ideal selectivity. However, this SAPO-34 zeolite was synthesized with double organic structure directing agent at high temperature (200 °C). The high energy cost and poor general applicability is not suit for a large-scale application of the SAPO-34/PES MMMs.

In this study, we tried to blend a commercially available SAPO-34 zeolite in the PES membrane. The comparison of the influence of the commercial and the lab-made SAPO-34 zeolite on the CO_2 and CH_4 diffusivity and solubility of the PES membrane as well as the gas permeability and ideal selectivity was conducted.

3.2 Experimental

3.2.1 Materials and Instrumental

Table 3-1 lists the materials and instrumental for the preparation and characterization of the SAPO-34/PES mixed matrix membranes. The commercial SAPO-34 (S1) powder was kindly provided by Nikki Universal Co., Ltd. The home-made SAPO-34 zeolite (S2) and S2 filled PES MMMs produced by Dr. Wu in our lab was used as a reference [16].

Table 3-1 Materials and Instrumental of SAPO-34/PES mixed matrix membranes

Materials	Abbreviation/Code	Manufacturer, Model	Purity (wt%)
Polyethersulfone	PES	BASF Chemical	—
Commercial SAPO-34 zeolite	S1	Nikki Universal	—
Lab-made SAPO-34 zeolite	S2	Dr. Wu [14]	—

3.2.2 Preparation of neat PES membrane

The PES solid was divided into four equal parts to be dissolved in the NMP solvent to prepare a 15 wt% PES/NMP solution. After stirring for 20 hours, the solution was treated by ultrasonic for 4 hours and then bubble removal for 30 min. The solution was cast on a A4-paper size glass plate with a glass rod. After vacuum drying at 200 °C for 20 hours, the membrane was peeled from the glass plate.

3.2.3 Preparation of SAPO-34/PES membrane

The commercial SAPO-34 (S1) was dried at 200 °C overnight before added in to the NMP solvent. The PES solid was divided into four equal parts to be added in the SAPO-34/NMP slurry sequentially. After mixing for 20 hours, the SAPO-34/PES/NMP solution was cast on a glass plate follow by the ultrasonic treatment for 4 hours. The membrane was peeled from the glass plate after vacuum drying at 200 °C for 20 hours. The membranes prepared using 20 wt% and 30 wt% of S1 and S2 zeolite filler were named as S1-20, S1-30, S2-20 and S2-30, respectively.

3.2.4 Characterization Methods

The X-ray diffraction (XRD) was used to analyze structure of the filler and membranes. The scanning electron microscopy (SEM) was applied to observe the morphology.

3.2.5 Single Gas Permeation

The single gas permeation through the membranes was tested by a home-made apparatus (Figure 2-3) with the vacuum method at 0.1 MPa and 35 °C. Before the gas

permeation, the membrane in the apparatus was degassed at 100 °C for more than 2 hours and then cooling to 35 °C. The gas permeability (P), diffusivity (D) and solubility (S) were calculated using the equations as described in Chapter 2 [17,18].

3.3 Results and Discussion

3.3.1 XRD Analysis

Figure 3-1 shows the XRD patterns of the neat PES membrane, commercial SAPO-34 powder (S1) and the 30 wt% S1 filled MMM (S1-30). The XRD patterns can be used to analysis the crystal structure of filler particles and confirm its presence in the membranes.

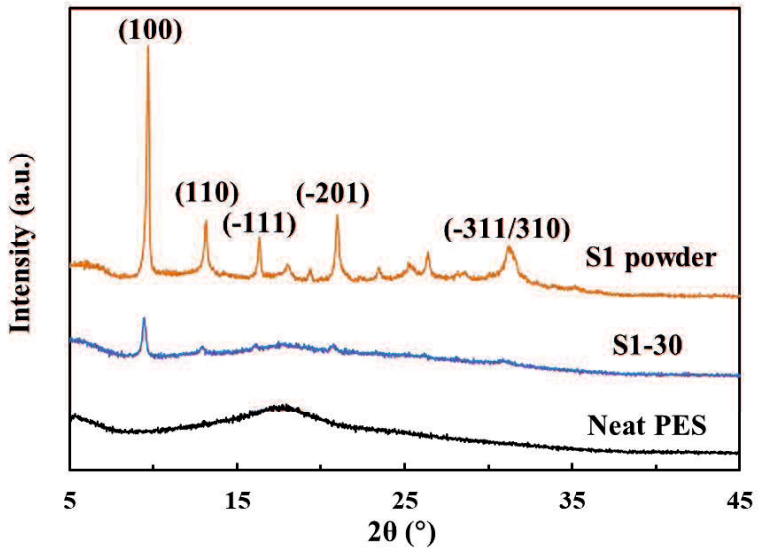

Figure 3-1. XRD patterns of the neat PES membrane, the commercial SAPO-34 powder (S1), and the S1-30 MMM using 30 wt% S1.

The neat PES has an amorphous halo. The S1 had main peaks at 2θ = 9.7°, 13.2°, 15.2°, 21.0°, 31.3°. These peak positions assigned to the crystalline plane of (100), (110), (−111), (−201) and (−311/310), respectively. It is in a good accordance with XRD pattern of the lab-made SAPO-34 zeolite (S2) in the previous study [16]. Compared to the S2 particles,

the priority growth of (100) occurred in the S1 particles. This kind of oriented growth had been reported by some literature [19,20]. This growth orientation facilitates more 8-member rings to be exposed, thereby promoting gas permeation [21]. The S1-30 membrane also possessed the XRD peaks of SAPO-34. The peak intensity of S1-30 membrane was lower than of S1 powder due to the presence of the amorphous PES matrix.

3.3.2 SEM Observation

Figure 3-2 shows the SEM images of the S1 powder and the cross-section of the MMMs including 20 wt% S1 filled MMMs (S1-20), and 30 wt% S1 filled MMMs (S1-30). These images can be used to observe the morphology of particles and membranes, and the compatibility of particles with polymer matrix.

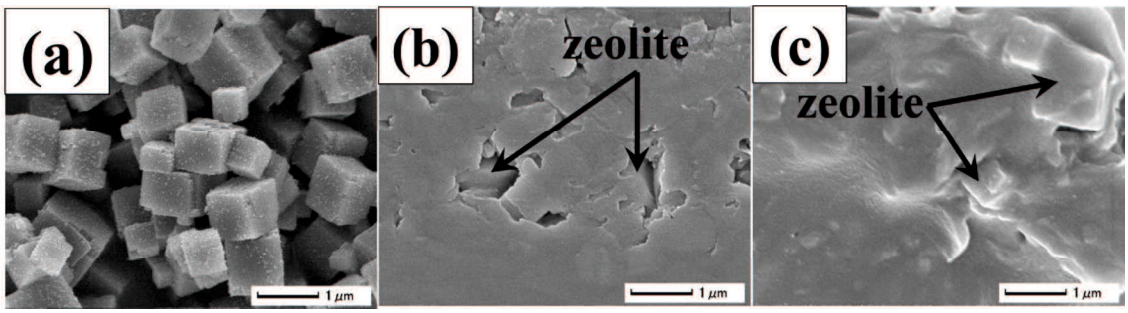

Figure 3-2. SEM images of the SAPO-34 zeolite powder and the cross-section of the SAPO-34/PES MMMs: (a) commercial zeolite S1; (b) S1-20 MMMs using 20 wt% S1; (c) S1-30 MMMs using 30 wt% S1. The magnification of each image is 20000.

The S1 powder had cubic crystals with the particle size around 1 μm. The cross-sectional SEM images of the MMMs shows that the amorphous polymer matrix almost covered all the S1 particles. Most areas of the membranes were dense except for a few amounts of the interfacial voids appeared between the filler particle and polymer matrix.

This defect also appeared in the reported SAPO-34 MMMs [10–14]. In addition, the agglomeration occurred in the MMMs using 20 wt% and 30 wt% S2 zeolite filler (S2-20 and S2-30) in our previous study [16]. This was due to the tiny particles with large surface area tend to agglomerate. The large agglomerates had internal voids to reduce the gas selectivity. The appearance of the cross-sectional SEM images of the S2 filled MMMs is different from that of the S1 filled MMMs.

3.3.4 Gas Separation Performance

The gas permeation mechanism in the polymeric membrane can be mainly described by the solution-diffusion model [22]. The gas diffusivity and solubility in the polymeric membrane determine the gas permeability. The adsorption and diffusion behavior of CO_2 and CH_4 molecules in the SAPO-34 would affect the gas diffusivity and solubility to change the gas permeability if the zeolite is blended into the PES membrane. Figure 3-3 presents the CO_2 and CH_4 permeability (P), diffusivity (D) and solubility (S) of the PES based membranes as a function of SAPO-34 filler content. Figure 3-4 shows their corresponding selectivity. The ideal selectivity (αP) was the ratio of CO_2 permeability to CH_4 permeability; diffusivity selectivity (αD) was the ratio of CO_2 diffusivity to CH_4 diffusivity; solubility selectivity (αS) was the ratio of CO_2 solubility to CH_4 solubility.

Compared to the neat PES membrane, the CO_2 and CH_4 permeability were increased as well as CO_2/CH_4 ideal selectivity with increasing filler content. The CO_2 permeability and CO_2/CH_4 ideal selectivity of the S1-30 membrane was 15 barrer and 51, respectively. These values were 170% and 39% higher than that of the neat PES membrane. These values of S2-30 membrane was 9 barrer and 48, respectively. These values were 64% and 31% higher than that of the neat PES membrane, respectively.

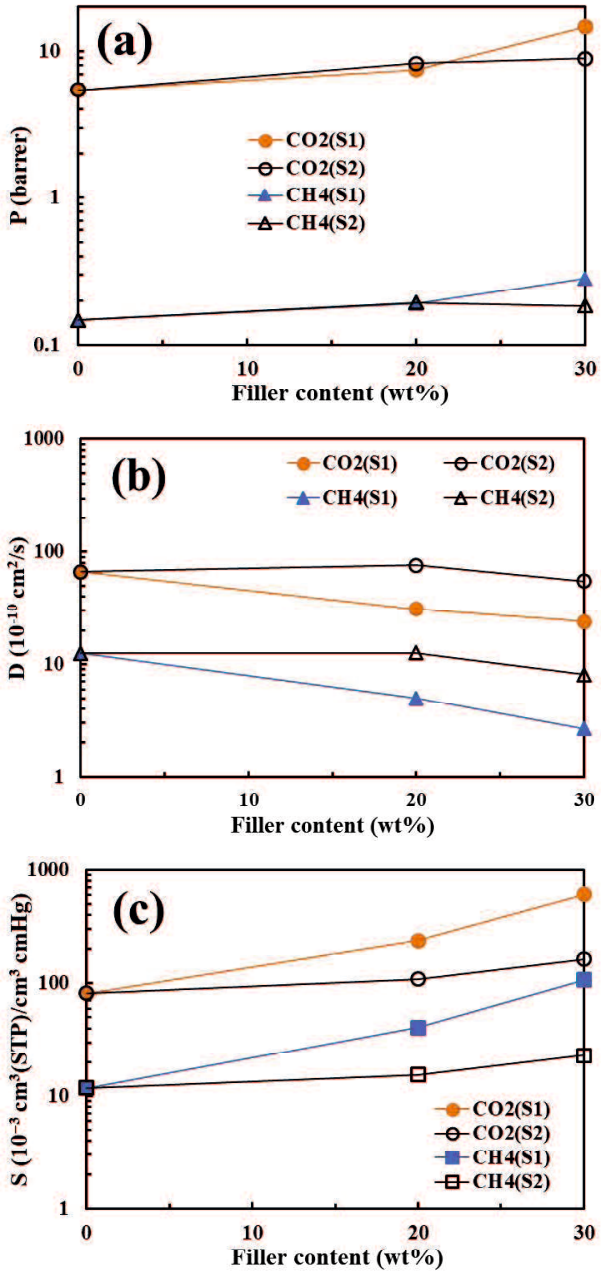

Figure 3-3. (a) Permeability, (b) diffusivity, (c) solubility of CO_2 and CH_4 of the SAPO-34/PES MMMs as function of different filler content. The S1 and S2 is the commercial and lab-made SAPO-34 zeolite filler, respectively. The values of the S2 filled MMMs were reported in our previous study [16].

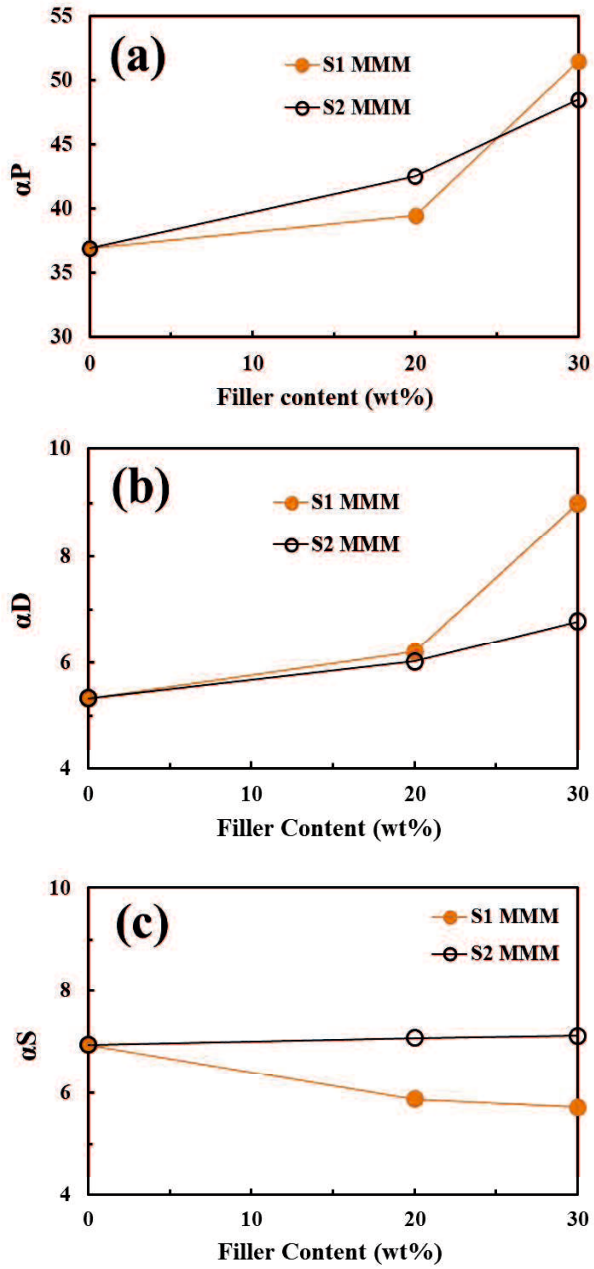

Figure 3-4. (a) Ideal selectivity, (b) diffusivity selectivity, (c) solubility selectivity of CO2/CH4 of the SAPO-34/PES MMMs as function of different filler content. The S1 and S2 is the commercial and lab-made SAPO-34 zeolite filler, respectively. The values of the S2 filled MMMs were reported in our previous study [16].

Figure 3-3(b) shows that the CO_2 and CH_4 diffusivity of the PES membrane was decreased with adding S1 and S2 filler. The CO_2 and CH_4 diffusivity in the pure SAPO-34 phase was 6×10^{-6} and 4.5×10^{-7} cm^2/s, respectively [23]. These values were both higher than in the neat PES. The gas diffusivity of the PES membrane should be increased with adding SAPO-34. However, Kaliaguine et al. had reported that the gas diffusivity of the 6FDA-DAM-HAB co-polyimide was decreased with adding MIL-53 [24]. Kawakami et al. also reported that the addition of the silica nanoparticles reduced the gas diffusivity of the PIM-1 polymer [25]. Therefore, the decrease in the gas diffusivity of the polymeric membrane after adding porous filler may occur.

Paul et al. had reported that the immobilizing adsorption of diffusing penetrants will cause very large increases in the diffusion time lag but will have only minor effects on the steady-state permeation [17]. The diffusivity used in this study is calculated from Equation (2) using the diffusion time lag. The diffusivity is apparently affected by partial immobilization of the adsorbed molecules. Therefore, the increase in the adsorption of the gas molecules may increase the time-lag and then reduce the value of the gas diffusivity apparently. This maybe one reason that why the gas diffusivity was decreased after adding SAPO-34 zeolite in this study. The Z1 particles can affect the gas adsorption greater than Z2 particles because of the priority growth of the (100) crystal plane, so the decreased ratio in the diffusivity of Z1 MMMs was larger than Z2 MMMs.

Figure 3-4(b) shows that the CO_2/CH_4 diffusivity selectivity was increased with adding S1 and S2 filler. The CO_2/CH_4 diffusivity selectivity in the pure SAPO-34 phase was 13 and higher than that in the neat PES membrane [18]. This is why the CO_2/CH_4 diffusivity selectivity of the S1-30 and S2-30 higher than the neat PES membrane, respectively. The increased ratio was 69% and 24% for S1-30 and S2-30, respectively. Besides, the

difference in the increased ratio is due to that the amount of defect in the former less than in the latter. This is in accordance with the results of SEM observation.

Figure 3-3(c) shows that the CO_2 and CH_4 solubility of the PES membrane was increased with increasing the filler content of S1 and S2. The CO_2 and CH_4 solubility of the neat PES was 0.082 and 0.012 cm^3(STP)/ (cm^3 cmHg). These values in the pure SAPO-34 phase at 0.1 MPa were 1.02 and 0.19 cm^3(STP)/ (cm^3 cmHg) [26]. Therefore, the CO_2 and CH_4 solubility of the PES membrane would be increased with adding SAPO-34. Due to the priority growth of (100) plane, the S1 particles can adsorb more amount of gas molecules than the S2 particles. In this case, the CO_2 and CH_4 solubility of the S1 based MMMs should be higher than that of the S2 based MMMs. Figure 3-4(c) displayed that the CO_2/CH_4 solubility selectivity after adding S1 and S2 filler was decreased. It was due to that the solubility selectivity in the pure SAPO-34 was 5 and less than in the neat PES about 7. The solubility selectivity of S1-30 was almost same as that of S2-30. Hence, the diffusion selectivity played an important role to the difference in the ideal selectivity of the S1-30 and S2-30 membranes.

3.3.5 Comparison with reported SAPO-34/PES MMMs

Figure 3-5 can compare the separation performance of the SAPO-34/PES MMMs in our study with the reported MMMs in literature by using the plot of CO_2/CH_4 ideal selectivity and CO_2 permeability. The circle symbol, triangle presents the separation performance of the commercial and lab-made SAPO-34 filled PES MMMs in our study; square symbols is separation performance of the reported SAPO-34-PES in literature. The hollow symbol and solid symbol present the MMMs using pristine SAPO-34 and modified SAPO-34, respectively.

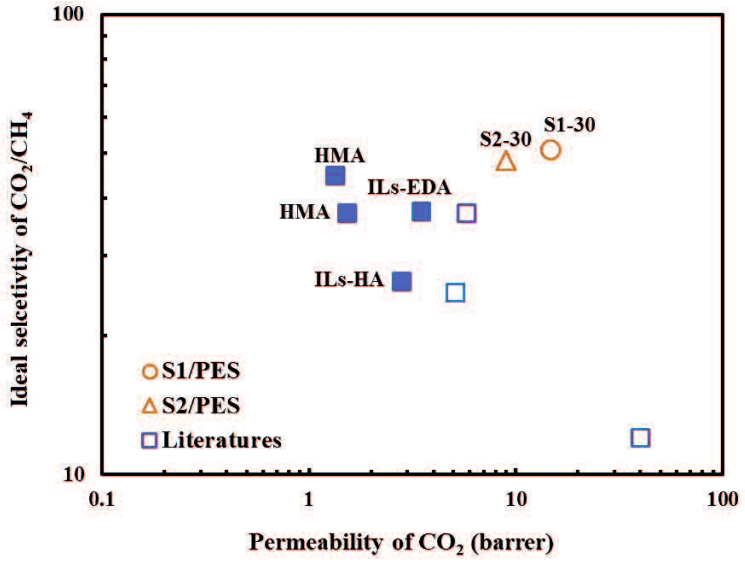

Figure 3-5. The CO_2/CH_4 separation performance comparison of the SAPO-34/PES MMMs in this study and in the literature [10–14]. The hollow symbol and solid symbol present the MMMs using pristine SAPO-34 and modified SAPO-34, respectively.

In the literatures, different reagents included HMA, EDA, HA and ILs were applied to modify the SAPO-34 zeolite and improve the structure of the PES based MMMs. These membranes still showed a lower separation performance than our membranes. This may be due to the different quality of the filler or different experimental conditions. Our membrane still has interfacial defects. The improvement of the MMMs by using modified zeolite filler in the literature suggested that using the suitable functional materials and the modified process can improve the structure and separation performance of our SAPO-34/PES MMMs in the future.

3.4 Conclusions

This study had used a commercial SAPO-34 to prepare the PES based MMMs for the CO_2/CH_4 separation. It is not only confirmed that the diffusivity selectivity was essential to the ideal selectivity but also identified that the commercial SAPO-34 was better than the lab-made SAPO-34 sample. A comparison with the reported MMMs and our MMMs reveals that it is possible to further improve the separation performance of the SAPO-34/PES MMMs. High-performance MMMs composited of the commercially available SAPO-34 and PES has a potential in the practical natural purification.

3.5 References

[1] D.Y.C. Leung, G. Caramanna, M.M. Maroto-Valer, An overview of current status of carbon dioxide capture and storage technologies, Renew. Sustain. Energy Rev. 39 (2014) 426–443.

[2] T. Koga, H. Kita, T. Suzuki, K. Uemura, K. Tanaka, I. Kawafune, M. Funaoka, Carbon Membranes from Wood Materials and their Separation Properties, Trans. Mater. Res. Soc. Japan. 33 (2008) 825–828.

[3] Y. Zhang, M. Wang, H. Qiu, L. Kong, N. Xu, X. Tang, D. Meng, X. Kong, Y. Zhang, Synthesis of thin SAPO-34 zeolite membranes in concentrated gel, J. Memb. Sci. 612 (2020) 118451.

[4] B. Zhou, Q. Li, Q. Zhang, J. Duan, W. Jin, Sharply promoted CO_2 diffusion in a mixed matrix membrane with hierarchical supra-nanostructured porous coordination polymer filler, J. Memb. Sci. 597 (2020) 117772.

[5] L.M. Robeson, The upper bound revisited, J. Memb. Sci. 320 (2008) 390–400.

[6] M. Pera-Titus, Porous inorganic membranes for CO_2 capture: Present and prospects, Chem. Rev. 114 (2014) 1413–1492.

[7] H.J.C. te Hennepe, D. Bargeman, M.H.V. Mulder, C.A. Smolders, Zeolite-filled silicone rubber membranes, J. Memb. Sci. 35 (1987) 39–55.

[8] Y. Cheng, Z. Wang, D. Zhao, Mixed Matrix Membranes for Natural Gas Upgrading: Current Status and Opportunities, Ind. Eng. Chem. Res. 57 (2018) 4139–4169.

[9] T. Marino, E. Blasi, S. Tornaghi, E. Di, A. Figoli, Polyethersulfone membranes prepared with Rhodiasolv ® Polarclean as water soluble green solvent, J. Memb.

Sci. 549 (2018) 192–204.

[10] C. Zhao, J. Xue, F. Ran, S. Sun, Modification of polyethersulfone membranes - A review of methods, Prog. Mater. Sci. 58 (2013) 76–150.

[11] Y. Mansourpanah, S.S. Madaeni, A. Rahimpour, M. Adeli, M.Y. Hashemi, M.R. Moradian, Fabrication new PES-based mixed matrix nanocomposite membranes using polycaprolactone modi fi ed carbon nanotubes as the additive : Property changes and morphological studies, Desalination. 277 (2011) 171–177.

[12] E. Karatay, H. Kalipçilar, L. Yilmaz, Preparation and performance assessment of binary and ternary PES-SAPO-34-HMA based gas separation membranes, J. Memb. Sci. 364 (2010) 75–81.

[13] U. Cakal, L. Yilmaz, H. Kalipcilar, Effect of feed gas composition on the separation of CO_2/CH_4 mixtures by PES-SAPO-34-HMA mixed matrix membranes, J. Memb. Sci. 417–418 (2012) 45–51.

[14] N.N.R. Ahmad, H. Mukhtar, D.F. Mohshim, R. Nasir, Z. Man, Effect of different organic amino cations on SAPO-34 for PES/SAPO-34 mixed matrix membranes toward CO_2/CH_4 separation, J. Appl. Polym. Sci. 133 (2016) 1–6.

[15] R. Nasir, N.N.R. Ahmad, H. Mukhtar, D.F. Mohshim, Effect of ionic liquid inclusion and amino-functionalized SAPO-34 on the performance of mixed matrix membranes for CO_2/CH_4 separation, J. Environ. Chem. Eng. 6 (2018) 2363–2368.

[16] T. Wu, Y. Liu, I. Kumakiri, K. Tanaka, X. Chen, H. Kita, Preparation and permeation properties of PESU-based mixed matrix membranes with nano-sized CHA zeolites, J. Chem. Eng. Japan. 52 (2019) 514–520.

[17] D.R. Paul, D.R. Kemp, The diffusion time lag in polymer membranes containing adsorptive fllers, J. Polym. Sci. Polym. Symp. 93 (1973) 79–93.

[18] K. Tanaka, M.N. Islam, M. Kido, H. Kita, K. ichi Okamoto, Gas permeation and separation properties of sulfonated polyimide membranes, Polym. 47 (2006) 4370–4377.

[19] B. Engineering, Alumina-Supported SAPO-34 Membranes for CO_2/CH_4 Separation Moises A. Carreon, J. Am. Chem. Soc. 130 (2008) 5412–5413.

[20] S. Li, Z. Zong, S. James, Y. Huang, Z. Song, X. Feng, R. Zhou, H.S. Meyer, M. Yu, M.A. Carreon, SAPO-34 Membranes for N_2/CH_4 separation : Preparation , characterization , separation performance and economic evaluation, J. Memb. Sci. 487 (2015) 141–151.

[21] M. Lee, S. Hong, D. Kim, E. Kim, K. Lim, J.C. Jung, H. Richter, J. Moon, N. Choi, J. Nam, J. Choi, Chabazite-Type Zeolite Membranes for Effective CO_2 Separation : The Role of Hydrophobicity and Defect Structure, ACS Appl. Mater. Interfaces, 11 (2019) 3946−3960.

[22] R.W. Baker, Future directions of membrane gas separation technology, Ind. Eng. Chem. Res. 41 (2002) 1393–1411.

[23] B. Liu, C. Tang, X. Li, B. Wang, R. Zhou, High-performance SAPO-34 membranes for CO_2 separations from simulated flue gas, Micropor. Mesopor. Mater. 292 (2020) 109712.

[24] N. Tien-Binh, H. Vinh-Thang, X.Y. Chen, D. Rodrigue, S. Kaliaguine, Polymer functionalization to enhance interface quality of mixed matrix membranes for high CO_2/CH_4 gas separation, J. Mater. Chem. A. 3 (2015) 15202–15213.

[25] A. Imai, H. Mikami, E. Ito, M. Tanaka, M. Yamato, H. Kawakami, Influence of chemical modification on CO_2 permeability of polymers of intrinsic microporosity / silica nanoparticles composite membranes, J. Photopolym. Sci. Technol. 32

(2019) 457–461.

[26] Y. Luo, H.H. Funke, J.L. Falconer, R.D. Noble, Adsorption of CO_2, CH_4, C_3H_8, and H_2O in SSZ-13, SAPO-34, and T-Type Zeolites, Ind. Eng. Chem. Res. 55 (2016) 9749–9757.

Chapter 4 Silane surface modified SAPO-34 zeolite blended into 6FDA-mDAT membranes for gas separation

4.1 Introduction

The mixed matrix membranes (MMMs) is composited of inorganic filler and polymer matrix. The separation performance of the MMMs is influenced by the nature of filler and polymer matrix [1–4]. Due to the polymer as the main component, its property plays an important role in the performance of the MMMs. Therefore, it is necessary to focus on the choice of polymer matrix [5]. The 6FDA-TrMPD and 6FDA-mDAT polyimides (PI) are made by the polymerization of the 4,4'- (hexafluoroisopropylidene)diphthalic anhydride (6FDA) with the diamines, 2,4,6-trimethyl-1,3-phenylenediamine (TrMPD) and 2,6-diaminotoluene (mDAT) [6][7]. Figure 4-1 shows that the 6FDA based polyimides especially 6FDA-mDAT provide a promising CO_2/CH_4 separation performance among the polymeric membrane including the polyethersulfone (PES) membrane [8].

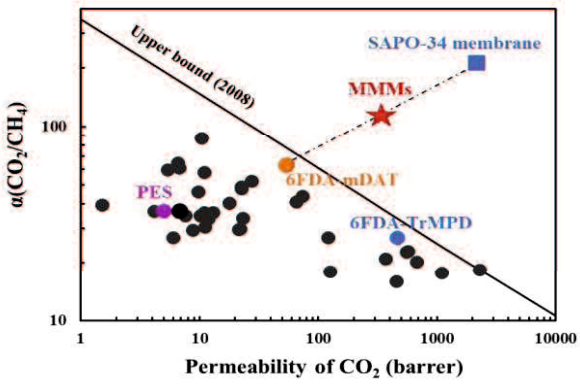

Figure 4-1 CO_2/CH_4 separation performance comparison of the polymeric membranes [8].

In Chapter 3, the commercial SAPO-34 had been proved to enhance the separation

performance of the PES membrane [9]. In this case, the MMMs prepared by blending the commercial SAPO-34 into 6FDA-mDAT polyimides is worth expecting, as shown in Figure 4-1. However, the sieve-in-a-cages appeared in the SAPO-34/PES membranes [10]. The sieve-in-a-cage is one kind of the defects in the MMMs [11]. This was due to the poor compatibility of the inorganic filler particles and polymer matrix. The defects allow the gas molecules to pass through, and then result in a low ideal selectivity. The PES has more flexible backbone than the polyimides. There is also a possibility that the defects appear in the SAPO-34/polyimide MMMs.

In order to eliminate the defect, aminosilane had been used to modify the surface of the zeolite [12,13]. The 3-aminopropyltrimethoxysilane (APTMS) is one common-used aminosilane. Hydroxyl groups of the APTMS can react with the silanol on the surface of the zeolite. This process is so-called silane coupling reaction, as shown in Scheme 4-1. The silane-modified zeolite particles possess a good compatibility with polymer matrix.

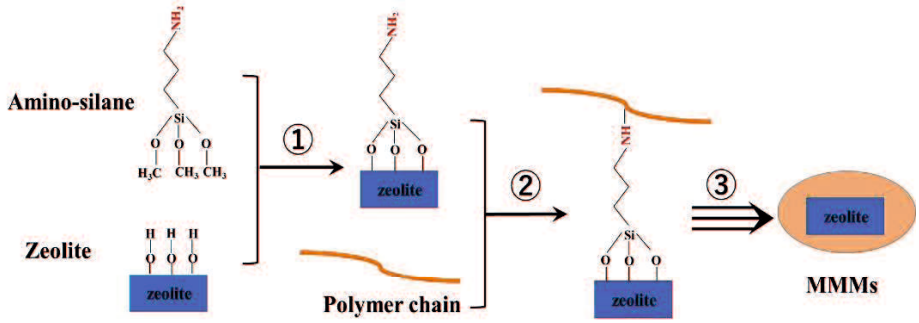

Scheme 4-1. Compatibility of zeolite and polymer improved by Silane coupling reaction [12,13].

The organic group of the aminosilane has good affinity with the polymer chain. Hence, the interaction of the zeolite particles with the polymer has been enhanced [14]. However, the linear structure with amino group of the APTMS molecules may enter the pore of SAPO-34 zeolite. This will result in the pore blockage of the zeolite [5,15]. Using *N*-phenylaminotrimethoxysilane (PhAPTMS) may avoid this issue because of the benzene-

ring. In this study we had selected the PhAPTMS as well as the APTMS to modify the SAPO-34 zeolite for the fabrication of the 6FDA-mDAT as based MMM. The phenyltrimethoxysilane (PhTMS) which contains benzene-ring and without amino group was used as a reference. Scheme 4-2 shows the formula structure of these tree kinds of silane. The influence of the different silane coupling reagent on the structure of the zeolite and separation performance of the MMMs had been investigated in this study.

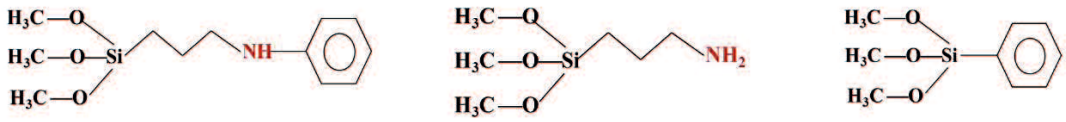

Scheme 4-2. Chemical Structure of silane coupling reagent

4.2 Experimental

4.2.1 Materials and Instrumental

Table 4-1 lists the materials and instrumental for the preparation of the SAPO-34/6FDA-mDAT MMMs. The SAPO-34 powder was provided by Mitsubishi Chemical Company. It was named as S3 to distinguish it from the SAPO-34 zeolite in Chapter 3.

Table 4-1 Materials and instrumental of SAPO-34/polyimide mixed matrix membranes.

Materials	**Abbreviation/Code**	**Manufacturer, Model**	**Purity** (wt%)
2,6-Diaminotoluene	mDAT	Tokyo Chemical Industry (TCI)	98
Commercial SAPO-34 zeolite	S3	Mitsubishi Chemical Company	—
Phenyl-3-amino-propyltrimethoxysilane	PhAPTMS	TCI	98
3-amino-propyltrimethoxysilane	APTMS	TCI	96
Phenyltrimethoxsilane	PhTMS	TCI	96
Toluene	TOL	TCI	97
Brunauer-Emmett-Teller Instrument	BET	Bel-sorp mini II	—

4.2.2 Silane surface modification of SAPO-34 zeolite

The silane surface modification of the SAPO-34 zeolite powder was based on the literature reported by Asghari et al. [16]. The detail process was as following:

(1) The SAPO-34 zeolite powder provided by Mitsubishi Chemical Company was dried at 200 °C overnight before modification.

(2) The dried zeolite powder was dispersed in to the toluene (TOL) and stirred at room temperature for 10 minutes. The ratio of zeolite to the TOL was 0.1g/mL.

(3) The silane coupling reagent was added to the zeolite/TOL slurry and stirred at room temperature for 6 hours to form a homogenous solution. The ratio of silane to zeolite was 3 mmol/g.

(4) The solution was heated at 110 °C for 4 hours under a reflux condition.

(5) The reacted zeolite sample were washed by using 300 mL ethanol and then dried at 80 °C overnight.

Herein, the original SAPO-34 was presented as S3. The zeolite sample modified by using PhAPTMS, APTMS, PhTMS were named as S4, S5, and S6 respectively.

4.2.3 Synthesis of 6FDA-mDAT Polymer

The 6FDA-mDAT polyimides were synthesized by the imidization of the polyamic acid which was generated from the 6FDA monomer reacted with the mDAT diamine monomer as shown in the Scheme 4-3. The equipment was shown in Figure 2-2.

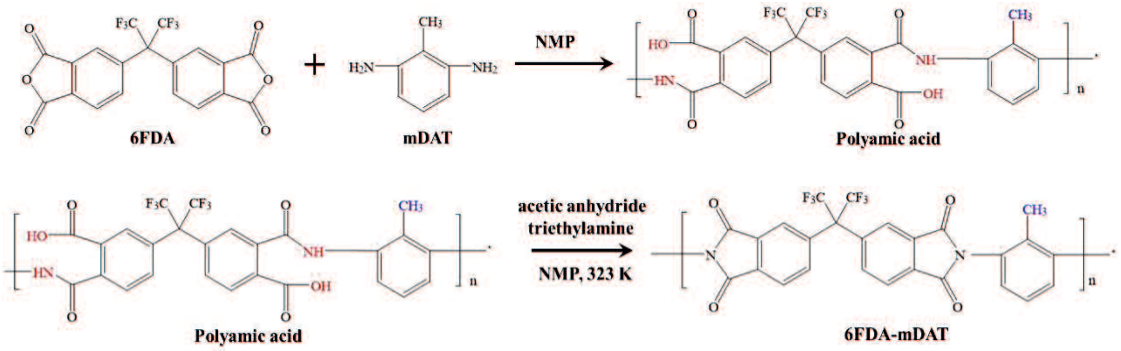

Scheme 4-3 Synthesis mechanism of 6FDA-mDAT polyimide.

The reaction of 6FDA with mDAT monomers was carried out in the four-neck round flask under nitrogen atmosphere. Acetic anhydride and triethylamine were used as the catalysts. The molar ratio of mDAT monomer: 6FDA: acetic anhydride: triethylamine was 1: 1: 4: 4. The detail experimental process is as follows:

(1) The mDAT monomer was mixed with the NMP solvent for 30 minutes to form a clear solution, and then the 6FDA was separately added to the solution.

(2) After mixing 6FDA and mDAT monomers in the NMP, the solution was kept overnight to form a medium product, polyamic acid.

(3) The polyamic acid was converted to the polyimide at 50 °C in the presence of acetic anhydride and triethylamine.

(4) The obtained solution was slowly poured into 800 mL of ethanol and washed thrice.

(5) The washed polymer was dried at 80 °C with vacuum condition overnight.

4.2.4 Preparation of neat 6FDA-mDAT membrane

The 6FDA-mDAT polyimide (PI) solid was divided into four equal parts to be dissolved in the NMP solvent to prepare a 15 wt% PI/NMP solution. After stirring for 20 hours, the solution was treated by ultrasonic for 4 hours and then bubble removal for 30

min. The solution was cast on the glass plate with a glass rod. After vacuum drying at 200 °C for 20 hours, the membrane was peeled from the glass plate.

4.2.5 Preparation of SAPO-34/6FDA-mDAT MMMs

The preparation of the modified SAPO-34/6FDA-mDAT MMMs was same to that of the original SAPO-34/PES MMMs as described in Chapter 3. The filler content of the zeolite in the membranes was in range of 0–20 wt%. Table 4-2 lists the preparation condition and code of the membranes.

Table 4-2 Preparation condition and code of the SAPO-34/6FDA-mDAT MMMs.

Filler content (wt%)	**Original filler (S3)**	**PhAPTMS-modified (S4)**	**APTMS-modified (S5)**	**PhTMS-modified (S6)**
0	M0	M0	M0	M0
5	M1	M4	—	M9
10	M2	M5	M7	M10
20	M3	M6	M8	M11

Note:

(1) M0 was the neat 6FDA-mDAT membrane

4.2.4 Characterization Methods

The surface area and the pore volume of the zeolite was measured by N_2 adsorption using BET instrument at 77 K [16,17]. Before the BET measurement, all the sample was degassed at 250 °C for 3 hours. The structure of the filler and membranes was analyzed by XRD. The morphology of the membranes was observed by using SEM.

4.2.5 Single Gas Permeation

The single gas permeation (H_2, CO_2 and CH_4) through the membranes was measured at 0.1 MPa and 35 °C. The gas permeability (*P*), diffusivity (*D*) and solubility (*S*) and their ideal selectivity were calculated as described in the Chapter 2.

4.3 Results and Discussion

Due to the original SAPO-34 particles has been modified by different silane coupling reagent. This is worth for analysis the variety of the zeolite before and after modification.

4.3.1 Characterization of Filler

4.3.1.1 SEM Images of Zeolite

Figure 4-2 shows the SEM images of the original and modified SAPO-34 particles. The S3, S4, S5 and S6 sample were original, PhAPTMS-modified, APTMS-modified, and PhTMS modified SAPO-34 zeolite. The SEM images can be used to observe the morphology of zeolite particles before and after modification.

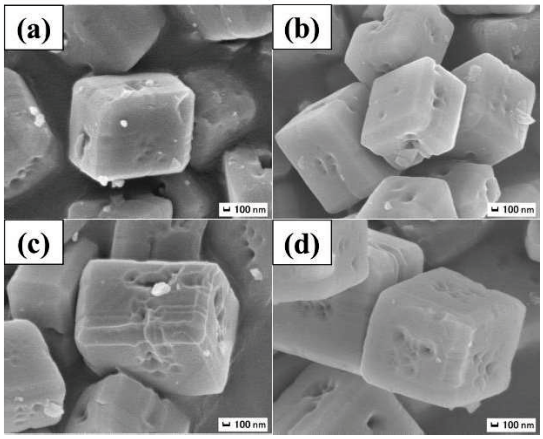

Figure 4-2. SEM images of (a) original (S3), (b) PhAPTMS-modified (S4), (c) APTMS-modified

filler (S5), and (d) PhTMS-modified (S6) SAPO-34 zeolite particles. The magnification of each image was 30,000.

All the zeolite powder had cubic crystals with around 2 μm of particle size. There was no agglomeration occurred among these sample. The surface of the modified zeolite (S4, S5 and S6) was same as the original SAPO-34 (S3). Hence, there was no difference in the morphology of the zeolite before and after modification. This also indicates that the crystallinity of the zeolite would not be affected by surface modification.

4.3.1.2 BET Analysis of Zeolite

Figure 4-3 shows the N_2 adsorption isotherm of the zeolite samples. The S3, S4, S5 and S6 sample were original, PhAPTMS-modified, APTMS-modified, and PhTMS modified SAPO-34 zeolite. These adsorption isotherms all assigned to the Type-I curve [18]. It confirmed that all the sample had the micropore structure. The order of the N_2 capacity in the powder was S3 > S6 > S4 > S5.

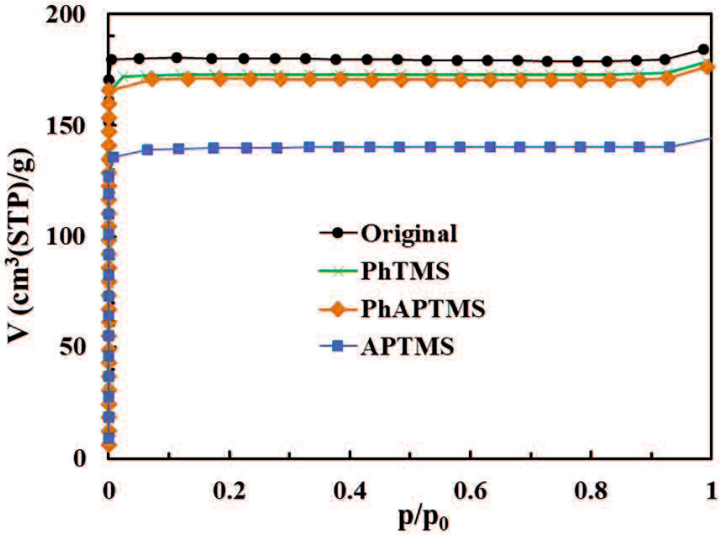

Figure 4-3. N_2 adsorption isotherm of original and modified SAPO-34 powder at 77 K.

Table 4-2 lists the results of the N_2 adsorption of the original and modified SAPO-34 powder. Two parameters are included: BET surface area and total pore volume.

Table 4-2 N_2 adsorption results of pristine and functionalized SAPO-34 zeolite at 77 K.

Sample	Silane	BET surface area (m^2/g)	Total pore volume (cm^3/g)
S3	no	553	0.28
S4	PhAPTMS	509	0.27
S5	APTMS	423	0.22
S6	PhTMS	522	0.28

The value order of surface area or pore volume of the samples was S3 > S6 > S4 > S5. This was corresponding to the adsorption amount of N_2 as shown in Figure 4-3. The original SAPO-34 sample (S3) has 553 m^2/g of BET surface area and 0.28 cm^3/g of total pore volume. The BET surface area of the PhAPTMS modified sample (S4) were 8% lower than that of the S3 sample. Their pore volume was considered almost same. These two values of the APTMS modified zeolite (S5) were 24% and 21% lower than the S3 sample. This indicates that the APTMS silane blocked the pore of the SAPO-34 zeolite. The difference in S4 and S5 was due to the presence of the benzene ring. The sample (S6) modified by using PhTMS with benzene-ring and without NH– group was used a reference. Compared to the original zeolite (S3), the surface area and pore volume almost remained after PhTMS modification. This confirm that the presence of the benzene-ring can prevent the blockage of the zeolite pore.

4.3.2 Characterization of Membranes

4.3.2.1 XRD Analysis

Figure 4-4 shows the XRD patterns of the original SAPO-34 powder (S3) and the

MMMs using 20 wt% of filler. This figure can be used to analysis the crystal structure of SAPO-34 zeolite, and then compare the crystallinity of the SAPO-34 zeolite before and after silane modification, and confirm the presence of the zeolite in the MMMs.

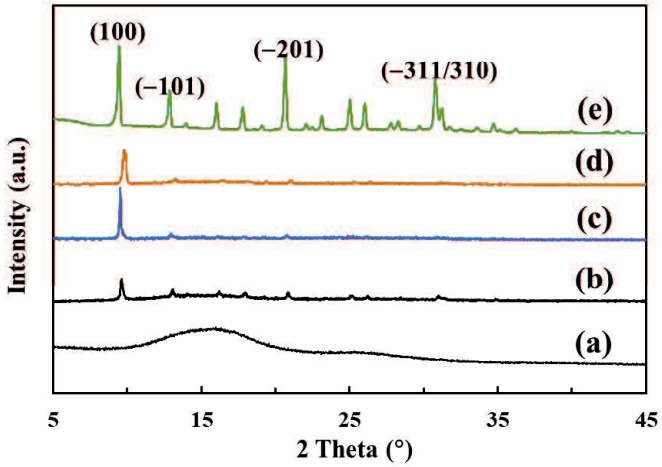

Figure 4-4. XRD patterns of the neat 6FDA-mDAT membranes and the MMMs using 20 wt% original and modified SAPO-34 filler: (a) neat membrane (M0), (b) original S3 filled MMMs (M3), (c) PhAPTMS-modified MMMs (M6), (d) APTMS-modified MMMs (M8), and (e) original SAPO-34 powder (S3).

The neat polymer membranes had an amorphous structure. The SAPO-34 powder (S3) had main peaks at 2θ = 9.4°, 12.8°, 20.7°, 30.7°. These peak positions assigned to the crystalline plane of (100), (–101), (–201) and (–311/310), respectively. This was in good agreement with the XRD pattern of CHA-type zeolite in the literature. Hence, the S3 powder possessed a typical XRD peaks belong to CHA structure. The peak intensity of zeolite in the MMMs were all weak than the original S3 powder due to the presence of the amorphous polymer matrix. The modified SAPO-34 MMMs had stronger XRD peak than the original SAPO-34 MMM. This may be due to the aminosilane resulted in the agglomeration of the zeolite particles near the outside surface of the MMMs.

4.3.2.2 SEM Observation

Figure 4-5 shows the cross-sectional SEM images of the MMMs using 5 wt% of filler. The cubic crystal was the SAPO-34 zeolite particle; the amorphous structure was the polymer matrix.

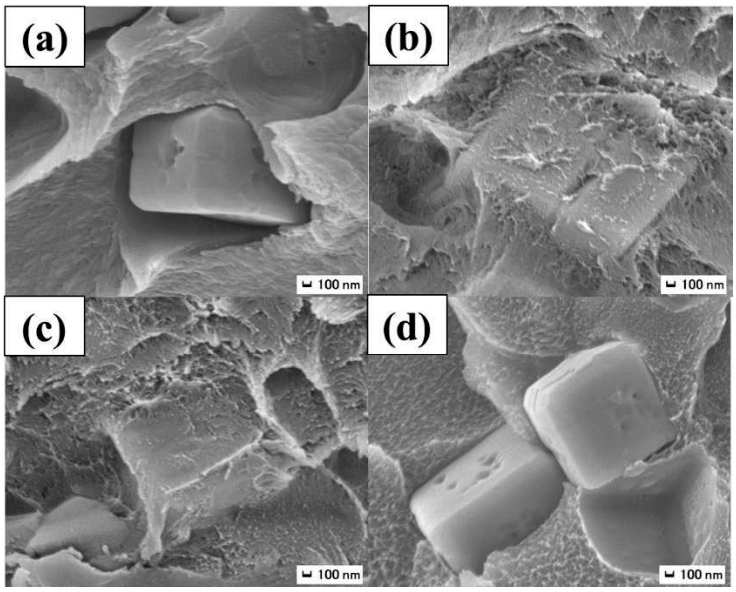

Figure 4-5 Cross-sectional SEM images of the MMMs: (a) M1 using 5 wt% S3, (b) M4 using 5 wt% S4, (c) M8 using 20 wt% of S5, and (d) M11 using 20 wt% of S6. Magnification of each image is 30,000.

Figure 4-5(a) shows that the sieve-in-a-cage existed around the particles. There was free-space between the particles and polymer matrix. This means the original filler has no obvious interaction with the polymer matrix. Figure 4-5(b) shows that the particles appear to be mostly buried in the polymer. This indicated an excellent wettability of filler particles and polymer matrix. There are obvious amorphous polymer sticks on the surface of crystals, which not presented in the original S4 zeolite sample. Figure 4-5(c) shows that the morphology of the APTMS-modified zeolite (S5) filled membrane (M8) was

same to that of the S4 filled MMMs. The wettability of the filler particles and polymer matrix in the M11 membrane that using PhAPTMS and ATMS-modified zeolite was better than in the membranes using PhTMS-modified zeolite. This due to the absence of the amino group which can react with polymer chains to enhance the affinity of the zeolite surface with the polymer.

Figure 4-6 further displayed the cross-sectional SEM images of the MMMs all using 20 wt% of filler. The M3 membrane was using original SAPO-34 zeolite (S3), as displayed by Figure 4-6(a) and (e); M6 membrane using the PhAPTMS-modified zeolite (S4) as displayed by Figure 4-6(b) and (f); the M8 membrane using APTMS-modified zeolite (S5) as displayed by Figure 4-6(c) and (g); the M11 membrane using PhTMS-modified zeolite (S6) as displayed by Figure 4-6(d) and (h). The upper row using a higher magnification of image, and the below row using the corresponding lower magnification of image.

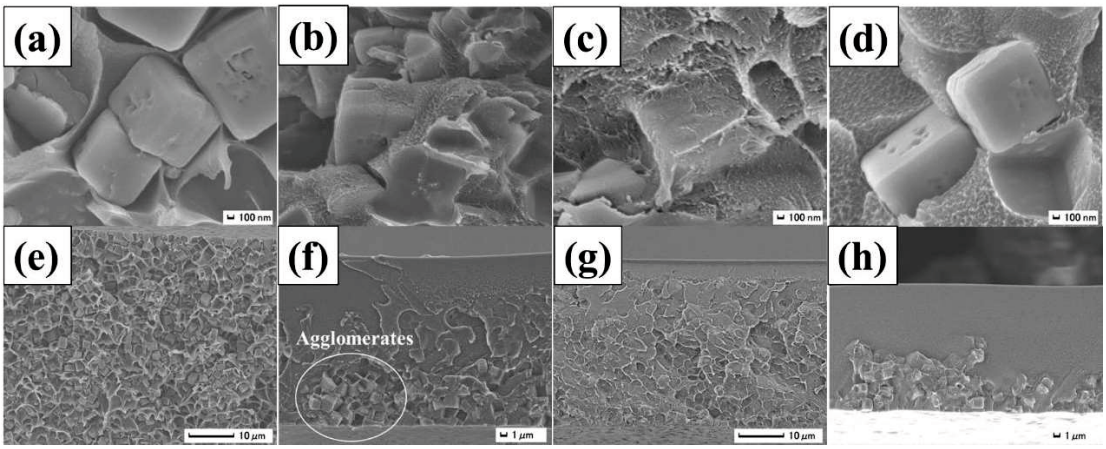

Figure 4-6 Cross-sectional SEM images of the MMMs using 20 wt% of filler: (a,e) M3 using S3, (b,f) M6 using S4, and (c,g) M8 using S5, and (d,h) M11 using S6.

The 20 wt% of the S3 filled M3 membrane possessed a same structure to the 5wt% S3 filled MMMs (M1). Sieve-in-a-cages also appeared in the M3 membranes. The amount was more than M1 membrane. The homogenously dispersion of S3 in the M3 membrane was same as in the M1 membrane. The 20 wt% of the S4 particles was covered by the polymer matrix. However, the agglomeration of the filler particles occurred near the out surface of the M6 membrane as shown Figure 4-6(f). This maybe due to that increasing the content of particles would increase the probability of silane-modified zeolite contact with the same part of the polymer chains, thereby causing the agglomeration. Figure 4-6(c) and (g) shows the cross-sectional SEM images of 20 wt% of S5 filled MMMs (M8). The filler particles provided a good compatibility with the polymer matrix. However, the agglomeration occurred in the cross-section of the M8. The upper part of the membrane which touches the air during casting was almost a neat polymer layer. This was due to that the APTMS strongly contact the polymer chains together and then the sedimentation occurred near the bottom surface (which touches the glass plate during casting) of the membrane. This phenomenon may be occurred during the phase conversion of polymer from liquid to solid. Figure 4-6(d) and (h) shows that the agglomeration also occurred in the PhTMS-modified zeolite (S6) filled membrane (M11). Therefore, the silane-modification could improve the wettability/compatibility of the particles and polymer matrix, but it will result in agglomeration when using high content of modified zeolite.

4.3.3 Gas Separation Performance

Figure 4-7 and Figure 4-8 showed the gas permeability and ideal selectivity of the MMMs, respectively. In each graph, the X axis presents the filler content, Y axis presents the values of gas permeability or ideal selectivity.

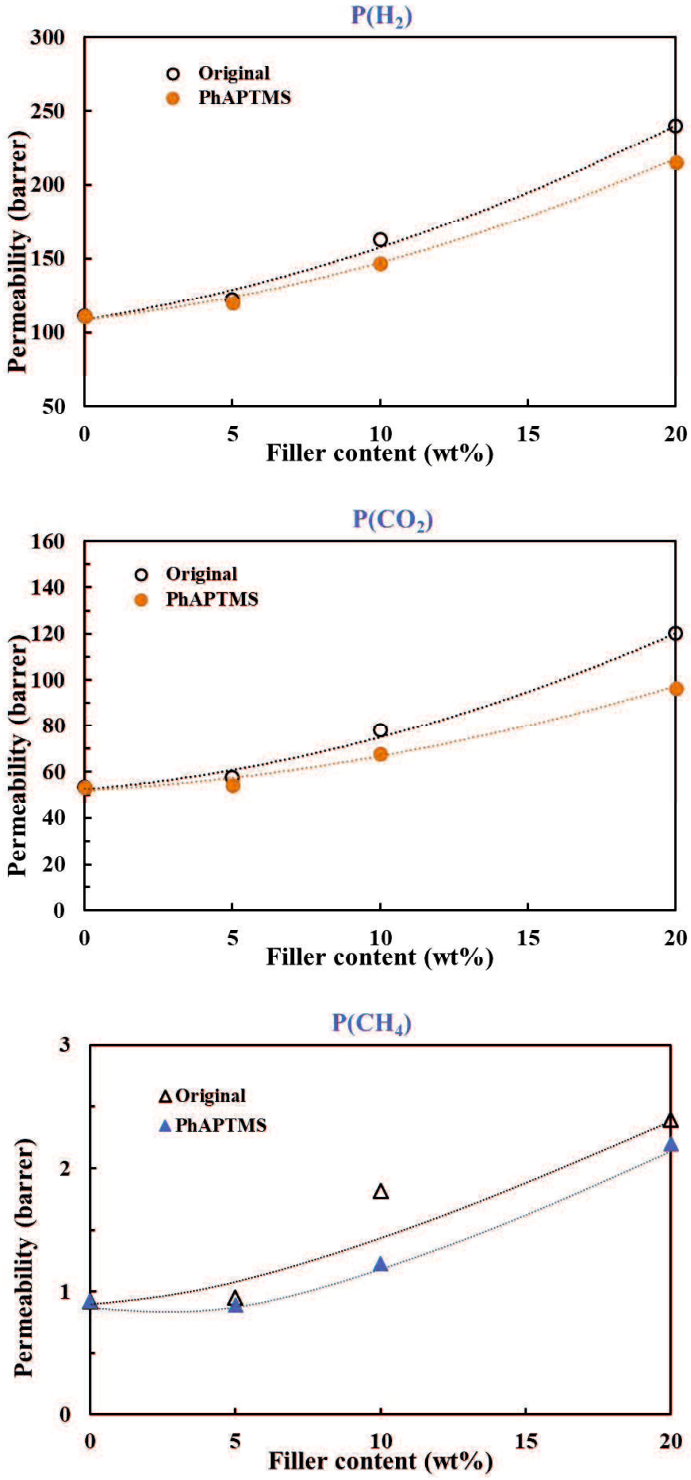

Figure 4-7. Permeability of H_2, CO_2 and CH_4 of 6FDA based MMMs using original SAPO-34 and PhAPTMS-modified SAPO-34 as function of the filler content.

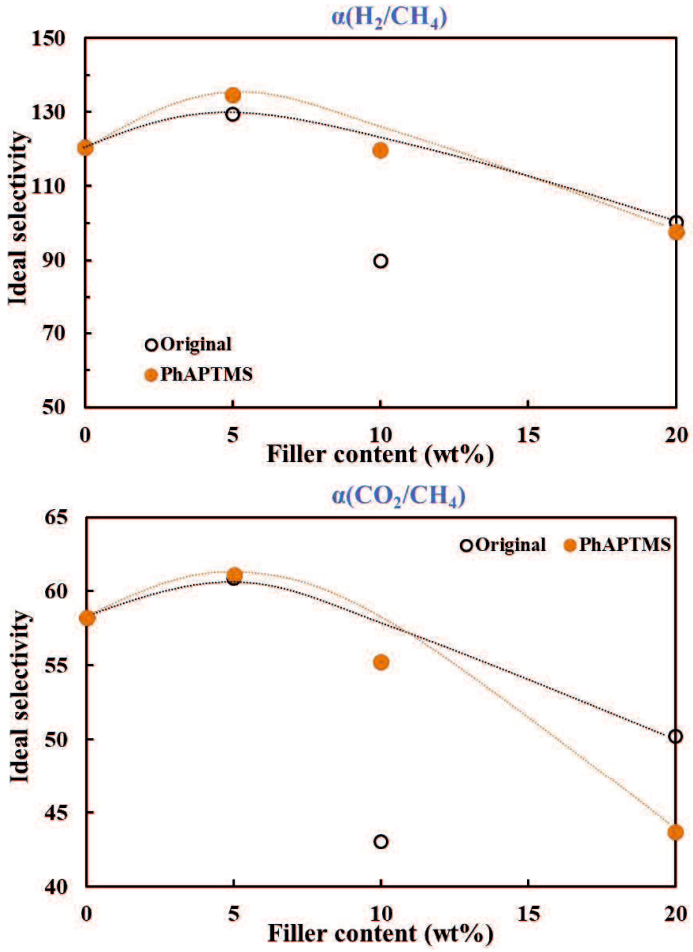

Figure 4-8. Ideal selectivity of H_2/CH_4 and CO_2/CH_4 of 6FDA based MMMs using original SAPO-34 and PhAPTMS-modified SAPO-34 as function of the filler content.

The CH_4 permeabilites of the 6FDA-mDAT membranes was both increased with increasing the original SAPO-34 (S3) filler as well as the H_2 and CO_2 permeability. Normally, the CH_4 permeability of the neat polymer membrane should be decreased with adding SAPO-34 zeolite. The result indicates that there were some defects in the original SAPO-34 filled MMMs. The H_2/CH_4 and CO_2/CH_4 ideal selectivity of the S3 MMM using 5 wt% of the original S3 filler were 7% and 5% higher than that of the neat polymer membrane. The increase ratio of the H_2 and CO_2 permeability greater than that of the CH_4 permeability. It due to that the positive effect (molecular sieving effect) of the zeolite pore

on the gas selectivity was greater than the negative effect of the defect (sieve-in-a-cage). When the filler content over 5 w%, the amount of the defects was increased. The negative effect of defects greater than positive effect of zeolite pore, so the ideal selectivity was decreased.

In terms of the comparison of the PhAPTMS-modified SAPO-34 (S4) and original zeolite (S3), the gas permeability of each MMMs using S4 zeolite was lower than the MMMs using the same content of S3 zeolite. This due to that the PhAPTMS eliminated the sieve-in-a-cage. The gas permeability was higher than that of the neat polymer membrane. This confirmed the PhAPTMS aminosilane didn't block the pore of the zeolite particles. In this case, using 5 wt% of S4 zeolite particles increased the ideal selectivity of H_2/CH_4 and CO_2/CH_4 better than using 5 wt% of the original S3 zeolite particles.

When the filler content increased to 20 wt%, the PhATMS modified MMM (M6) provided CO_2 permeability was 96 barrer, but the CO_2/CH_4 ideal selectivity was only 44. This value was lower than that of 20 wt% original SAPO-34 filled MMMs (M3). It due to that the agglomeration occurred in the M6 membrane and not in the M3 membrane. The agglomeration was formed due to that high content of aminosilane modified zeolite more possible contact with the same part of the polymer chains. Hence, the PhAPTMS aminosilane was effective on the improvement of separation performance of the SAPO-34/6FDA-mDAT MMMs when the filler content was 5 wt% in this study.

Figure 4-9 summarized of H_2/CH_4 and CO_2/CH_4 separation performance of the SAPO-34/6FDA-mDAT MMMs. The X axis was the permeability ratio of the MMMs to the neat membrane; Y axis was the ideal selectivity ratio of the MMMs to the neat membrane. The cross composed of two dashed lines divides each graph into four parts. The upper-right part means the permeability and ideal selectivity of the membrane are both higher than

that of the neat polymer membrane which located at the dotted line intersection. Therefore, the upper-right part of each graph presents the ideal region for the gas separation performance of the MMMs.

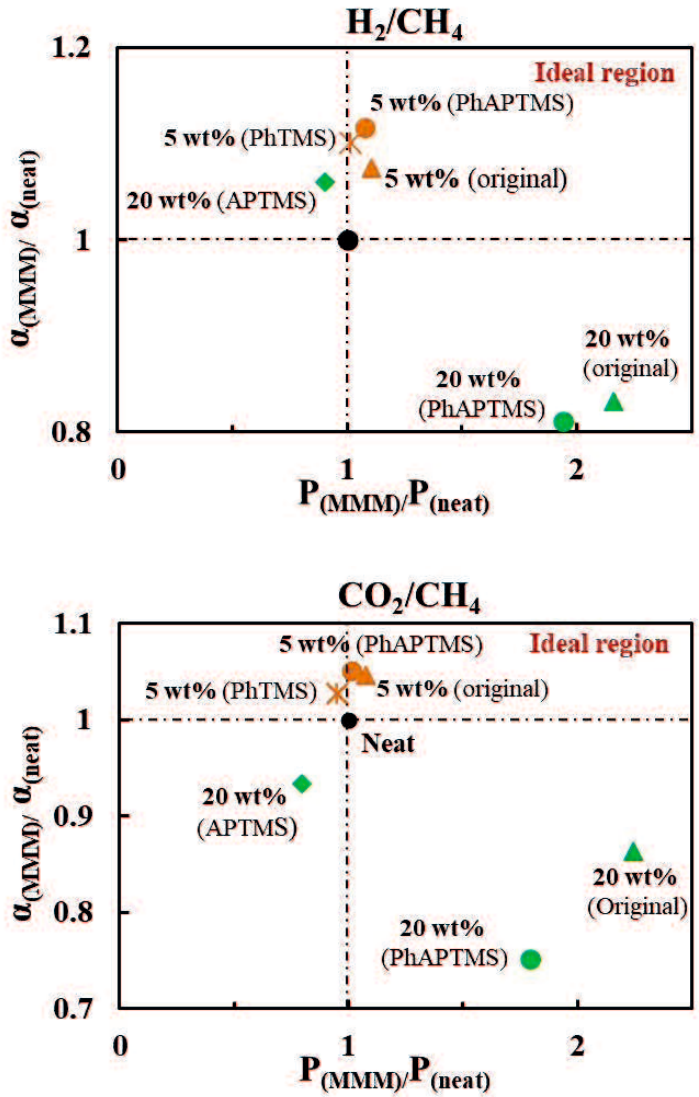

Figure 4-9. Summary of CO_2/CH_4 separation performance of the SAPO-34/6FDA-mDAT MMMs using original zeolite (triangle), PhAPTMS-modified (circle), APTMS-modified (diamond) and PhTMS-modified (star) zeolite particles.

Figure 4-9 shows that the almost all the MMMs using 5 wt% of zeolites located at the ideal region that provided both higher gas permeability and ideal selectivity than the neat

polymer membrane. In terms of the ideal selectivity, the value order of the MMMs was PhATMS-modified > PhTMS-modified > original zeolite. This was due to the PhATMS improved the wettability of the zeolite particle and polymer matrix better than the PhTMS.

When increasing the content of the original and PhAPTMS-modified zeolite to 20 wt%, the values dropped to the bottom-right part. This means the MMMs had higher permeability and lower selectivity than that of the neat polymer membrane. It due to that sieve-in-cage appeared in the membrane using original zeolite and agglomeration occurred in the membrane using PhAPTMS-modified zeolite, as shown in Figure 4-6. The ideal selectivity ratio of H_2/CH_4 and CO_2/CH_4 of the membrane using PhTMS-modified zeolite to the neat polymer membrane was 0.21 and 0.22, which were not displayed in the Figure 4-9. These values of ideal selectivity were all poor than that of the membrane using PhAPTMS-modified zeolite. This was due to the agglomeration of the membrane using PhTMS was much serious than the MMMs. In terms of the MMMs using APTMS-modified zeolite, the values located at the left part. This was due to the APTMS blocked the pore of zeolite seriously.

4.4 Conclusions

The SAPO-34/6FDA-mDAT MMMs were prepared with silane surface modification for gas separation. The silane coupling reagent, PhAPTMS, was the first time applied to modify the surface of the SAPO-34 particles in order to improve the compatibility of the filler and 6FDA-mDAT matrix. When the filler content was 5 wt%, the PhAPTMS-modified SAPO-34 both increased the gas permeability and selectivity compared with the neat polymer membrane and the original SAPO-34 MMMs. This was attributed to that the PhAPTMS enhanced the affinity of the filler particles with polymer matrix. When the filler content over 10 wt%, the separation performance of the PhAPTMS-modified SAPO-34 MMM was lower than the original SAPO-34 MMM. This was due to that the agglomeration occurred in the PhAPTMS-modified filler in the MMMs. Therefore, there was an antagonism effect on the membrane performance: positive effect from zeolite pore (molecular sieving effect); negative effect from defects (sieve-in-a-cage/agglomeration). The PhAPTMS was effective to enhance the separation performance of the SAPO-34/6FDA-mDAT MMMs when the filler content less than 10 wt% in this study.

4.5 References

[1] T.S. Chung, L.Y. Jiang, Y. Li, S. Kulprathipanja, Mixed matrix membranes (MMMs) comprising organic polymers with dispersed inorganic fillers for gas separation, Prog. Polym. Sci. 32 (2007) 483–507.

[2] B. Shimekit, H. Mukhtar, T. Murugesan, Prediction of the relative permeability of gases in mixed matrix membranes, J. Memb. Sci. 373 (2011) 152–159.

[3] H. Vinh-Thang, S. Kaliaguine, Predictive models for mixed-matrix membrane performance: A review, Chem. Rev. 113 (2013) 4980–5028.

[4] M. Galizia, W.S. Chi, Z.P. Smith, T.C. Merkel, R.W. Baker, B.D. Freeman, 50th Anniversary perspective: Polymers and mixed matrix Membranes for gas and vapor separation: A review and prospective opportunities, Macromolecules. 50 (2017) 7809–7843.

[5] Y. Cheng, Z. Wang, D. Zhao, Mixed Matrix Membranes for Natural Gas Upgrading: Current Status and Opportunities, Ind. Eng. Chem. Res. 57 (2018) 4139–4169.

[6] K. Tanaka, J. Taguchi, J.Q. Hao, H. Kita, K. Okamoto, Permeation and separation properties of polyimide membranes to olefins and paraffins, J. Membr. Sci. 121 (1996) 197–207.

[7] C. Cao, R. Wang, T.S. Chung, Y. Liu, Formation of high-performance 6FDA-2,6-DAT asymmetric composite hollow fiber membranes for CO_2/CH_4 separation, J. Memb. Sci. 209 (2002) 309–319.

[8] L.M. Robeson, The upper bound revisited, J. Memb. Sci. 320 (2008) 390–400.

[9] T. Wu, Y. Liu, I. Kumakiri, K. Tanaka, X. Chen, H. Kita, Preparation and

permeation properties of PESU-based mixed matrix membranes with nano-sized CHA zeolites, J. Chem. Eng. Japan. 52 (2019) 514–520.

[10] E. Karatay, H. Kalipçilar, L. Yilmaz, Preparation and performance assessment of binary and ternary PES-SAPO 34-HMA based gas separation membranes, J. Memb. Sci. 364 (2010) 75–81.

[11] M. Wang, Z. Wang, N. Li, J. Liao, S. Zhao, J. Wang, S. Wang, Relationship between polymer-filler interfaces in separation layers and gas transport properties of mixed matrix composite membranes, J. Memb. Sci. 495 (2015) 252–268.

[12] C. Takai, M. Fuji, M. Takahashi, A novel surface designed technique to disperse silica nano particle into polymer, Colloids Surfaces A Physicochem. Eng. Asp. 292 (2007) 79–82.

[13] N.N. Rosyadah Ahmad, H. Mukhtar, D.F. Mohshim, R. Nasir, Z. Man, Surface modification in inorganic filler of mixed matrix membrane for enhancing the gas separation performance, Rev. Chem. Eng. 32 (2016) 181–200.

[14] M.U.M. Junaidi, C.P. Khoo, C.P. Leo, A.L. Ahmad, The effects of solvents on the modification of SAPO-34 zeolite using 3-aminopropyl trimethoxy silane for the preparation of asymmetric polysulfone mixed matrix membrane in the application of CO_2 separation, Micropor. Mesopor. Mater. 192 (2014) 52–59.

[15] Y. Li, H.M. Guan, T.S. Chung, S. Kulprathipanja, Effects of novel silane modification of zeolite surface on polymer chain rigidification and partial pore blockage in polyethersulfone (PES)-zeolite A mixed matrix membranes, J. Memb. Sci. 275 (2006) 17–28.

[16] M. Mosadegh, F. Amirkhani, H. Riasat Harami, M. Asghari, M.J. Parnian, Effect of Nafion and APTEOS functionalization on mixed gas separation of PEBA-FAU

membranes: Experimental study and MD and GCMC simulations, Sep. Purif. Technol. 247 (2020).

[17] H.R. Amedi, M. Aghajani, Aminosilane-functionalized ZIF-8/PEBA mixed matrix membrane for gas separation application, Micropor. Mesopor. Mater. 247 (2017) 124–135.

[18] M. Thommes, K. Kaneko, A. V. Neimark, J.P. Olivier, F. Rodriguez-Reinoso, J. Rouquerol, K.S.W. Sing, Physisorption of gases, with special reference to the evaluation of surface area and pore size distribution (IUPAC Technical Report), Pure Appl. Chem. 87 (2015) 1051–1069.

Chapter 5 Summary and Prospects

5.1 Summary

In this thesis, we had investigated the preparation and separation performance of mechano-synthesized ZIF-8/6FDA-TrMPD, SAPO-34/PES, and SAPO-34/6FDA-mDAT MMMs. All the MMMs provided a higher separation performance than their neat polymer membranes.

The MMMs composited of mechanochemically synthesized ZIF-8 nanoparticles and 6FDA-TrMPD polyimide were prepared in **Chapter 2**. The pre-treatment of the ZIF-8 nanoparticles by using ball milling helps the dispersion of the filler in the MMMs. The C_3H_6 permeability and C_3H_6/C_3H_8 ideal selectivity of a 20 wt% mechano-synthesized ZIF-8/6FDA-TrMPD MMM were 70% and 32% higher than those of the neat polymer membrane at 0.1 MPa and 308 K, respectively. The C_3H_6/C_3H_8 separation performance of the mechano-synthesized ZIF-8 MMM was similar to that of the conventional solvothermal-synthesized ZIF-8 MMM. This separation performance was in good agreement with the Maxwell model. Temperature and pressure dependence analyses confirmed that the mechano-synthesized ZIF-8 nanoparticles acted as molecular sieves in the MMMs for the C_3H_6 and C_3H_8 permeation.

The CO_2/CH_4 separation performance of commercialized SAPO-34 zeolite/PES MMMs as well as the gas diffusivity and solubility had been investigated in **Chapter 3**. The MMMs using 30 wt% SAPO-34 provided a CO_2 permeability and CO_2/CH_4 ideal selectivity at 0.1 MPa and 35 °C about 15 barrer and 51, respectively. In our previous paper, the PES MMMs using laboratory-made SAPO-34 provided both higher

permeability and selectivity than the neat PES membrane. The performance of the commercial SAPO-34 filled MMMs in this study exceeded their performance. We also investigated the performance of these MMMs in terms of gas diffusivity and solubility. The increase in the diffusivity selectivity was greater for the commercial SAPO-34 MMMs than for the laboratory-made SAPO-34 MMMs. The difference was attributed to the amounts of defects. The performance of the MMMs in this study was also superior to that of the reported SAPO-34/PES MMMs in literature where the filler surface was modified to improve the compatibility of the filler and PES matrix. These results suggest that the use of the commercial SAPO-34 and an appropriate surface modification has the potential to improve the performance of the MMMs

Due to the high CO_2/CH_4 selectivity, the 6FDA-mDAT polyimide was selected as a polymer matrix to be blended with the SAPO-34 zeolite in **Chapter 4**. The silane coupling reagent, PhAPTMS aminosilane, was the first time applied to modify the surface of the SAPO-34 particles. Compared to the common used APTMS aminosilane block the pore of the zeolite seriously, the presence of benzene-ring in the PhAPTMS can avoid this problem. Due to the presence of the amino-group, the PhAPTMS can improve the compatibility of the zeolite and polymer better than the PhTMS which only contains benzene-ring. Therefore, the PhAPTMS is a promising silane coupling reagent for the improvement on the separation performance of the MMMs.

5.2 Prospects

The Maxwell model predicts that high content of mechano-synthesized ZIF-8/6FDA-TrMPD MMMs can provide a better separation performance than the current result. The preparation process of the MMMs should be improved. The agglomeration of mechano-synthesized ZIF-8 nanoparticles can be improved by priming, beads milling, chemical functionalization and so on.

The separation performance of the SAPO-34/PES membrane can be improved by eliminating the sieve-in-a-cages. The silane coupling reaction and amine functionalization are the promising improvement methods.

In order to avoid the agglomeration of PhAPTMS-modified SAPO-34 zeolite in the 6FDA-mDAT MMMs, the amount of the PhAPTMS (the ratio of the aminosilane to the zeolite particles) and the time of the modification reaction time should be optimized.

Novel microporous materials such as AEI zeolite (por size: 0.38×0.38 nm), AFX zeolite (0.34×0.36 nm) and SAS zeolite (0.42×0.42 nm) could be used to prepare the MMMs for gas separation.

List of Publications

1. Mechanochemically synthesized ZIF-8 nanoparticles blended into 6FDA-TrMPD membranes for C_3H_6/C_3H_8 separation

   Yongsheng Liu, Hidetoshi Kita, Kazuhiro Tanaka*, Kouta Imawaka, Shunsuke Tanaka, Takahiko Takewaki

   Journal of Applied Polymer Science, 2021;138:e50251.

2. Preparation and permeation properties of PESU-based mixed matrix membranes with nano-sized CHA zeolites

   Ting Wu, **Yongsheng Liu**, Izumi Kumakiri, Kazuhiro Tanaka*, Xiangshu Chen*, Hidetoshi Kita

   Journal of Chemical Engineering of Japan, 52 (2019) 514–520.

3. Investigation of gas diffusivity and solubility of PES based mixed matrix membranes using commercial SAPO-34 zeolite

   Yongsheng Liu, Kyosuke Takata, Hidetoshi Kita and Kazuhiro Tanaka*

   Transactions of the Materials Research Society of Japan, Accepted

4. Nano-porous zeolite and MOF filled mixed matrix membranes for gas separation

   Yongsheng Liu, Kyosuke Takata, Yu Mukai, Hidetoshi Kita and Kazuhiro Tanaka*

   The Proceeding of 18th Asian Pacific Confederation of Chemical Engineering Congress (APCChE 2019), MATEC Web of Conferences, 333 (2021) 04008.

Acknowledgements

First and foremost, I would like to express my deepest appreciate to my supervisor, Professor Kazuhiro Tanaka. Thanks for guiding, supporting, and giving me a lot of delightful ideas throughout my research. I have learned a great deal from his unique perspective on research, scientific attitude, sharp insight on issue, personal integrity, and expectations of excellence.

I would like to extend my sincere gratitude to Professor Hidetoshi Kita who offered me this wonderful opportunity to continue my research and given his kind assistance and valuable advice for me. Your enthusiastic, endless interest on study, devoted academic attitude also guided me in my personal and latter academic life. I am very grateful to Professor Yoshihisa Sakata for his kind help and valuable suggestions.

Special appreciation would go to my master's supervisor Professor Xiangshu Chen, thanks for leading me to the membrane research and recommending me to study the Ph.D program in Yamaguchi University. Moreover, I would like to appreciate, Dr. Meihua Zhu, who has given me much advice and assistance to my research. Thanks to every member in our laboratory, Ting Wu, Jing Nie, Kyosuke Takata, Yu Mukai, Koji Takahashi, Yushi Imamura, and so on, for giving me a lot of assistance.

I'd like to give my special thanks to my wife, Junzhe Jiang, who has studied the Master and Ph.D program together with me. Her accompany and encouragement gives me endless motivation. Thanks very much to beloved family and friends for 100% supporting and endless love throughout my life.

Yongsheng Liu

Appendix: Conflict of Interest Statement

The content of **Chapter 2** had been published in *Journal of Applied Polymer Science* (DOI: 10.1002/app.50251). The author has obtained permission from the publisher, John Wiley and Sons, to reuse the full article in this dissertation. License Terms and Conditions provided by John Wiley and Sons and Copyright Clearance Center are as follows.

- **License number**: 5007040694230
- **License date**: February 13, 2021
- **License content title**: Mechanochemically synthesized ZIF-8 nanoparticles blended into 6FDA-TrMPD membranes for C_3H_6/C_3H_8 separation
- **License content author**: Yongsheng Liu, Hidetoshi Kita, Kazuhiro Tanaka, Kota Imawaka, Shunsuke Tanaka, Takahiko Takewaki
- **Requestor location**: Dr. Yongsheng Liu, Yamaguchi University

A manuscript related to the content of **Chapter 3** will be published in *Transactions of the Materials Research Society of Japan*, Vol. 46, No.1. The information of the manuscript to be published is as follows.

- **Manuscript ID**: MRSJ-2020-0032.R1
- **Publication**: Transactions of the Materials Research Society of Japan
- **Publisher**: The Materials Research Society of Japan
- **Tittle**: Investigation of Gas Diffusivity and Solubility of PES based Mixed Matrix Membranes Using Commercial SAPO-34 Zeolite
- **Autor**: Yongsheng Liu, Kyosuke Takata, Hidetoshi Kita and Kazuhiro Tanaka